

INFERRING MANIFOLDS USING GAUSSIAN PROCESSES

DAVID B DUNSON AND NAN WU

ABSTRACT. It is often of interest to infer lower-dimensional structure underlying complex data. As a flexible class of non-linear structures, it is common to focus on Riemannian manifolds. Most existing manifold learning algorithms replace the original data with lower-dimensional coordinates without providing an estimate of the manifold or using the manifold to denoise the original data. This article proposes a new methodology to address these problems, allowing interpolation of the estimated manifold between the fitted data points. The proposed approach is motivated by the novel theoretical properties of local covariance matrices constructed from samples near a manifold. Our results enable us to turn a global manifold reconstruction problem into a local regression problem, allowing for the application of Gaussian processes for probabilistic manifold reconstruction. In addition to the theory justifying our methodology, we provide simulated and real data examples to illustrate the performance.

Keywords: Data denoising; Dimension reduction; Manifold learning; Manifold reconstruction; Non-parametric regression

1. INTRODUCTION

It is common to characterize low-dimensional structures in data using Riemannian manifolds. The literature on manifold learning focuses mainly on dimensionality reduction algorithms; some well-known examples include Isomap [36], Laplacian Eigenmaps [3], Locally Linear Embeddings [32], and Diffusion Maps [7]. The focus of this article is instead on developing a new local regression-based approach to manifold reconstruction, which goes beyond dimensionality reduction to exploit the manifold structure in modeling the original data.

We provide a concrete illustration through bird vocalization data. Audio files are converted via discrete short-time Fourier transform into spectrograms. In Figure 1, we present five annotated spectrograms of a specific call type of *Anthus trivialis* (tree pipit) from [29]. Similar spectrogram data are routinely collected in studying birds, and it is of interest to develop realistic statistical models for such data that can be used to infer variation in vocalizations between individuals and according to geographical location and habitat conditions. With this goal in mind, we propose a method based on characterizing the data as noisy observations around a manifold.

This article proposes Manifold reconstruction via Gaussian processes (MrGap). Our main contributions are: (1) bias and variance analyses and spectral properties of the local covariance matrix constructed from samples near a manifold; and (2) a novel local regression formulation of manifold reconstruction, enabling application of Gaussian process regression and avoidance of restrictive assumptions on the noise or distribution of the denoised data on the manifold. We apply MrGap to the bird vocalization spectrogram data illustrated in Figure 1, interpolating 10 points near each sample in the manifold and showing the corresponding spectrograms near sample 1 in Figure 1. The generated samples incorporate the audio information from sample 1 and its neighboring samples. Such interpolation provides insights into variation across birds and provides a natural starting point for extensions for inference on covariate effects. Refer to Section 5 for details and results.

We briefly review the literature relevant to our first main contribution. [34] analyzes the bias and variance of the local covariance matrix constructed through a smooth kernel, assuming samples without noise from a closed submanifold. Focusing on the local covariance constructed from a $0-1$ kernel, [37] consider data having specific distributions on closed manifolds while [39, 41] assume samples without

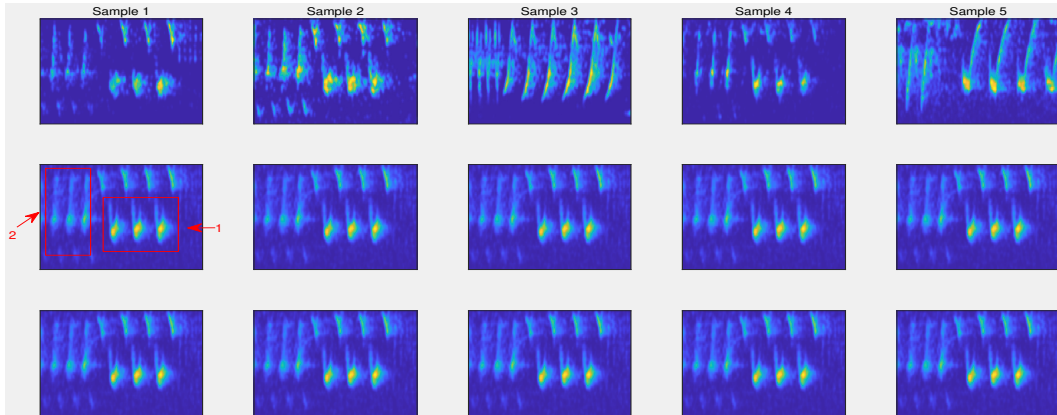


FIGURE 1. Top row: 5 out of 83 spectrograms corresponding to a call type of *Anthus trivialis*. The rows of the $\mathbb{R}^{75 \times 197}$ matrices correspond to frequency (kHz), and the columns correspond to time (ms) and entries measure amplitude of the signal. Samples 2 and 4 are near Sample 1. Second and third rows: 10 generated samples near Sample 1 using MrGap. Region 2 in the generated sample is similar to Sample 1, while region 1 is similar to Samples 2 and 4.

noise from a closed submanifold and a compact submanifold with boundary. [19] studies the local covariance constructed from k nearest neighbors under heavy restrictions on the embedded submanifold and sampling distribution. We consider much more realistic sampling conditions, and our theory generalizes [39] to allow Gaussian noise.

Relevant to our second main contribution, there is a literature on manifold reconstruction. Principal curves provide a fitted value for a one-dimensional manifold [18, 20, 22], while principal manifolds extend this to higher dimensions [35, 23]. Assuming Gaussian noise, [16, 17] reconstruct a manifold by approximating its normal bundle using noisy samples. [1] and [2] apply local polynomial fitting to reconstruct a manifold. [1] assumes bounded noise in the normal direction, while [2] consider uniformly distributed noise in a tubular neighborhood. [30] assume samples with bounded noise and estimate a projection operator onto the manifold. Assuming uniform samples on the manifold and Gaussian noise with known variance, [42] estimate the orthogonal projection map.

Most of these approaches are highly restrictive in terms of the distributions of data over the manifold and/or noise. Our proposed local regression approach motivated by novel theoretical findings represents an innovative general solution to the manifold modeling problem, which can avoid these restrictive assumptions and provide a useful starting point for regression with noisy outcomes on an unknown manifold or manifolds. We summarize our notations in Table 1.

2. MANIFOLD RECONSTRUCTION VIA GAUSSIAN PROCESSES

2.1. Setup of the manifold reconstruction problem. In this section, we propose a method to reconstruct an unknown embedded submanifold of Euclidean space from noisy samples. We first make the following assumption about the samples.

Assumption 2.1. M is a d -dimensional smooth, closed, and connected Riemannian manifold isometrically embedded in \mathbb{R}^D though $\iota : M \rightarrow \mathbb{R}^D$. P is a probability density function on M , which is smooth, bounded from below by $P_m > 0$ and bounded from above by P_M . The observed data follow $y_i = \iota(x_i) + \eta_i$, with $x_i \sim P$ and $\eta_i \sim \mathcal{N}(0, \sigma^2 I_{D \times D})$ independently for $i = 1, \dots, n$.

TABLE 1. Commonly used notations in this paper.

<i>Symbol</i>	<i>Meaning</i>
M	d -dimensional smooth Riemannian manifold
ι	An isometric embedding of M in \mathbb{R}^D
$\{e'_i\}_{i=1}^d, \{e_i\}_{i=1}^D$	The standard orthonormal basis of \mathbb{R}^d and \mathbb{R}^D respectively
P	Probability density function on M
$\{x_i\}_{i=1}^n$	Points sampled based on P from M
$\{\eta_i\}_{i=1}^n$	Noise sampled from a Gaussian distribution in \mathbb{R}^D
$\{y_i\}_{i=1}^n$	Noisy data points around $\iota(M)$
$\{\hat{y}_i\}_{i=1}^n$	Denoisied data points corresponding to $\{y_i\}_{i=1}^n$
ε	The bandwidth of the local covariance matrix
$C_{n,\varepsilon}(y_k)$	The local covariance matrix at y_k with bandwidth ε
J, \bar{J}	The projections from \mathbb{R}^D to the subspaces \mathbb{R}^d and \mathbb{R}^{D-d} respectively
$\mathcal{P}_{y_k}, \mathcal{P}_{y_k}^\perp$	Two major operators in constructing local regression
δ	A scale in \mathbb{R}^D to perform $\mathcal{P}_{y_k}, \mathcal{P}_{y_k}^\perp$ in the algorithm
$G(S_1, S_2)$	The geometric root mean square error between subsets S_1 and S_2 in \mathbb{R}^D

The information of $\iota(M)$ is not accessible and we are only given the Euclidean coordinates of $\{y_i\}_{i=1}^n$. For each y_k , our goals are to (i) estimate a fitted value $\hat{y}_k \in \iota(M)$ while controlling $\frac{1}{n} \sum_{i=1}^n \|\iota(x_i) - \hat{y}_i\|_{\mathbb{R}^D}^2$; (ii) interpolate around \hat{y}_k using a local parameterization of $\iota(M)$.

Under Assumption 2.1, we provide a method to estimate the dimension d in Section I of the Supplementary Material. The assumption that M is connected is made for simplicity in the statements of the main theorems and is not necessary for MrGap to function. When M is the disjoint union of smooth and closed Riemannian manifolds of the same dimension, our algorithm can be applied directly to denoise and interpolate on $\iota(M)$, without the need to test whether M is connected. In contrast, when M is the disjoint union of smooth and closed Riemannian manifolds of different dimensions, we propose a method to reconstruct $\iota(M)$ by applying MrGap to the samples corresponding to each connected component. Refer to Section K.4 of the Supplementary Material for details and numerical simulations. In Section L.2 of the Supplementary Material, we illustrate the performance of MrGap when M is a compact manifold with boundary.

There are two main ingredients in our methodology: the local covariance matrix and Gaussian process regression. We review these briefly in the following two subsections.

2.2. Local covariance matrix. Let $\{e_i\}_{i=1}^D$ be the standard orthonormal basis of \mathbb{R}^D , where $e_i = [0, \dots, 1, \dots, 0]^\top$ with 1 in the i -th entry. Similarly, let $\{e'_i\}_{i=1}^d$ be the standard orthonormal basis of \mathbb{R}^d . Letting $\chi(t) = 1$ for $t \in [0, 1]$ and $\chi(t) = 0$ for $t > 1$ denote a 0–1 kernel, we define a local covariance matrix at y_k ,

$$(1) \quad C_{n,\varepsilon}(y_k) = \frac{1}{n} \sum_{i=1}^n (y_i - y_k)(y_i - y_k)^\top \chi\left(\frac{\|y_i - y_k\|_{\mathbb{R}^D}}{\varepsilon}\right),$$

where $\varepsilon > 0$. Consider the eigen decomposition

$$(2) \quad C_{n,\varepsilon}(y_k) = U_{n,\varepsilon}(y_k) \Lambda_{n,\varepsilon}(y_k) U_{n,\varepsilon}(y_k)^\top,$$

with $U_{n,\varepsilon}(y_k) \in \mathbb{O}(D)$ and $\Lambda_{n,\varepsilon}(y_k) \in \mathbb{R}^{D \times D}$ a diagonal matrix of eigenvalues of $C_{n,\varepsilon}(y_k)$ in decreasing order, $e_1^\top \Lambda_{n,\varepsilon}(y_k) e_1 \geq e_2^\top \Lambda_{n,\varepsilon}(y_k) e_2 \geq \dots \geq e_D^\top \Lambda_{n,\varepsilon}(y_k) e_D$. The column vectors of $U_{n,\varepsilon}(y_k)$ are orthonormal eigenvectors in decreasing order of eigenvalues. The eigenvectors form an orthonormal basis of \mathbb{R}^D . We define two operators in \mathbb{R}^D associated with $U_{n,\varepsilon}(y_k)$ as follows.

Define projection matrices $J \in \mathbb{R}^{D \times d}$ such that $J_{ij} = 1$ when $i = j$ and $J_{ij} = 0$ when $i \neq j$ and $\bar{J} \in \mathbb{R}^{D \times (D-d)}$ such that $\bar{J}_{ij} = 1$ when $i = d + j$ and $\bar{J}_{ij} = 0$ otherwise, so that J and \bar{J} are projections from \mathbb{R}^D to subspaces \mathbb{R}^d and \mathbb{R}^{D-d} respectively. For any $y \in \mathbb{R}^D$, let $\mathcal{P}_{y_k}(y) : \mathbb{R}^D \rightarrow \mathbb{R}^d$ with

$$(3) \quad \mathcal{P}_{y_k}(y) = J^\top U_{n,\varepsilon}(y_k)^\top (y - y_k),$$

and let $\mathcal{P}_{y_k}^\perp(y) : \mathbb{R}^D \rightarrow \mathbb{R}^{D-d}$ with

$$(4) \quad \mathcal{P}_{y_k}^\perp(y) = \bar{J}^\top U_{n,\varepsilon}(y_k)^\top (y - y_k).$$

The operators \mathcal{P}_{y_k} and $\mathcal{P}_{y_k}^\perp$ depending on d are key components in our methodology.

2.3. Gaussian process regression. Suppose $F : \mathbb{R}^d \rightarrow \mathbb{R}^q$ is an unknown regression function with $F = (f_1, \dots, f_q)^\top$. Letting $z_i \in \mathbb{R}^q$ denote the response vector and $u_i \in \mathbb{R}^d$ the predictor vector, for $i = 1, \dots, N$, we have

$$(5) \quad z_i = F(u_i) + \eta_i, \quad \eta_i \sim \mathcal{N}(0, \sigma^2 I_{q \times q}).$$

We assign independent Gaussian process priors to each f_j with mean 0 and covariance function

$$(6) \quad C(u, u') = A \exp\left(-\frac{\|u - u'\|_{\mathbb{R}^d}^2}{\rho}\right),$$

implying $\tilde{z}_j^\top = \{f_j(u_1), \dots, f_j(u_N)\}^\top \sim \mathcal{N}(0, \Sigma_1)$, for $j = 1, \dots, q$, where $\Sigma_1 \in \mathbb{R}^{N \times N}$ has (j, k) element $C(u_j, u_k)$, for $1 \leq j, k \leq N$. Let $Z \in \mathbb{R}^{N \times q}$ with i th row z_i^\top for $i = 1, \dots, N$ and j th column \tilde{z}_j for $j = 1, \dots, q$. Marginalizing over the Gaussian process priors, we obtain the log-likelihood

$$(7) \quad \log p(Z|A, \rho, \sigma) = -\text{tr}\{z^\top (\Sigma_1 + \sigma^2 I_{N \times N})^{-1} z\} - q \log\{\det(\Sigma_1 + \sigma^2 I_{N \times N})\} - \frac{qN}{2} \log(2\pi).$$

To estimate the covariance parameters A, ρ, σ via an empirical Bayes approach that protects against overfitting, we maximize this marginal likelihood. Refer to Section A of the Supplementary Material for a detailed discussion and the derivation of (7).

2.4. Main challenges and motivation. Suppose y is a point on the embedded manifold $\iota(M)$. The tangent space of $\iota(M)$ at y , $T_y \iota(M)$, is a subspace of \mathbb{R}^D . $y + T_y \iota(M)$ is the affine subspace tangent to $\iota(M)$ at y . It is well known that $\iota(M)$ can be locally parametrized as a graph of a function over $y + T_y \iota(M)$. Consider neighborhood $B_{\delta}^{\mathbb{R}^D}(y) \cap \iota(M)$ for some $\delta > 0$. Then, there is a function $F(u) : O \subset \mathbb{R}^d \rightarrow \mathbb{R}^{D-d}$ with $F(0) = 0$ and $\nabla F(0) = 0$ such that the graph of F over O , after a rotation and a translation in \mathbb{R}^D , is a parametrization of $B_{\delta}^{\mathbb{R}^D}(y_k) \cap \iota(M)$. The parametrization can be expressed as $\Phi(u) = y + U \begin{bmatrix} u \\ F(u) \end{bmatrix} : O \rightarrow \mathbb{R}^D$, with $U \in \mathbb{O}(D)$ an orthogonal matrix mapping from the subspace generated by e_1, \dots, e_d to $T_y \iota(M)$. Refer to Figure 2 and the technical description in Proposition B.2 in the Supplementary Material. Since $\iota(M)$ is unknown, we cannot recover the tangent spaces of $\iota(M)$ from noisy data. Thus, we do not know the matrix U or the function F . The key idea of the paper is to take advantage of the properties of local covariance to construct alternative affine subspaces where $\iota(M)$ can be parametrized locally by the graph of a function. This allows us to conduct manifold denoising and interpolation by locally applying nonparametric regression.

2.5. Denoising phase of MrGap. Let $\mathcal{H}_k = y_k + \mathcal{T}_k$ be an affine subspace through y_k , with \mathcal{T}_k the subspace generated by the first d eigenvectors of $C_{n,\varepsilon}(y_k)$ in (1). In Section 3, we show that under certain relations between bandwidth ε , noise variance σ^2 , and sample size n , with high probability, the neighborhood $B_{3\delta}^{\mathbb{R}^D}(y_k) \cap \iota(M)$ can be parametrized as the graph of a function over \mathcal{H}_k for $\delta > \varepsilon$. Refer to Section K.1 in the Supplementary Material for an illustration of \mathcal{H}_k and more discussions. Importantly, the affine subspace \mathcal{H}_k is not required to accurately approximate the affine subspace tangent to $\iota(M)$ at

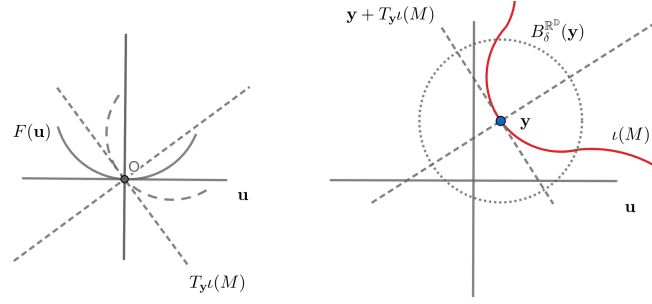


FIGURE 2. Left Panel: The solid lines are the standard coordinates of \mathbb{R}^D . The solid curve is the plot of $[u, F(u)]^\top$. The dashed lines show the rotation of the coordinates under U and the plot of $U[u, F(u)]^\top$. Right Panel: The solid curve is $\iota(M)$. After a translation by y , the graph of $y + U[u, F(u)]^\top$ gives a parametrization of $B_\delta^{\mathbb{R}^D}(y) \cap \iota(M)$.

$\iota(x_k)$. However, the parameterization can be expressed similarly as when the affine subspace is tangent to the manifold:

$$(8) \quad \Phi_k(u) = y_k + U_{n,\varepsilon}(y_k) \begin{bmatrix} u \\ F_k(u) \end{bmatrix}$$

where $F_k(u) : O_k \rightarrow \mathbb{R}^{D-d}$ for a connected open set O_k containing 0 in \mathbb{R}^d and $U_{n,\varepsilon}(y_k)$ is the orthogonal matrix that maps the subspace generated by e_1, \dots, e_d to \mathcal{T}_k as defined in (2). The parameterization $\Phi_k(u)$ is constructed from a rotation under $U_{n,\varepsilon}(y_k)$ and a translation under y_k of the graph of $F_k(u)$, and we have

$$(9) \quad \hat{y}_k = y_k + U_{n,\varepsilon}(y_k) \begin{bmatrix} 0 \\ F_k(0) \end{bmatrix}$$

is a point on $\iota(M)$. Hence, if we can estimate $F_k(0)$, then (9) provides a fitted value for y_k .

We rely on Gaussian process regression to infer F_k and hence $F_k(0)$. The operations \mathcal{P}_{y_k} and $\mathcal{P}_{y_k}^\perp$ in (3) and (4) are compositions of (a) a translation under $-y_k$, (b) a rotation under $U_{n,\varepsilon}(y_k)^\top$, and (c) projections onto \mathbb{R}^d and \mathbb{R}^{D-d} , respectively. Since $\Phi_k(u)$ is a parametrization of $B_{3\delta}^{\mathbb{R}^D}(y_k) \cap \iota(M)$ and there is noise in the data, we use points in a smaller neighborhood of y_k to estimate $F_k(0)$: $B_\delta^{\mathbb{R}^D}(y_k) \setminus y_k \cap \{y_1, \dots, y_n\} = \{y_{k,1}, \dots, y_{k,N_k}\}$. Refer to Section 3 for details. Then, $w_{k,j} = \mathcal{P}_{y_k}(y_{k,j})$ are the inputs for F_k and $z_{k,j} = \mathcal{P}_{y_k}^\perp(y_{k,j})$ are the response variables for $j = 1, \dots, N_k$. Refer to Figure 3.

Hence, the denoising phase of MrGap consists of the following steps. Inputs include data $\{y_i\}_{i=1}^n$, a bandwidth ε of the local covariance matrix $C_{n,\varepsilon}(y_k)$, and a scale δ of the maps \mathcal{P}_{y_k} and $\mathcal{P}_{y_k}^\perp$. The output is the denoised data $\{\hat{y}_1, \dots, \hat{y}_n\}$. In Step 1, for each data point y_k , we flag nearby points $\{y_{k,1}, \dots, y_{k,N_k}\}$ in $B_\delta^{\mathbb{R}^D}(y_k) \setminus y_k$. We construct the predictors and responses for a regression function F_k as described above. In Step 2, we calculate the covariance matrix between 0 and $\{w_{k,j}\}_{j=1}^{N_k}$. In Step 3, we apply Gaussian process regression to estimate $F_k(0)$ and denoise the data, using the covariance matrix in Step 2, while estimating the tuning parameters. Let \mathcal{A}_k be an affine subspace defined as

$$(10) \quad \mathcal{A}_k = y_k + V_k,$$

where V_k is the $D-d$ dimensional subspace generated by the last $D-d$ column vectors of $U_{n,\varepsilon}(y_k)$. The predictive distribution of the denoised y_k is Gaussian in \mathcal{A}_k centered at \hat{y}_k . We iteratively apply steps 1 to 3 to refine the results. Figure 3 illustrates the first 3 steps, and Step 4 is discussed in more detail in Section 3. Detailed steps are summarized in Algorithm 1.

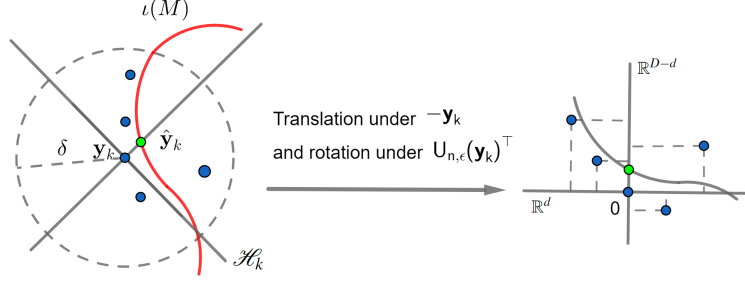


FIGURE 3. Left Panel: The solid curve is $\iota(M)$. The solid lines are affine subspace \mathcal{H}_k and affine normal subspace of \mathcal{H}_k . The blue points are noisy data points in the δ neighborhood of y_k . Right Panel: The solid lines are coordinates in \mathbb{R}^D and the graph of function F_k . After (a) a translation under $-y_k$ and (b) a rotation under $U_{n,\varepsilon}(y_k)^\top$, blue points in the left panel (the noisy data points) are mapped to blue points in the right panel. In particular, y_k is mapped to the origin. If we project the blue points except $0 \in \mathbb{R}^D$ in the right panel onto \mathbb{R}^d and \mathbb{R}^{D-d} which are the last operations (c) in \mathcal{P}_{y_k} and $\mathcal{P}_{y_k}^\perp$, then we have inputs $w_{k,j}$ and response variables $z_{k,j}$ for F_k respectively. The green point in the right panel is $[0, F_k(0)]^\top$. We apply (9) to get the denoised output \hat{y}_k indicated by the green point in the left panel.

Algorithm 1: MrGap denoising steps to produce estimates of $\hat{y}_1, \dots, \hat{y}_n$ from y_1, \dots, y_n .

- 1 For each y_k , construct $C_{n,\varepsilon}(y_k)$ as in (1). Let $\{y_{k,1}, \dots, y_{k,N_k}\}$ denote samples in $B_\delta^{\mathbb{R}^D}(y_k) \setminus y_k$, $w_{k,j} = \mathcal{P}_{y_k}(y_{k,j})$ and $z_{k,j} = \mathcal{P}_{y_k}^\perp(y_{k,j})$ for $j = 1, \dots, N_k$, with $\mathcal{P}_{y_k}(y)$ and $\mathcal{P}_{y_k}^\perp(y)$ defined in (3) and (4). The k th regression has responses $z_{k,j}$ and predictors $w_{k,j}$.
- 2 For each y_k , construct covariance $\Sigma_k = \begin{bmatrix} \Sigma_{k,1} & \Sigma_{k,2} \\ \Sigma_{k,3} & \Sigma_{k,4} \end{bmatrix} \in \mathbb{R}^{(N_k+1) \times (N_k+1)}$ over $\{w_{k,1}, \dots, w_{k,N_k}, 0\}$ induced by C in (6), with $\Sigma_{k,1} \in \mathbb{R}^{N_k \times N_k}$. Denote $Z_k \in \mathbb{R}^{N_k \times (D-d)}$ with i th row $z_{k,i}^\top$.
- 3 For the k th local regression, calculate the log marginal likelihood $\log p_k(Z_k|A, \rho, \sigma)$ using (7) with $Z = Z_k$, $\Sigma_1 = \Sigma_{k,1}$ and $N = N_k$. Estimate A, ρ, σ by maximizing the sum of log marginal likelihoods $L = \sum_{k=1}^n \log p_k(Z_k|A, \rho, \sigma)$. The predictive distribution of the denoised output of y_k is Gaussian in \mathcal{A}_k with mean

$$(11) \quad \hat{y}_k = y_k + U_{n,\varepsilon}(y_k) \left[\begin{array}{c} 0 \\ \{\Sigma_{k,3}(\Sigma_{k,1} + \sigma^2 I_{N_k \times N_k})^{-1} Z_k\}^\top \end{array} \right],$$

and covariance $\{\Sigma_{k,4} - \Sigma_{k,3}(\Sigma_{k,1} + \sigma^2 I_{N_k \times N_k})^{-1} \Sigma_{k,2}\} I_{(D-d) \times (D-d)}$, where $U_{n,\varepsilon}(y_k)$ and \mathcal{A}_k are defined in (2) and (10), respectively.

- 4 Repeat Steps 1-3 using the denoised data in Step 3 as the input in Step 1. Stop iterating when the change in σ is below a small tolerance and output the final denoised data.
-

2.6. Interpolation phase of the MrGap algorithm. Interpolation produces additional points on $\iota(M)$. In the presence of non-negligible noise, Algorithm 1 needs to be iterated until convergence; refer to Section 3.5. For illustration purposes, here we assume that the noise is small. Consequently, we are allowed to use the noisy data $\{y_i\}_{i=1}^n$ directly as inputs in the interpolation phase and adopt the same notation as in the previous section for clarity. Recall that (8) is a local parametrization of $\iota(M)$. A straightforward approach to interpolation is to generate new inputs $\{\tilde{u}_{k,1}, \dots, \tilde{u}_{k,K}\}$ randomly within

domain O_k and then apply

$$(12) \quad y_k + U_{n,\varepsilon}(y_k) \left[\frac{\tilde{\mathbf{u}}_{k,j}}{F_k(\tilde{\mathbf{u}}_{k,j})} \right]$$

to produce the j th point on $\iota(M)$ around the denoised point \hat{y}_k , for $j = 1, \dots, K$.

There are two issues involved. First, we need to ensure that the inputs $\{\tilde{\mathbf{u}}_{k,i}\}_{i=1}^K$ are distributed within the domain O_k . To achieve this, we use the predictors $\{w_{k,j}\}_{j=1}^{N_k}$ to estimate a ball in O_k and then generate $\{\tilde{\mathbf{u}}_{k,i}\}_{i=1}^K$ uniformly in that ball. The second issue is that the interpolated points around \hat{y}_k and around $\hat{y}_{k'}$ may have noticeable gaps in the intersection region of their local neighborhoods due to statistical errors in the estimation of F_k and $F_{k'}$. To address this issue, we perform iterative interpolation around each \hat{y}_k for k from 1 to n . Specifically, we identify all interpolated points around every $\hat{y}_{k'}$ with $k' < k$, falling within $B_\delta^{\mathbb{R}^D}(y_k)$, denoted as $\tilde{M}_{k-1} = \{\tilde{y}_{k,j}\}_{j=1}^{L_{k-1}}$. In fitting the regression for F_k , we augment the predictors $\{w_{k,j}\}_{j=1}^{N_k}$ with $\tilde{w}_{k,j} = \mathcal{P}_{y_k}(\tilde{y}_{k,j})$ for $j = 1, \dots, L_{k-1}$ and the responses $\{z_{k,j}\}_{j=1}^{N_k}$ with $\tilde{z}_{k,j} = \mathcal{P}_{y_k}^\perp(\tilde{y}_{k,j})$ for $j = 1, \dots, L_{k-1}$. Then, by applying (12) we produce smoother interpolations in the intersection regions. Refer to Figure 4 for an illustration. The interpolation steps are summarized in Algorithm 2 in Section C of the Supplementary Material. In Section K of the Supplementary Material, we demonstrate that results of interpolation are robust to permutations of the order of $\{\hat{y}_i\}_{i=1}^n$.

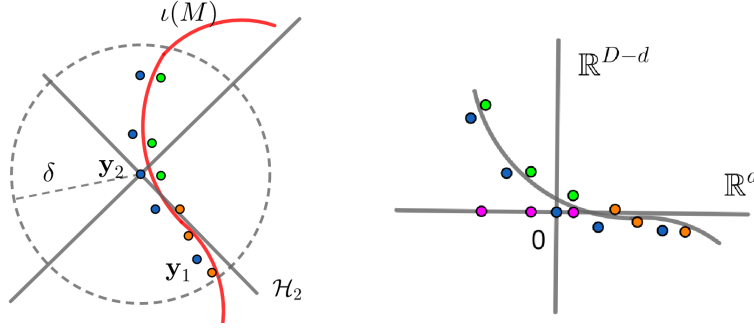


FIGURE 4. We focus our discussion on the point \mathbf{y}_2 . Left Panel: The blue points are $B_\delta^{\mathbb{R}^D}(\mathbf{y}_2) \cap \{y_i\}_{i=1}^n$. Suppose we interpolated K points around \mathbf{y}_1 on $\iota(M)$ whose union is \tilde{M}_1 . We find $\tilde{M}_1 \cap B_\delta^{\mathbb{R}^D}(\mathbf{y}_2)$ (orange points). Right Panel: The solid curve is the graph of the function F_2 . After a translation under $-\mathbf{y}_2$ and a rotation under $U_{n,\varepsilon}(\mathbf{y}_2)^\top$, the blue points and the orange points in the left panel are mapped to the blue points and orange points in the right panel. The purple points $\{\tilde{\mathbf{u}}_{2,j}\}_{j=1}^K$ are generated in the domain O_2 of F_2 in \mathbb{R}^d for the prediction. The blue points except 0 and the orange points are projected onto \mathbb{R}^d and \mathbb{R}^{D-d} to be the predictors and the response variables for the predictions whose coordinates are $\{[\tilde{\mathbf{u}}_{2,j}, F_2(\tilde{\mathbf{u}}_{2,j})]^\top\}_{j=1}^K$ (green points in the right panel). The green points in the right panel are mapped back to green points in the left panel through (12) which are the interpolations around \mathbf{y}_2 .

2.7. Selection of parameters ε and δ . Let L denote the sum of log marginal likelihood in Step 3 of Algorithm 1. We propose estimating ε and δ by maximizing L over all $\varepsilon \leq \delta$ in the first round of Algorithm. L has an analytic expression in terms of the covariance parameters A, ρ , and σ for a fixed pair (ε, δ) , which allows us to apply gradient descent to the covariance parameters along with a grid search on (ε, δ) to maximize L . To improve efficiency, a lower bound b on ε is imposed such that each $C_{n,b}(y_k)$ has at least d positive eigenvalues for all k . Refer to Section J of the Supplementary Material for an example.

3. THEORETICAL ANALYSIS

3.1. Geometric preliminaries. Suppose $x \in M$. Let $T_x M$ be the tangent space of M at x . Let $T_{\iota(x)} \iota(M)$ be the tangent space of $\iota(M)$ at $\iota(x)$ which is a subspace of \mathbb{R}^D . Let $T_{\iota(x)} \iota(M)^\perp$ be the normal subspace of $T_{\iota(x)} \iota(M)$ in \mathbb{R}^D . Recall the definition of a chart for $\iota(M)$. For any $x \in M$, we can find an open set $U_x \subset \mathbb{R}^D$ with $\iota(x) \in U_x$. V_x is an open topological ball in \mathbb{R}^d . A chart of $\iota(M)$ over $U_x \cap \iota(M)$ is a map $\Phi_x : V_x \rightarrow U_x \cap \iota(M)$ such that Φ_x is a diffeomorphism, a smooth bijective map with a smooth inverse. The reach $\tau_{\iota(M)}$ of $\iota(M)$ is the largest number such that any point in \mathbb{R}^D at distance less than the reach from $\iota(M)$ has a unique nearest point on $\iota(M)$ [15]. Refer to Section B of the Supplementary Material for detailed definitions.

3.2. Local covariance matrix on manifold with noise. $C_{n,\varepsilon}(y_k)$ from (2) is invariant under the translation of $\iota(M)$ in \mathbb{R}^D . Hence, to simplify the notation, we make the following assumption for the results in this subsection.

Assumption 3.1. For any fixed $x_k \in M$, we first translate $\iota(M)$ so that $\iota(x_k) = 0 \in \mathbb{R}^D$. Then, we apply an orthogonal transformation in \mathbb{R}^D so that $\{e_i\}_{i=1}^d$ form a basis of $T_{\iota(x_k)} \iota(M)$.

In the following theorem, we provide bias and variance analyses of $C_{n,\varepsilon}(y_k)$. The proofs are in Sections D and E of the Supplementary Material.

Theorem 3.1. Under Assumptions 2.1-3.1, suppose ε is small enough depending on d, D , scalar curvature of M and second fundamental form of $\iota(M)$. For $\beta > 1$, if $\sigma \leq \min \left\{ \frac{1}{\sqrt{-4(d+5)\log \varepsilon}}, \frac{1}{\sqrt{12\log(2n)}} \right\} \varepsilon^\beta$, then for all x_k , with probability greater than $1 - \frac{1}{n^2}$, we have $\|\eta_k\|_{\mathbb{R}^D} \leq \varepsilon^\beta$ and

$$C_{n,\varepsilon}(y_k) = \varepsilon^{d+2} \left\{ \frac{|S^{d-1}|P(x_k)}{d(d+2)} \begin{bmatrix} I_{d \times d} & 0 \\ 0 & 0 \end{bmatrix} + \mathcal{E} \right\},$$

where

$$\mathcal{E} = \begin{bmatrix} O\{\varepsilon^{\min(\beta-1,2)} + \sqrt{\frac{\log n}{ne^d}}\} & O\{\varepsilon^{2\min(\beta-1,1)} + \sqrt{\frac{\log n}{ne^{d-2\min(\beta-1,1)}}}\} \\ O\{\varepsilon^{2\min(\beta-1,1)} + \sqrt{\frac{\log n}{ne^{d-2\min(\beta-1,1)}}}\} & O\{\varepsilon^{2\min(\beta-1,1)} + \sqrt{\frac{\log n}{ne^{d-2\min(\beta-1,1)}}}\} \end{bmatrix}.$$

The top left block of \mathcal{E} is a d by d matrix. The constant factors in \mathcal{E} depend on d , the C^2 norm of P , the second fundamental form of $\iota(M)$ and its derivative, and the Ricci curvature of M .

The following theorem characterizes the orthonormal eigenvector matrix of $C_{n,\varepsilon}(y_k)$. The proof relies on applying the Davis-Kahan theorem [8, 43] to Theorem 3.1. The proof of the theorem is given in Section E of the Supplementary Material.

Theorem 3.2. Under Assumptions 2.1-3.1, for $\beta > 1$, suppose ε is small enough depending on β, d, D, P_m, C^2 norm of P , the second fundamental form of $\iota(M)$ and its derivative and the Ricci curvature of M . Suppose n is large enough so $\varepsilon^{-d-2\min(\beta-1,1)} \leq \frac{n}{\log n}$. If $\sigma \leq \min \left\{ \frac{1}{\sqrt{-4(d+5)\log \varepsilon}}, \frac{1}{\sqrt{12\log(2n)}} \right\} \varepsilon^\beta$, then for all x_k , with probability greater than $1 - \frac{1}{n^2}$, we have $\|\eta_k\|_{\mathbb{R}^D} \leq \varepsilon^\beta$, and $U_{n,\varepsilon}(y_k) = \begin{bmatrix} X_1 & 0 \\ 0 & X_2 \end{bmatrix} + O\{\varepsilon^{2\min(\beta-1,1)}\}$, where $X_1 \in \mathbb{O}(d)$, $X_2 \in \mathbb{O}(D-d)$. $O\{\varepsilon^{2\min(\beta-1,1)}\}$ is a D by D matrix whose entries are of order $O\{\varepsilon^{2\min(\beta-1,1)}\}$, where constant factors depend on d, D, P_m, C^2 norm of P , the second fundamental form of $\iota(M)$ and its derivative and the Ricci curvature of M .

We discuss Theorem 3.2 from the following two aspects.

Interpretation of the conclusion. We explain the dominating and error terms in the expansion of $U_{n,\varepsilon}(y_k)$. By Assumption 3.1, $\begin{bmatrix} X_1 \\ 0 \end{bmatrix}$ forms an orthonormal basis of $T_{\iota(x_k)} \iota(M)$ and $\begin{bmatrix} 0 \\ X_2 \end{bmatrix}$ forms an orthonormal basis of $T_{\iota(x)} \iota(M)^\perp$. We use the first d column vectors of $U_{n,\varepsilon}(y_k)$ to construct a map $\mathcal{P}_{y_k}(y)$ from \mathbb{R}^D to \mathbb{R}^d defined in (3). In the proof of Theorem 3.3, we allow the first d column vectors of $U_{n,\varepsilon}(y_k)$

to deviate from $\begin{bmatrix} x_1 \\ 0 \end{bmatrix}$ by an order 1 term, while $\mathcal{P}_{y_k}(y)$ on $\iota(M)$ still remains a local diffeomorphism. Therefore, it suffices that $U_{n,\varepsilon}(y_k) - \begin{bmatrix} x_1 & 0 \\ 0 & x_2 \end{bmatrix}$ is of order $O\{\varepsilon^{2\min(\beta-1,1)}\}$.

Conditions on n , ε and σ . For any $\beta > 1$, if we expect error between $U_{n,\varepsilon}(y_k)$ and $\begin{bmatrix} x_1 & 0 \\ 0 & x_2 \end{bmatrix}$ to be $O\{\varepsilon^{2\min(\beta-1,1)}\}$, we require ε to be smaller than a constant that depends on the factors in the theorem. Dependence of ε on β can be expressed as $\varepsilon \leq C^{\frac{1}{\min(\beta-1,1)}}$ based on the proof of Theorem 3.2, where C is a constant. Therefore, ε is independent of β if $\beta \geq 2$. Since Theorem 3.2 depends on Theorem 3.1, a lower bound on n depending on ε is needed. We impose $\varepsilon^{-d-2\min(\beta-1,1)} \leq \frac{n}{\log n}$ to balance bias and variance errors in Theorem 3.1. Finally, we can achieve the desired error bound of $O\{\varepsilon^{2\min(\beta-1,1)}\}$ whenever the standard deviation of the noise σ is of order $O(\varepsilon^\beta)$, up to a square root logarithmic factor.

3.3. Construction of a chart from noisy samples. In the following theorem, we show that, with high probability, the map $\mathcal{P}_{y_k}(y)$ in (3) is a diffeomorphism from $B_{3\delta}^{\mathbb{R}^D}(y_k) \cap \iota(M)$ onto its image for some $\delta > 0$. Consequently, its inverse defines a chart of $\iota(M)$. The proof of the theorem, in Section F of the Supplementary Material, relies on Theorem 3.2 and an analysis of perturbations of tangent spaces of $\iota(M)$ near y_k .

Theorem 3.3. *Under Assumption 2.1, for $\beta > 1$, suppose ε is small enough depending on β , d , D , P_m , C^2 norm of P , the second fundamental form of $\iota(M)$ and its derivative and the Ricci curvature of M . Suppose n is large enough such that $\varepsilon^{-d-2\min(\beta-1,1)} \leq \frac{n}{\log n}$. If $\sigma \leq \min\left\{\frac{1}{\sqrt{-4(d+5)\log\varepsilon}}, \frac{1}{\sqrt{12\log(2n)}}\right\}\varepsilon^\beta$, then for all x_k and any δ such that $\varepsilon^\beta < \delta < \frac{\tau_{\iota(M)}}{16}$, with probability greater than $1 - \frac{1}{n^2}$, we have the following facts:*

- (1) If $y_i \in B_{3\delta}^{\mathbb{R}^D}(y_k)$, then $\iota(x_i) \in B_{3\delta}^{\mathbb{R}^D}(y_k)$.
- (2) The map $\mathcal{P}_{y_k}(y)$ defined in (3) is a diffeomorphism from $B_{3\delta}^{\mathbb{R}^D}(y_k) \cap \iota(M)$ onto its image $O_k \subset \mathbb{R}^d$. O_k is homeomorphic to $B_1^{\mathbb{R}^d}(0)$.
- (3) There is a point $u_{k,0}$ in O_k such that $0 \in B_{R_k}^{\mathbb{R}^d}(u_{k,0}) \subset O_k \subset B_{3\delta}^{\mathbb{R}^d}(0)$. Let $A = 1 - \Omega\varepsilon^{2\min(\beta-1,1)}$ and $B = \frac{8\delta+2\varepsilon^\beta}{\tau_{\iota(M)}}$, where Ω is a constant depending on d , D , P_m , C^2 norm of P , the second fundamental form of $\iota(M)$ and its derivative and the Ricci curvature of M . Then

$$R_k \geq (\sqrt{A^2 - A^2B} - \sqrt{B - A^2B})(3\delta - \varepsilon^\beta).$$

We discuss some of the conditions in the above theorem.

Discussion of the magnitude of σ . In the above theorem, we require the condition

$$\sigma \leq \min\left\{\frac{1}{\sqrt{-4(d+5)\log\varepsilon}}, \frac{1}{\sqrt{12\log(2n)}}\right\}\varepsilon^\beta,$$

which allows for any $\beta > 1$. This relation implies that σ is not small; in fact, it can be close to the order ε up to a square root logarithmic factor. The reason why σ is not allowed to be too large compared to ε is due to the use of the $0-1$ kernel in the construction of the local covariance matrix. A large σ can result in too few points within the ε neighborhood of y_k , causing the local covariance matrix at y_k to have a rank less than d . In such a case, the map $\mathcal{P}_{y_k}(y)$ cannot be constructed. One possible improvement to the condition on σ would be to apply a different kernel, such as a squared exponential kernel. This would require analyzing the spectral behavior of the local covariance matrix with a more general kernel, constructed from noisy samples around a manifold, analogous to the result in Theorem 3.1. Moreover, the relationship between σ and ε , along with condition $\varepsilon^\beta < \frac{\tau_{\iota(M)}}{16}$, ensures that y_k is close to $\iota(x_k)$ relative to the reach, with high probability. We illustrate in Section K of the Supplementary Material that we may not reconstruct $\iota(M)$ accurately if y_k is too far from $\iota(x_k)$ compared to the reach.

The relation between σ and the shape of the set O_k . Depending on σ , the last part of the theorem describes how close to round O_k is. Consider the case of no noise. Equivalently, we can take $\beta \rightarrow \infty$. By the discussion after Theorem 3.2, ε is independent of β if $\beta \geq 2$. By applying an approximation for small ε and δ , $R_k \geq 3(1 - \frac{4\delta}{\tau_{\iota(M)}} - \Omega'\varepsilon)\delta$ for some constant Ω' depending on $\tau_{\iota(M)}$ and Ω . Hence, O_k is close to round in the sense that O_k is contained in the round ball of radius 3δ and contains a round ball of radius close to 3δ . In general, when σ is small, we can choose β to be large so that R_k is closer to 3δ .

The implications of Theorem 3.3 are explored in the following two subsections. In Section 3.4, under the proposed relations between ε , δ , σ , and n in the theorem, we connect the manifold reconstruction problem to a series of local regressions. Section 3.5 addresses the impact of Theorem 3.3 on the evolution of the geometry of O_k throughout the iterations of Algorithm 1. We demonstrate that as the domain becomes more regular through iterations, interpolation improves.

3.4. Setup of the regression functions. Suppose ε , δ , σ and n satisfy the conditions in Theorem 3.3. Then, all the following statements hold with probability greater than $1 - \frac{1}{n^2}$.

Statement (2) of Theorem 3.3 shows that for any y_k , $\mathcal{P}_{y_k}(y)$ is a diffeomorphism on $B_{3\delta}^{\mathbb{R}^D}(y_k) \cap \iota(M)$. Then, the inverse of $\mathcal{P}_{y_k}(y)$ denoted as $\Phi_k : O_k \rightarrow \mathbb{R}^D$ with $O_k \subset \mathbb{R}^d$ is a chart of $\iota(M)$. As illustrated in Figure 3, since $\mathcal{P}_{y_k}(y)$ is constructed from a projection and is a diffeomorphism,

$$(13) \quad \Phi_k(u) = y_k + U_{n,\varepsilon}(y_k) \begin{bmatrix} u \\ F_k(u) \end{bmatrix},$$

where $F_k(u) : O_k \rightarrow \mathbb{R}^{D-d}$ is a smooth function. Since $\iota(M)$ is unknown, F_k and the domain O_k are unknown. Moreover, statement (3) in Theorem 3.3 confirms $0 \in O_k$ which is not straightforward as y_k is not necessarily on $\iota(M)$. Thus, (3) implies that $\mathcal{P}_{y_k}(y_k) = 0$, suggesting that $\Phi_k(0)$ serves as a denoised output for y_k .

The reconstruction of $B_{3\delta}^{\mathbb{R}^D}(y_k) \cap \iota(M)$ is based on the prediction of $F_k(u)$ for $u \in O_k$. We find $B_{3\delta}^{\mathbb{R}^D}(y_k) \cap \{y_1, \dots, y_n\} = \{y_{k,1}, \dots, y_{k,N_k}\}$ with $y_{k,i} = \iota(x_{k,i}) + \eta_{k,i}$. Statement (1) in Theorem 3.3 justifies that the clean data $\{\iota(x_{k,i})\}_{i=1}^{N_k}$ are in the domain $B_{3\delta}^{\mathbb{R}^D}(y_k) \cap \iota(M)$ on which \mathcal{P}_{y_k} is a diffeomorphism. By (3), (4) and (13), the following equations hold:

$$\begin{aligned} \mathcal{P}_{y_k}\{\iota(x_{k,i})\} &= \mathcal{P}_{y_k}\{\Phi_k(u_{k,i})\} = u_{k,i} \in O_k, \\ \mathcal{P}_{y_k}^\perp\{\iota(x_{k,i})\} &= \mathcal{P}_{y_k}^\perp\{\Phi_k(u_{k,i})\} = F_k(u_{k,i}). \end{aligned}$$

Therefore, we apply $\{y_{k,1}, \dots, y_{k,N_k}\}$ to construct the predictors and responses for F_k . Specifically, let $\eta_{k,i,1} = J^\top U_{n,\varepsilon}(y_k)^\top \eta_{k,i} \in \mathbb{R}^d$ and $\eta_{k,i,2} = \bar{J}^\top U_{n,\varepsilon}(y_k)^\top \eta_{k,i} \in \mathbb{R}^{D-d}$. By (3) and (4)

$$(14) \quad \mathcal{P}_{y_k}(y_{k,i}) = \mathcal{P}_{y_k}\{\iota(x_{k,i}) + \eta_{k,i}\} = \mathcal{P}_{y_k}\{\iota(x_{k,i})\} + J^\top U_{n,\varepsilon}(y_k)^\top \eta_{k,i} = u_{k,i} + \eta_{k,i,1},$$

$$(15) \quad \mathcal{P}_{y_k}^\perp(y_{k,i}) = \mathcal{P}_{y_k}^\perp\{\iota(x_{k,i}) + \eta_{k,i}\} = \mathcal{P}_{y_k}^\perp\{\iota(x_{k,i})\} + \bar{J}^\top U_{n,\varepsilon}(y_k)^\top \eta_{k,i} = F_k(u_{k,i}) + \eta_{k,i,2}.$$

Since $U_{n,\varepsilon}(y_k)^\top \eta_{k,i} \sim \mathcal{N}(0, \sigma^2 I_{D \times D})$, from properties of the normal distribution, $\eta_{k,i,1} \sim \mathcal{N}(0, \sigma^2 I_{d \times d})$ and $\eta_{k,i,2} \sim \mathcal{N}(0, \sigma^2 I_{(D-d) \times (D-d)})$.

We summarize the above observations through the errors-in-variables regression model. Suppose $F = (f_1, \dots, f_q) : O \subset \mathbb{R}^d \rightarrow \mathbb{R}^q$, with $q = D - d$, is an unknown regression function, where O is an unknown open subset in \mathbb{R}^d . We observe the labeled training data $(w_i, z_i)_{i=1}^N$, where

$$(16) \quad w_i = u_i + \eta_{i,1}, \quad z_i = F(u_i) + \eta_{i,2}, \quad \eta_{i,1} \sim \mathcal{N}(0, \sigma^2 I_{d \times d}), \quad \eta_{i,2} \sim \mathcal{N}(0, \sigma^2 I_{q \times q}),$$

and $\{u_i\}_{i=1}^N \subset O$. We apply Gaussian process regression to predict $F(u)$ for $u \in O$.

3.5. Discussion of interpolation. For any $i > 1$, denote the denoised outputs of the $(i-1)$ th iteration of Steps 1-3 of Algorithm 1 as $\{y_1^{(i-1)}, \dots, y_n^{(i-1)}\}$. We assume

$$(17) \quad y_k^{(i-1)} = \iota(x_k^{(i-1)}) + \eta_k^{(i-1)} \text{ for } x_k^{(i-1)} \in M \text{ and } \eta_k^{(i-1)} \sim \mathcal{N}(0, \sigma^{(i-1)2} I_{D \times D}),$$

where $\sigma^{(i-1)}$ decreases as i increases. In the i th iteration, for each $y_k^{(i-1)}$, there is a chart $\Phi_k^{(i-1)}$ and regression function $F_k^{(i-1)}$ associated with unknown domain $O_k^{(i-1)}$. Suppose Algorithm 1 stops at the I th round. We use the outputs $\{y_1^{(I-1)}, \dots, y_n^{(I-1)}\}$ as inputs to interpolate the points on $\iota(M)$. In the I th iteration, if we generate K points in each domain $O_k^{(I-1)}$, then we can interpolate K points on $\iota(M)$ through reconstruction of $F_k^{(I-1)}$. Since $O_k^{(I-1)}$ is unknown, we outline a method to generate samples in $O_k^{(I-1)}$ with an explanation by the results in Theorem 3.3.

For each $y_k^{(I-1)}$, we construct $C_{n,\varepsilon}^{(I-1)}(y_k^{(I-1)})$ through $\{y_1^{(I-1)}, \dots, y_n^{(I-1)}\}$ as in (1). We find an orthonormal eigenvector matrix $U_{n,\varepsilon}^{(I-1)}(y_k^{(I-1)})$ of $C_{n,\varepsilon}^{(I-1)}(y_k^{(I-1)})$ to construct $\mathcal{P}_{y_k^{(I-1)}}(y)$ and $\mathcal{P}_{y_k^{(I-1)}}^\perp(y)$. Suppose $\{y_j^{(I-1)}\}_{j=1}^n \cap B_{\delta}^{\mathbb{R}^D}(y_k^{(I-1)}) = \{y_{k,1}^{(I-1)}, \dots, y_{k,N_k^{(I-1)}}^{(I-1)}\}$. Let $w_{k,j}^{(I-1)} = \mathcal{P}_{y_k^{(I-1)}}(y_{k,j}^{(I-1)})$ and $z_{k,j}^{(I-1)} = \mathcal{P}_{y_k^{(I-1)}}^\perp(y_{k,j}^{(I-1)})$. We estimate a small round ball contained in $O_k^{(I-1)}$ using $\{w_{k,1}^{(I-1)}, \dots, w_{k,N_k^{(I-1)}}^{(I-1)}\}$ and sample K points, $\{\tilde{u}_{k,1}, \dots, \tilde{u}_{k,K}\}$, uniformly at random from the ball. The center of the ball is

$$\mathcal{U}_k = \frac{1}{N_k^{(I-1)}} \sum_{j=1}^{N_k^{(I-1)}} w_{k,j}^{(I-1)} = \frac{1}{N_k^{(I-1)}} \sum_{j=1}^{N_k^{(I-1)}} u_{k,j}^{(I-1)} + \frac{1}{N_k^{(I-1)}} \sum_{j=1}^{N_k^{(I-1)}} \eta_{k,j,1}^{(I-1)} \in \mathbb{R}^d,$$

where $u_{k,j}^{(I-1)} \in O_k^{(I-1)}$ and $\eta_{k,j,1}^{(I-1)} \sim \mathcal{N}(0, \sigma^{(I-1)2} I_{d \times d})$, $j = 1, \dots, N_k^{(I-1)}$. We set radius $m_k - s_k$, with m_k the mean and s_k the standard deviation of $\{\|w_{k,1}^{(I-1)} - \mathcal{U}_k\|_{\mathbb{R}^d}, \dots, \|w_{k,N_k^{(I-1)}}^{(I-1)} - \mathcal{U}_k\|_{\mathbb{R}^d}\}$.

The method above to construct a small round ball in $O_k^{(I-1)}$ relates to the evolution of the shapes of the sets $\{O_k, O_k^{(1)}, \dots, O_k^{(I-1)}\}$ through the iteration process. If $O_k^{(I-1)} \subset \mathbb{R}^d$ is close to spherical, our algorithm produces a ball contained in $O_k^{(I-1)}$. By (17) and statement (3) in Theorem 3.3, all sets $\{O_k, O_k^{(1)}, \dots, O_k^{(I-1)}\}$ are contained in $B_{3\delta}^{\mathbb{R}^d}(0)$. Since $\sigma^{(i-1)}$ decreases as i increases, compared to $\{O_k, O_k^{(1)}, \dots, O_k^{(I-2)}\}$, $O_k^{(I-1)}$ is close to spherical, as it contains a larger radius ball closer to 3δ . In Figure 5, we illustrate sets O_k and $O_k^{(I-1)}$. Hence, we perform the interpolation after sufficient iterations of Steps 1-3 in Algorithm 1 to ensure that the generated K samples $\{\tilde{u}_{k,i}\}_{i=1}^K$ are within the domain. Refer to Section C of the Supplementary Material for explicit expressions of interpolations constructed through $\{\tilde{u}_{k,i}\}_{i=1}^K$ and estimated parameters.

3.6. Performance evaluation. We evaluate the performance of MrGap in manifold reconstruction, assessing deviation of the interpolated points from the embedded submanifold $\iota(M)$. For any $y \in \mathbb{R}^D$, the distance from y to $S \subset \mathbb{R}^D$ is $\text{dist}(y, S) = \inf_{y' \in S} \|y - y'\|_{\mathbb{R}^D}$. Given $\mathcal{Y} = \{y_1, \dots, y_n\} \subset \mathbb{R}^D$, the geometric root mean square error from \mathcal{Y} to S is $G(\mathcal{Y}, S) = \sqrt{\frac{1}{n} \sum_{i=1}^n \text{dist}(y_i, S)^2}$, with $G(\mathcal{Y}, S) = 0$ if and only if \mathcal{Y} is in the closure of S . When S is compact, $G(\mathcal{Y}, S) = 0$ if and only if $\mathcal{Y} \subset S$. In the following theorem, we show that when \mathcal{Y}_{true} is sampled in $\iota(M)$ based on a density function with a positive lower bound, as the sample size of \mathcal{Y}_{true} goes to infinity, $G(\mathcal{Y}, \mathcal{Y}_{true}) \rightarrow G\{\mathcal{Y}, \iota(M)\}$ almost surely. We also provide the convergence rate. The proof is given in Section G of the Supplementary Material.

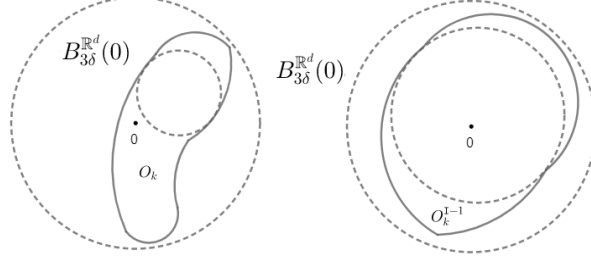


FIGURE 5. Both O_k and $O_k^{(I-1)}$ are contained in $B_{3\delta}^{\mathbb{R}^d}(0)$. Left: An illustration of $O_k \subset \mathbb{R}^d$ where O_k contains a small round ball. Right: An illustration of $O_k^{(I-1)} \subset \mathbb{R}^d$ where $O_k^{(I-1)}$ contains a larger round ball of radius close to 3δ .

Theorem 3.4. Suppose $\mathcal{Y} = \{y_1, \dots, y_n\} \subset \mathbb{R}^D$. $\{x_1, \dots, x_m\}$ are samples on M based on a C^1 p.d.f q on M such that $q > q_{\min} > 0$. Let $\mathcal{Y}_{true} = \{\iota(x_1), \dots, \iota(x_m)\}$. Suppose C is a constant depending on d, D, C^1 norm of q , the curvature of M and the second fundamental form of $\iota(M)$, and $r = \left[\max\left\{\frac{2}{q_{\min}}, \left(\frac{2C}{q_{\min}}\right)^2\right\} \frac{\log m}{m} \right]^{1/d}$, then with probability greater than $1 - \frac{1}{m^2}$,

- (1) $0 \leq \text{dist}\{y_i, \mathcal{Y}_{true}\} - \text{dist}\{y_i, \iota(M)\} \leq r$,
- (2) $G(\mathcal{Y}, \mathcal{Y}_{true})^2 - 2rG\{\mathcal{Y}, \iota(M)\} - r^2 \leq G\{\mathcal{Y}, \iota(M)\}^2 \leq G(\mathcal{Y}, \mathcal{Y}_{true})^2$.

Convergence in the above theorem follows from the fact that $r \rightarrow 0$ as the sample size $m \rightarrow 0$. Moreover, statement (2) implies that if m is large enough so that $r < \frac{1}{10}G\{\mathcal{Y}, \iota(M)\}$, then

$$(18) \quad G\{\mathcal{Y}, \iota(M)\} \leq G(\mathcal{Y}, \mathcal{Y}_{true}) \leq G\{\mathcal{Y}, \iota(M)\} + 1.3r.$$

Computing $\text{dist}\{y, \iota(M)\}$ is generally not computationally feasible. Therefore, we use samples \mathcal{Y}_{true} generated in $\iota(M)$ to estimate $G\{\mathcal{Y}, \iota(M)\}$. The limits given in (18) offer guidance on the sample sizes required for an accurate estimation. Furthermore, $q_{\min} \leq \frac{1}{\text{Vol}(M)}$, with equality holding when q is uniform. Thus, for a fixed sample size m , r is minimized when q is uniform. This suggests that the most efficient way to estimate $G\{\mathcal{Y}, \iota(M)\}$ is to sample \mathcal{Y}_{true} uniformly.

4. NUMERICAL SIMULATION

4.1. Cassini Oval in \mathbb{R}^3 . Let $r(\theta) = [\cos(2\theta) + \{\cos(2\theta)^2 + 0.2\}^{1/2}]^{1/2}$. A Cassini Oval $\iota(M)$ in \mathbb{R}^3 is parametrized by

$$(19) \quad X(\theta) = r(\theta)\cos(\theta), \quad Y(\theta) = r(\theta)\sin(\theta), \quad Z(\theta) = 0.3\sin(\theta + \pi),$$

where $\theta \in [0, 2\pi)$. We obtain non-uniform samples $\{X(\theta_i), Y(\theta_i), Z(\theta_i)\}_{i=1}^{102}$ on $\iota(M)$ from samples $\{\theta_i\}_{i=1}^{102}$ on $[0, 2\pi)$. Suppose $\eta_i \sim \mathcal{N}(0, \sigma^2 I_{3 \times 3})$, with $\sigma = 0.04$, $y_i = \{X(\theta_i), Y(\theta_i), Z(\theta_i)\}^\top + \eta_i$, $i = 1, \dots, 102$, and $\mathcal{Y} = \{y_i\}_{i=1}^{102}$. We uniformly sample $\{\phi_i\}_{i=1}^{10^5}$ on $[0, 2\pi)$ letting $\mathcal{Y}_{true} = \{X(\phi_i), Y(\phi_i), Z(\phi_i)\}_{i=1}^{10^5}$. For any sample points \mathcal{S} , $G\{\mathcal{S}, \iota(M)\}$ is approximated by $G(\mathcal{S}, \mathcal{Y}_{true})$. Without denoising, we obtain $G(\mathcal{Y}, \mathcal{Y}_{true}) = 0.059$.

Using the methods in Sections I and J of the Supplementary Material, we estimate dimension $d = 1$ and the scale parameters $\varepsilon = 0.3$ and $\delta = 0.6$ in MrGap. We iterate Steps 1-3 of Algorithm 1 twice. The estimated covariance parameters in the first round are $A^{(0)} = 0.014$, $\rho^{(0)} = 0.2$ and $\sigma^{(0)} = \sqrt{0.002}$, while the values in the last round are $A^{(1)} = 0.048$, $\rho^{(1)} = 0.3$ and $\sigma^{(1)} = \sqrt{2 \times 10^{-5}}$. The denoised outputs are $\mathcal{X}_1 = \{\hat{y}_i\}_{i=1}^{102}$, with $G(\mathcal{X}_1, \mathcal{Y}_{true}) = 0.0224$. In the interpolation phase, we construct 102 charts and interpolate $K = 20$ points in each chart. The outputs are $\mathcal{X}_2 = \{\hat{y}_i\}_{i=1}^{2040}$ with $G(\mathcal{X}_2, \mathcal{Y}_{true}) = 0.0216$. A comparison of \mathcal{Y} , \mathcal{X}_1 , and \mathcal{X}_2 with \mathcal{Y}_{true} is provided in Figure 6.

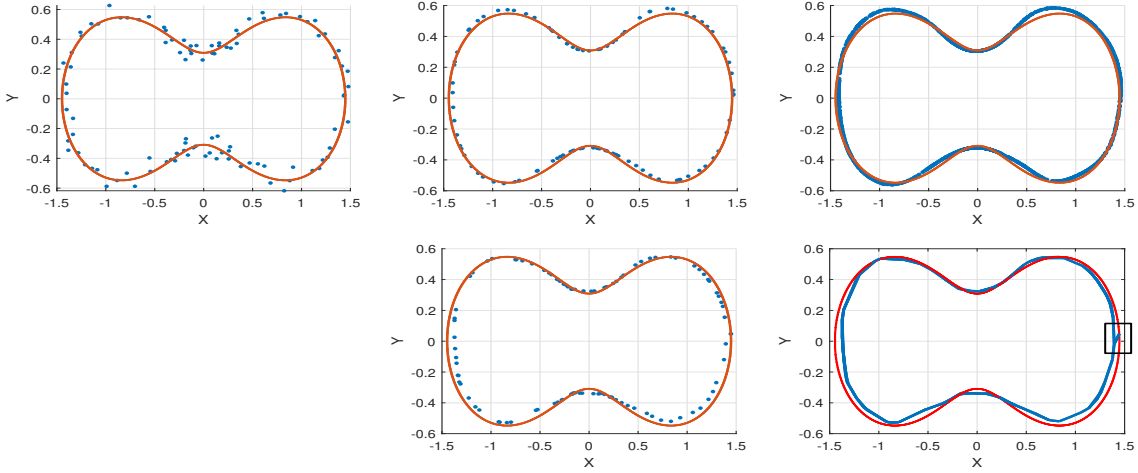


FIGURE 6. Red curves represent \mathcal{Y}_{true} consisting of 10^5 points on $\iota(M)$. Top row: left panel shows data \mathcal{Y} (blue) and \mathcal{Y}_{true} ($G(\mathcal{Y}, \mathcal{Y}_{true}) = 0.059$). Middle panel shows denoised samples \mathcal{X}_1 (blue) by MrGap and \mathcal{Y}_{true} ($G(\mathcal{X}_1, \mathcal{Y}_{true}) = 0.0224$). Right panel shows interpolations \mathcal{X}_2 (blue) by MrGap and \mathcal{Y}_{true} ($G(\mathcal{X}_2, \mathcal{Y}_{true}) = 0.0216$). Bottom row: middle panel shows denoised samples \mathcal{X}_p by principal graphs (blue) and \mathcal{Y}_{true} ($G(\mathcal{X}_p, \mathcal{Y}_{true}) = 0.0322$). Right panel shows principal graphs fit (blue) and \mathcal{Y}_{true} ; fit is not smooth at the indicated position.

We compare the performance of MrGap with principal graphs [22], which are a generalization of principal curves [18]. Principal graphs involve a number of nearest neighbors nn and tuning parameters σ_p , γ_p and λ_p . We choose $nn = 5$, $\sigma_p = 0.01$, $\gamma_p = 0.5$ and $\lambda_p = 1$ based on suggestions in their codes. We iterate their algorithm for 20 times to acquire 102 denoised data points \mathcal{X}_p , obtaining $G(\mathcal{X}_p, \mathcal{Y}_{true}) = 0.0322$. The principal graphs algorithm also generates a curve which fits \mathcal{Y} . One of the primary challenges in manifold reconstruction lies in addressing the non-smoothness problem during interpolations. In the principal graph method, non-smoothness is evident, while MrGap effectively eliminates this issue. Refer to Figure 6.

4.2. Torus in \mathbb{R}^3 . We consider a torus $\iota(M)$ in \mathbb{R}^3 parametrized by $u, v \in [0, 2\pi)$,

$$X(u, v) = \{2 + 0.8 \cos(u)\} \cos(v), \quad Y(u, v) = \{2 + 0.8 \cos(u)\} \sin(v), \quad Z(u, v) = 0.8 \sin(u).$$

We randomly sample 558 points $\{\iota(x_i)\}_{i=1}^{558}$ from the uniform density on $\iota(M)$. Let $\eta_i \sim \mathcal{N}(0, \sigma^2 I_{3 \times 3})$, with $\sigma = 0.12$, $y_i = \iota(x_i) + \eta_i$ for $i = 1, \dots, 558$, and $\mathcal{Y} = \{y_i\}_{i=1}^{558}$. We randomly sample 3.2×10^5 points from the uniform density on $\iota(M)$ to form \mathcal{Y}_{true} . We calculate the error from \mathcal{Y} to \mathcal{Y}_{true} which is $G(\mathcal{Y}, \mathcal{Y}_{true}) = 0.1238$. We plot \mathcal{Y} and \mathcal{Y}_{true} in Figure 20.

Using the methods in Sections I and J of the Supplementary Material, we estimate dimension $d = 2$ and the scale parameters $\varepsilon = 0.8$ and $\delta = 1$. We iterate Steps 1-3 of Algorithm 1 twice. The estimated covariance parameters are $A^{(0)} = 0.06$, $\rho^{(0)} = 0.2$ and $\sigma^{(0)} = \sqrt{0.03}$ in the first round, and $A^{(1)} = 0.2$, $\rho^{(1)} = 1.1$ and $\sigma^{(1)} = \sqrt{0.007}$ in the last round. The denoised outputs are $\mathcal{X}_1 = \{\hat{y}_i\}_{i=1}^{558}$ with $G(\mathcal{X}_1, \mathcal{Y}_{true}) = 0.0544$. We choose $K = 20$ in the interpolation phase, yielding the output $\mathcal{X}_2 = \{\hat{y}_i\}_{i=1}^{11160}$ with $G(\mathcal{X}_2, \mathcal{Y}_{true}) = 0.0605$. We plot $\mathcal{X}_1, \mathcal{X}_2$ in Figure 20.

We compare with the method of [2], which assumes data are uniformly distributed in a σ_a neighborhood of $\iota(M)$ in \mathbb{R}^D . We estimate $\sigma_a = 1.19$ and denoised data \mathcal{X}_a , which have $G(\mathcal{X}_a, \mathcal{Y}_{true}) = 0.2196$.

Although they do not provide an algorithm for interpolation, we modify their approach to produce interpolated points by uniformly generating 20 points in the $\frac{\sigma_a}{2}$ neighborhood of each denoised point in \mathcal{X}_a to obtain \mathcal{Y}_a , and then re-apply their algorithm with the same parameters to obtain new denoised data \mathcal{X}'_a that have $G(\mathcal{X}'_a, \mathcal{Y}_{true}) = 0.2424$. A comparison of \mathcal{X}_a and \mathcal{X}'_a with \mathcal{Y}_{true} in Figure 20 indicates the denoised points and interpolations lying on a thinner torus than the true one.

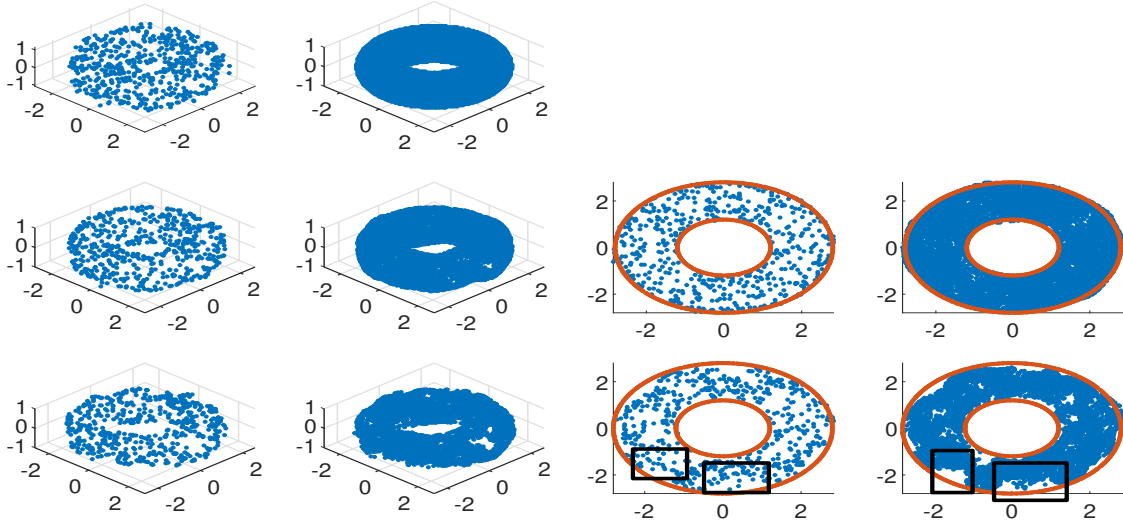


FIGURE 7. Top row: the first panel shows \mathcal{Y} containing 558 points around torus $\iota(M)$. The second panel shows \mathcal{Y}_{true} containing 3.2×10^5 points on $\iota(M)$ with $G(\mathcal{Y}, \mathcal{Y}_{true}) = 0.1238$. Middle row: the first panel shows denoised outputs \mathcal{X}_1 from MrGap with $G(\mathcal{X}_1, \mathcal{Y}_{true}) = 0.0544$. The second panel shows 11260 interpolated fits \mathcal{X}_2 from MrGap with $G(\mathcal{X}_2, \mathcal{Y}_{true}) = 0.0605$. In the last two panels, blue points are XY projections of \mathcal{X}_1 and \mathcal{X}_2 . Red circles are the intersection of the XY plane and the torus. Bottom row: first panel shows denoised outputs \mathcal{X}_a via [2] with $G(\mathcal{X}_a, \mathcal{Y}_{true}) = 0.2196$. The second panel shows 11260 interpolated fits \mathcal{X}'_a by their method with $G(\mathcal{X}'_a, \mathcal{Y}_{true}) = 0.2424$. In the last two panels, blue points are XY projections of \mathcal{X}_a and \mathcal{X}'_a . Since the clean data are uniformly distributed on $\iota(M)$, if the reconstructed torus matches the size of $\iota(M)$, the XY projections of denoised outputs and interpolation should lie within the annulus formed by the intersection of the XY plane and $\iota(M)$, with no significant gaps. The holes in the XY projections of \mathcal{X}_a and \mathcal{X}'_a near the annulus boundary shown in the figure suggest that the reconstructed torus is thinner than $\iota(M)$.

4.3. Additional simulations. In Section L, we illustrate the performance of MrGap on a real projective space, a 3 dimensional closed manifold embedded in \mathbb{R}^{10} . This section also shows the performances of MrGap under different assumptions about the manifold and data, specifically when the manifold has a boundary or the noise is not Gaussian.

5. MODELING OF BIRD VOCALIZATION DATA

Recall the bird vocalization data introduced in Section 1. Data consist of 83 matrices of dimension 75×197 corresponding to a type of call of *Anthus trivialis*; these matrices are submatrices of the spectrograms. Since we want to remove the impact of volume of the vocalizations, we normalize the

data after vectorizing to obtain the data in $x_i \in \mathbb{R}^{14775}$, for $i = 1, \dots, 83$. Following standard practice for extremely high-dimensional data, we project noisy data onto the first $n - 1 = 82$ principal components to obtain the data $\mathcal{Y} = \{y_i\}_{i=1}^{83} \subset \mathbb{R}^{82}$.

These are representative of data that are routinely collected in many biodiversity studies. Standard practice uses the spectrogram data to infer which species is vocalizing in each audio segment based on deep neural network classifiers [28]. Our collaborators are also interested in studying variation in vocalizations across individuals of the same species, both randomly and in relationship to spatial location and environmental covariates. Our proposed local Gaussian process regression framework provides a natural starting point for such analyses. By interpolating between different bird spectrograms of the same species we obtain insight into variation across individuals. By using local GP regressions to characterize a low dimensional bird vocalization manifold, we obtain a statistically efficient modeling approach that can naturally include sample covariates and/or spatial location. Here, we avoid the complexities of including such information and focus on showing that MrGap performs well in capturing the bird vocalization manifold from a small number of noisy samples.

To increase the difficulty, we add Gaussian noise $\eta_i \sim \mathcal{N}(0, \sigma^2 I_{14775 \times 14775})$, with $\sigma = 0.005$, to x_i . We evaluated the eigenvalues of the local covariance matrix constructed through \mathcal{Y} as in Section I of the Supplementary Material, producing an estimate of $d = 1$. Using the method in Section J, we estimate the scale parameters $\varepsilon = 1.27$ and $\delta = 1.27$. The estimated covariance parameters in the first round of Algorithm 1 are $A^{(0)} = 0.005$, $\rho^{(0)} = 0.2$ and $\sigma^{(0)} = 0.009$. We apply steps 1-3 of Algorithm 1 for only one round, as subsequent iterations do not significantly affect the estimate of σ . We choose $K = 10$ in the interpolation phase and generate 830 samples $\{\tilde{y}_i\}_{i=1}^{830}$ in the underlying manifold, representing new synthetic *Anthus trivialis* vocalizations in a space of 82-dimensional principal components. We map these samples back to the \mathbb{R}^{14775} space of the vectorized submatrices of the spectrogram, reconstructing the spectrograms from these.

In Figure 8, we present 10 such synthetic bird vocalization spectrograms generated by our methodology. To make the problem more challenging, we added noise to the original data. Nonetheless, we obtain excellent performance, with the spectrograms less noisy compared to the training data, successfully incorporating audio information from nearby denoised spectrograms that we are interpolating around. Our denoised spectrograms closely resemble those obtained in applying MrGap to the original data without noise added; some examples are shown in Figure 1.

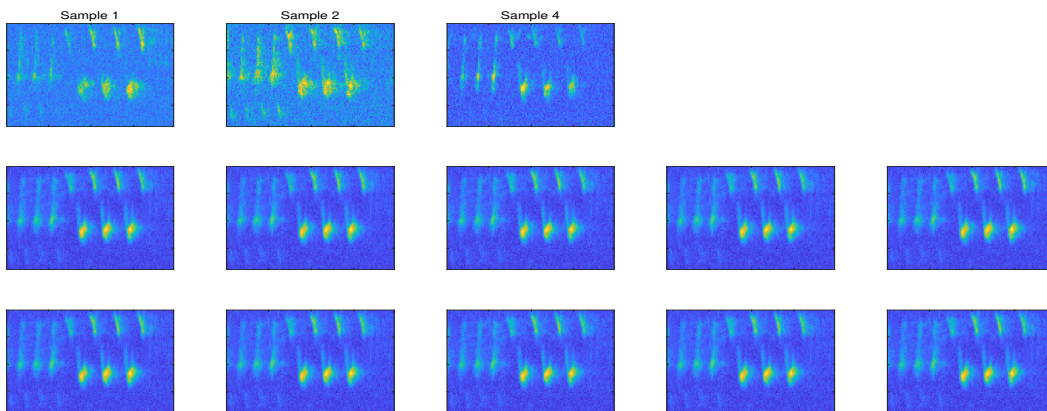


FIGURE 8. Top row: The data spectrograms with noise added. They correspond to Sample 1, 2 and 4, respectively, in Figure 1. Second and third rows: 10 synthetic bird vocalizations generated close to Sample 1 using MrGap.

We apply the method in [2] to the noisy data $\mathcal{Y} = \{\mathbf{y}_i\}_{i=1}^{83} \subset \mathbb{R}^{82}$, following the process described in Section 4.1, which estimates $\sigma_a = 1.427$ and produces 83 denoised samples. We then generate 10 samples uniformly in the $\frac{\sigma_a}{2}$ neighborhood of each denoised point. We obtain 830 clean new samples $\{\tilde{\mathbf{y}}_i^{as}\}_{i=1}^{830}$ on the 1 dimensional manifold by reapplying the algorithm with the same parameters. We map these samples back to the \mathbb{R}^{14775} space of the vectorized submatrices of the spectrogram, reconstructing 830 new spectrograms from these. In Figure 9, we present 10 generated spectrograms around Sample 1. Comparing these to the given noisy Sample 1 and the nearby Samples 2 and 4 in Figure 8 (corresponding to clean Samples 1, 2 and 4 in Figure 1), it is evident that important audio information is missing in the indicated regions.

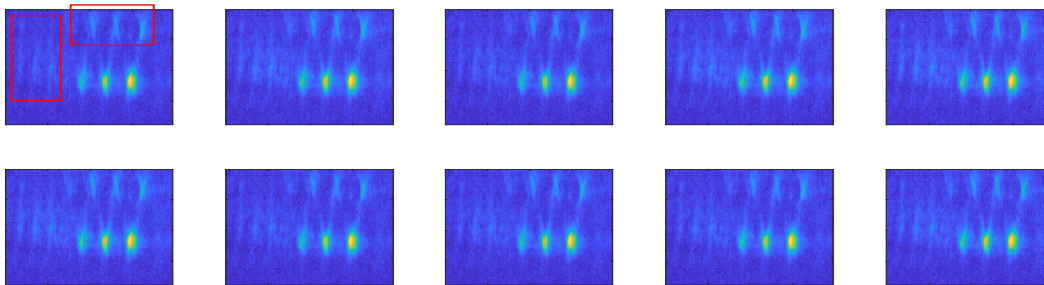


FIGURE 9. First and second rows: 10 generated samples around Sample 1 by the method in [2]. Audio information is missing at the indicated regions in the spectrograms.

6. DISCUSSION

This article proposed a local regression modeling framework for inferring manifold structure underlying noisy data, leveraging on novel theory on properties of local covariance matrices. While adding to the literature on manifold reconstruction, the fact that we obtain a statistical modeling framework is highly appealing in providing a starting point for many interesting extensions. For example, motivated by ecology applications we are currently pursuing extensions that include sample covariates and spatio-temporal dependence within the local Gaussian process regressions. Such models can allow intricate features of bird vocalizations to change depending on context.

There are many other interesting future directions. First, we can consider broader classes of covariance functions in the local Gaussian process regressions, including locally adaptive approaches accommodating complex manifolds that have varying smoothness. For example, we may consider a Matérn covariance instead of the squared exponential and can allow the local bandwidth parameters in the covariance functions to vary. Potentially, this can be done in a spatially smooth manner so that local neighborhoods that are close together in the ambient space have bandwidth parameters that tend to be closer together *a priori*. Another key direction is to obtain a theoretical justification in terms of uncertainty quantification. In this article, we have focused on using the local regressions for point estimation, but the posterior distributions clearly contain substantial information about uncertainty.

7. SUPPLEMENTARY MATERIAL AND CODES

The Supplementary Material include the proofs of the theorems and additional examples. The MATLAB implementation of the method and the data sets in Sections 4 and 5 are available on <https://github.com/wunan3/Manifold-reconstruction-via-Gaussian-processes>.

8. ACKNOWLEDGEMENT

The authors acknowledge the support of the European Research Council (ERC) under the European Union's Horizon 2020 research and innovation program (grant agreement No 856506) and the National Science Foundation (IIS-2426762).

APPENDIX A. REVIEW OF GAUSSIAN PROCESS REGRESSION

Suppose $F : \mathbb{R}^d \rightarrow \mathbb{R}^q$ is an unknown regression function with $F = (f_1, \dots, f_q)^\top$. Letting $z_i \in \mathbb{R}^q$ denote the response vector and $u_i \in \mathbb{R}^d$ denote the predictor vector, for $i = 1, \dots, N$, we have

$$(20) \quad z_i = F(u_i) + \eta_i, \quad \eta_i \sim \mathcal{N}(0, \sigma^2 I_{q \times q}).$$

We assign independent Gaussian process priors to each f_j with mean 0 and covariance function

$$(21) \quad C(u, u') = A \exp\left(-\frac{\|u - u'\|_{\mathbb{R}^d}^2}{\rho}\right).$$

Denote $f'_j \in \mathbb{R}^N$ as the discretization of f_j over $\{u_i\}_{i=1}^N$ so that $f'_j = \{f_j(u_1), \dots, f_j(u_N)\}^\top$ for $j = 1, \dots, q$. A Gaussian process prior for f_j implies $p(f'_j | u_1, u_2, \dots, u_N) = \mathcal{N}(0, \Sigma_1)$, where $\Sigma_1 \in \mathbb{R}^{N \times N}$ is the covariance matrix induced from C , with element (j, k) of Σ_1 corresponding to $C(u_j, u_k)$, for $1 \leq j, k \leq N$. Prior distribution $\mathcal{N}(0, \Sigma_1)$ can be combined with information in the likelihood function under model (20) to obtain the posterior distribution, which will be used as a basis for inference.

Suppose that we want to predict F at $\{u_i\}_{i=N+1}^{N+m}$. Define $f_j^* \in \mathbb{R}^m$ as $f_j^* = \{f_j(u_{N+1}), \dots, f_j(u_{N+m})\}^\top$ for $j = 1, \dots, q$. Denote $F \in \mathbb{R}^{m \times q}$ with j th column f_j^* . Under a Gaussian process prior for f_j , the joint distribution of f'_j and f_j^* is $p(f'_j, f_j^*) = \mathcal{N}(0, \Sigma)$, where $\Sigma = \begin{bmatrix} \Sigma_1 & \Sigma_2 \\ \Sigma_3 & \Sigma_4 \end{bmatrix}$, with $\Sigma_2 \in \mathbb{R}^{N \times m}$, $\Sigma_3 \in \mathbb{R}^{m \times N}$, and $\Sigma_4 \in \mathbb{R}^{m \times m}$ induced from covariance function C .

Denote $Z \in \mathbb{R}^{N \times q}$ with i th row z_i^\top for $i = 1, \dots, N$. Denote \tilde{z}_j for $j = 1, \dots, q$ as the j th column of Z consisting of the responses of f_j over $\{u_i\}_{i=1}^N$. Under model (20) and a Gaussian process prior, we have $p(\tilde{z}_j, f_j^*) = \mathcal{N}(0, \tilde{\Sigma})$, where

$$\tilde{\Sigma} = \Sigma + \begin{bmatrix} \sigma^2 I_{N \times N} & 0 \\ 0 & 0 \end{bmatrix} = \begin{bmatrix} \Sigma_1 + \sigma^2 I_{N \times N} & \Sigma_2 \\ \Sigma_3 & \Sigma_4 \end{bmatrix}.$$

For $j = 1, \dots, q$, the predictive distribution of f_j^* is

$$(22) \quad p(f_j^* | \tilde{z}_j) = \mathcal{N}\{\Sigma_3(\Sigma_1 + \sigma^2 I_{N \times N})^{-1} \tilde{z}_j, \Sigma_4 - \Sigma_3(\Sigma_1 + \sigma^2 I_{N \times N})^{-1} \Sigma_2\}.$$

Then, prediction for F can be expressed using the means of the above distributions:

$$\Sigma_3(\Sigma_1 + \sigma^2 I_{N \times N})^{-1} Z.$$

In the special case $m = 1$, so we want to predict F at only one point u_{N+1} , we have $F^\top = F(u_{N+1}) \in \mathbb{R}^q$. By (22), the predictive distribution of F^\top is

$$p(F^\top | Z) = \mathcal{N}\{\{\Sigma_3(\Sigma_1 + \sigma^2 I_{N \times N})^{-1} Z\}^\top, \{\Sigma_4 - \Sigma_3(\Sigma_1 + \sigma^2 I_{N \times N})^{-1} \Sigma_2\} I_{q \times q}\}.$$

For each \tilde{z}_j , the covariance parameters A , ρ and σ can be estimated by maximizing the natural log of the marginal likelihood, obtained by marginalizing over the Gaussian process prior,

$$\log p_j(\tilde{z}_j | A, \rho, \sigma) = -\tilde{z}_j^\top (\Sigma_1 + \sigma^2 I_{N \times N})^{-1} \tilde{z}_j - \log\{\det(\Sigma_1 + \sigma^2 I_{N \times N})\} - \frac{N}{2} \log(2\pi).$$

To estimate the parameters A , ρ and σ , we maximize $\log \{ \prod_{j=1}^q p_j(\tilde{z}_j|A, \rho, \sigma) \}$,

$$\begin{aligned} \log p(Z|A, \rho, \sigma) &= \log \{ \prod_{j=1}^q p_j(\tilde{z}_j|A, \rho, \sigma) \} = \sum_{j=1}^q \log p_j(\tilde{z}_j|A, \rho, \sigma) \\ &= - \sum_{j=1}^q \tilde{z}_j^\top (\Sigma_1 + \sigma^2 I_{N \times N})^{-1} \tilde{z}_j - q \log \{ \det(\Sigma_1 + \sigma^2 I_{N \times N}) \} - \frac{qN}{2} \log(2\pi) \\ &= - \text{tr} \{ Z^\top (\Sigma_1 + \sigma^2 I_{N \times N})^{-1} Z \} - q \log \{ \det(\Sigma_1 + \sigma^2 I_{N \times N}) \} - \frac{qN}{2} \log(2\pi). \end{aligned}$$

This empirical Bayes approach for parameter estimation protects against over-fitting.

APPENDIX B. SOME BASIC CONCEPTS ABOUT SMOOTH EMBEDDED MANIFOLDS

B.1. Diffeomorphism and chart. Suppose $U \subset \mathbb{R}^p$, $V \subset \mathbb{R}^q$ where U and V are not necessarily open. Suppose $\Phi : U \rightarrow V$ is continuous. Then Φ is a smooth map whenever it can be extended locally to a smooth map from an open set in \mathbb{R}^p to \mathbb{R}^q . More precisely, we have the following definition.

Definition B.1. *Suppose $U \subset \mathbb{R}^p$, $V \subset \mathbb{R}^q$. $\Phi : U \rightarrow V$ is a smooth map if for any $u \in U$ there is an open subset O_u of \mathbb{R}^p containing u and a smooth map $\tilde{\Phi} : O_u \rightarrow \mathbb{R}^q$ such that $\Phi = \tilde{\Phi}$ on O_u .*

Suppose $\Phi : U \rightarrow V$ is bijective. Then Φ^{-1} exists. We say that Φ is a diffeomorphism if both Φ and Φ^{-1} are smooth.

Suppose M is a d -dimensional smooth, closed and connected Riemannian manifold isometrically embedded in \mathbb{R}^D through ι . We define a chart of the embedded submanifold $\iota(M)$.

Definition B.2. *A map Φ is a chart (local parametrization) of $\iota(M)$, if there is an open subset U of \mathbb{R}^d and V of \mathbb{R}^D such that $\Phi : U \rightarrow V \cap \iota(M)$ is a diffeomorphism.*

We refer the reader to [25] for the above definitions. The definitions of diffeomorphisms and charts can be generalized to the abstract manifold M . Since our proofs of the main results focus on $\iota(M)$, we discuss only the relevant definitions for $\iota(M)$. We refer the reader to [21] for more general definitions.

B.2. The reach of an embedded submanifold. We recall the definition of the reach of an embedded submanifold in Euclidean space [15], which is an important concept in manifold reconstruction.

Definition B.3. *For any point $y \in \mathbb{R}^D$, the distance between y and $\iota(M)$ is $\text{dist}\{y, \iota(M)\} = \inf_{y' \in \iota(M)} \|y - y'\|_{\mathbb{R}^D}$. The reach of $\iota(M)$ is the supremum of all ℓ such that if $y \in \mathbb{R}^D$ and $\text{dist}\{y, \iota(M)\} < \ell$ then there is a unique $y' \in \iota(M)$ with $\text{dist}\{y, \iota(M)\} = \|y - y'\|_{\mathbb{R}^D}$. We denote the reach of $\iota(M)$ as $\tau_{\iota(M)}$.*

The reach $\tau_{\iota(M)}$ of $\iota(M)$ is the largest number such that any point in \mathbb{R}^D at distance less than the reach of $\iota(M)$ has a unique nearest point in $\iota(M)$. The reaches of some special embedded submanifolds can be explicitly calculated. For example, the reach of a d -dimensional sphere in \mathbb{R}^D is the radius of the sphere.

Suppose M is equipped with a Riemannian metric g and isometrically embedded in \mathbb{R}^D via ι . The geometric properties of M , and hence those of $\iota(M)$, which depend only on the metric g are called intrinsic properties. Examples include the volume, diameter, and curvature tensor of M . In contrast, the geometric properties of $\iota(M)$ that also depend on the embedding ι are known as the extrinsic properties of $\iota(M)$. These include the second fundamental form and the reach of $\iota(M)$. We illustrate the dependence of the reach on ι through the following example: Consider S^1 as the unit circle in \mathbb{R}^2 and let $a \in S^1$. Define $\iota_1(M) = S^1 \setminus a \subset \mathbb{R}^2$ and $\iota_2(M) = (0, 2\pi) \times \{0\}$, an interval on the x -axis in \mathbb{R}^2 . Both $\iota_1(M)$ and $\iota_2(M)$ are different isometric embeddings of the same manifold M , but they have different reaches.

A relevant topological result on the reach of $\iota(M)$ suggests that if there exists a point $y \in \mathbb{R}^D$ and a radius ξ such that $B_\xi^{\mathbb{R}^D}(y) \cap \iota(M)$ has more than one connected component, then $\tau_{\iota(M)} < \xi$. Figure 10 illustrates this concept. We summarize this result in the following proposition.

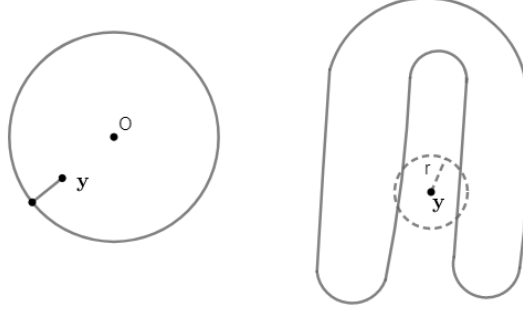


FIGURE 10. Left panel: The reach of a circle in the plane is the radius. For the center of the circle, the nearest point on the circle is the whole circle. For any point y whose distance to the circle is less than the radius, there is a unique nearest point on the circle. Right panel: A closed curve in the plane with small reach. We can find a point y and a small ball of radius r centered at y . The intersection between the ball and the curve has two connected components. Hence, by the consequence of Proposition B.1, the reach of the curve is smaller than r .

Proposition B.1 (Proposition 1 [4]). *Suppose $0 < \xi < \tau_{\iota(M)}$. For any $y \in \mathbb{R}^D$, if $B_\xi^{\mathbb{R}^D}(y) \cap \iota(M) \neq \emptyset$, then $B_\xi^{\mathbb{R}^D}(y) \cap \iota(M)$ is an open subset of $\iota(M)$ that is homeomorphic to $B_1^{\mathbb{R}^d}(0)$.*

B.3. Uniform construction of charts. As we introduced in the definition, for any $x \in M$, there is a chart of $\iota(M)$ over a neighborhood $U_x \cap \iota(M) \subset \mathbb{R}^D$ around $\iota(x)$. However, the size of U_x may not be uniform for all x . In the next proposition, by applying Proposition B.1, we show that we can choose the neighborhoods $\{U_x\}$ to be uniform for all x . In particular, we can construct a chart over $B_\xi^{\mathbb{R}^D}\{\iota(x)\} \cap \iota(M)$ for any $\xi < \frac{\tau_{\iota(M)}}{2}$. The proposition will be used later in the proof of the main theorem.

Proposition B.2. *Suppose $0 < \xi < \frac{\tau_{\iota(M)}}{2}$. For any $x \in M$, there is an open set $V_x \subset B_\xi^{\mathbb{R}^D}(0) \subset \mathbb{R}^d$ containing 0 such that for any $y \in B_\xi^{\mathbb{R}^D}\{\iota(x)\} \cap \iota(M)$, we have*

$$y = \iota(x) + X(x) \begin{bmatrix} u \\ G_x(u) \end{bmatrix},$$

where $u \in V_x$. Moreover,

- (1) $X(x) \in \mathbb{O}(D)$ is a $D \times D$ orthogonal matrix and $\{Xe_i\}_{i=1}^d$ form a basis of $T_{\iota(x)}\iota(M)$.
- (2) V_x is homeomorphic to $B_1^{\mathbb{R}^d}(0)$.
- (3) $G_x(u) = \{g_{x,1}(u), \dots, g_{x,D-d}(u)\}^\top \in \mathbb{R}^{D-d}$ and each $g_{x,i}$ is a smooth function on V_x .
- (4) $g_{x,i}(0) = 0$ and $\mathcal{D}g_{x,i}(0) = 0$ for $i = 1, \dots, D-d$, where $\mathcal{D}g_{x,i}$ is the derivative of $g_{x,i}$.

Proof. By Proposition B.1, $B_\xi^{\mathbb{R}^D}\{\iota(x)\} \cap \iota(M)$ is an open subset of $\iota(M)$ that is homeomorphic to $B_1^{\mathbb{R}^d}(0)$. Let f be the projection from \mathbb{R}^D to $T_{\iota(x)}\iota(M)$. For any $y \in B_\xi^{\mathbb{R}^D}\{\iota(x)\} \cap \iota(M)$, we express $g(y) = f\{y - \iota(x)\}$ in a chart around y , then by Lemma 5.4 in [27], $Dg(y)$ is not singular. By the inverse function theorem, $g(y)$ is a diffeomorphism. Hence, the image of $B_\xi^{\mathbb{R}^D}\{\iota(x)\} \cap \iota(M)$ under g is the open set V_x that is homeomorphic to $B_1^{\mathbb{R}^d}(0)$. Then g^{-1} is the chart with the described properties. \square

APPENDIX C. INTERPOLATION PHASE OF MRGAP

The steps of the interpolation phase of MrGap are listed as Algorithm 2. Suppose that the iterations in Algorithm 1 stop at the I th round. Then the final denoised outputs are $\{\hat{y}_k = y_k^{(I)}\}_{k=1}^n$. We use the outputs $\{y_1^{(I-1)}, \dots, y_n^{(I-1)}\}$ from the $I-1$ th iteration and the covariance parameters $A^{(I-1)}$, $\rho^{(I-1)}$, and $\sigma^{(I-1)}$ from the I th iteration as the inputs to interpolate points on $\iota(M)$.

Algorithm 2: MrGap steps to iteratively interpolate K points around each \hat{y}_k .

- 1 **for** $k = 1, \dots, n$ **do**
 - 2 Let \tilde{M}_{k-1} be the union of the $K(k-1)$ points already interpolated around $\{\hat{y}_1, \dots, \hat{y}_{k-1}\}$.
 Use $\{y_1^{(I-1)}, \dots, y_n^{(I-1)}\}$ as input to repeat Step 1 of Algorithm 1. Construct $\mathcal{P}_{y_k^{(I-1)}}(y_{k,j}^{(I-1)})$ and $\mathcal{P}_{y_k^{(I-1)}}^\perp$. Find $\{y_j^{(I-1)}\}_{j=1}^n \cap B_\delta^{\mathbb{R}^D}(y_k^{(I-1)}) = \{y_{k,1}^{(I-1)}, \dots, y_{k,N_k}^{(I-1)}\}$ and let $w_{k,j}^{(I-1)} = \mathcal{P}_{y_k^{(I-1)}}(y_{k,j}^{(I-1)})$ and $z_{k,j}^{(I-1)} = \mathcal{P}_{y_k^{(I-1)}}^\perp(y_{k,j}^{(I-1)})$.
 - 3 Let $\mathcal{U}_k = \frac{1}{N_k^{(I-1)}} \sum_{j=1}^{N_k^{(I-1)}} w_{k,j}^{(I-1)}$, and (m_k, s_k) denote the mean and standard deviation of $\{\|w_{k,1}^{(I-1)} - \mathcal{U}_k\|_{\mathbb{R}^d}, \dots, \|w_{k,N_k^{(I-1)}}^{(I-1)} - \mathcal{U}_k\|_{\mathbb{R}^d}\}$. Let $\{\tilde{u}_{k,1}, \dots, \tilde{u}_{k,K}\}$ be K samples generated uniformly in $B_{m_k - s_k}^{\mathbb{R}^d}(\mathcal{U}_k)$. Suppose $B_\delta^{\mathbb{R}^D}(y_k^{(I-1)}) \cap \tilde{M}_{k-1} = \{\tilde{y}_{k,1}, \dots, \tilde{y}_{k,L_k}\}$. Let $\tilde{w}_{k,j} = \mathcal{P}_{y_k^{(I-1)}}(\tilde{y}_{k,j})$ and $\tilde{z}_{k,j} = \mathcal{P}_{y_k^{(I-1)}}^\perp(\tilde{y}_{k,j})$ for $j = 1, \dots, L_k$.
 - 4 Construct the covariance matrix $\tilde{\Sigma}_k = \begin{bmatrix} \tilde{\Sigma}_{k,1} & \tilde{\Sigma}_{k,2} \\ \tilde{\Sigma}_{k,3} & \tilde{\Sigma}_{k,4} \end{bmatrix}$ over $\{w_{k,1}^{(I-1)}, \dots, w_{k,N_k}^{(I-1)}, \tilde{w}_{k,1}, \dots, \tilde{w}_{k,L_k}, \tilde{u}_{k,1}, \dots, \tilde{u}_{k,K}\}$ using covariance C in (21) and the covariance parameters $A^{(I-1)}$ and $\rho^{(I-1)}$, with $\tilde{\Sigma}_{k,1}$ corresponding to $\{w_{k,1}^{(I-1)}, \dots, w_{k,N_k}^{(I-1)}, \tilde{w}_{k,1}, \dots, \tilde{w}_{k,L_k}\}$.
 - 5 Denote $Z_k^{(I-1)} \in \mathbb{R}^{N_k \times (D-d)}$ with j th row $z_{k,j}^{(I-1)\top}$, and $\tilde{Z}_k \in \mathbb{R}^{L_k \times (D-d)}$ with j th row $\tilde{z}_{k,j}^\top$. Let $\mathbf{1}_K$ denote a K -vector of ones. Then, the column vectors of
$$y_k^{(I-1)} \mathbf{1}_K^\top + U_{n,\varepsilon}^{(I-1)}(y_k^{(I-1)}) \left[\begin{array}{c} \tilde{u}_{k,1}, \dots, \tilde{u}_{k,K} \\ \tilde{\Sigma}_{k,3} \{ \tilde{\Sigma}_{k,1} + \sigma^{(I-1)2} I_{(N_k^{(I-1)} + L_k) \times (N_k^{(I-1)} + L_k)} \}^{-1} \left[\begin{array}{c} Z_k^{(I-1)} \\ \tilde{Z}_k \end{array} \right] \right]^\top \end{array} \right] \in \mathbb{R}^{D \times K}$$
 give the Euclidean coordinates of the points that we interpolate around \hat{y}_k .
 - 6 **end**
-

APPENDIX D. BIAS ANALYSIS OF THE LOCAL COVARIANCE MATRIX

Recall Assumption 2.1, and let $G_\sigma(\eta)$ denote the $\mathcal{N}(0, \sigma^2 I_{D \times D})$ probability density function of η . Since samples $\{\eta_1, \dots, \eta_n\}$ are independent of $\{x_1, \dots, x_n\}$, pairs $\{(x_i, \eta_i)\}_{i=1}^n$ can be regarded as n independent and identically distributed samples based on the probability density function $P(x)G_\sigma(\eta)$ in $M \times \mathbb{R}^D$. For simplicity of notation, we provide the bias analysis under Assumption 3.1.

Suppose \mathbb{X} is a random variable associated with the probability density function $P(x)$ on M . Suppose \mathbb{H} is a random variable associated with the probability density function $G_\sigma(\eta)$ on \mathbb{R}^D . Since $\iota(x_k) = 0$ by the Assumption 3.1, we have $y_k = \iota(x_k) + \eta_k = \eta_k$. The expectation of the local covariance matrix

at y_k is defined as follows:

$$(23) \quad C_\varepsilon(y_k) = \mathbb{E} \left[\{ \iota(\mathbb{X}) + \mathbb{H} - \eta_k \} \{ \iota(\mathbb{X}) + \mathbb{H} - \eta_k \}^\top \chi \left(\frac{\| \iota(\mathbb{X}) + \mathbb{H} - \eta_k \|_{\mathbb{R}^D}}{\varepsilon} \right) \right] \\ = \int_{\mathbb{R}^D} \int_M \{ \iota(x) + \eta - \eta_k \} \{ \iota(x) + \eta - \eta_k \}^\top \chi \left(\frac{\| \iota(x) + \eta - \eta_k \|_{\mathbb{R}^D}}{\varepsilon} \right) P(x) G_\sigma(\eta) dV d\eta.$$

Remark D.1. Suppose $f : \mathbb{R}^D \rightarrow \mathbb{R}$ is a measurable function. Then, by a change of variables,

$$\int_{\mathbb{R}^D} \int_M f \{ \iota(x) + \eta \} P(x) G_\sigma(\eta) dV d\eta = \int_{\mathbb{R}^D} \int_M f(\eta) P(x) G_\sigma \{ \eta - \iota(x) \} dV d\eta \\ = \int_{\mathbb{R}^D} f(\eta) P \star G_\sigma(\eta) d\eta,$$

where the convolution $P \star G_\sigma(\eta) = \int_M P(x) G_\sigma \{ \eta - \iota(x) \} dV$ is the probability density function for the random variable $\iota(\mathbb{X}) + \mathbb{H}$. Hence, the definition in (23) is equivalent to

$$(24) \quad \mathbb{E} \left[\{ \iota(\mathbb{X}) + \mathbb{H} - \eta_k \} \{ \iota(\mathbb{X}) + \mathbb{H} - \eta_k \}^\top \chi \left(\frac{\| \iota(\mathbb{X}) + \mathbb{H} - \eta_k \|_{\mathbb{R}^D}}{\varepsilon} \right) \right] \\ = \int_{\mathbb{R}^D} (\eta - \eta_k) (\eta - \eta_k)^\top \chi \left(\frac{\| \eta - \eta_k \|_{\mathbb{R}^D}}{\varepsilon} \right) P \star G_\sigma(\eta) d\eta.$$

In the following proposition, we provide a bias analysis for the local covariance matrix. The proposition is proved later in this section.

Proposition D.1. Under Assumptions 2.1 and 3.1, suppose ε is small enough depending on d, D , the second fundamental form of $\iota(M)$ and the scalar curvature of M . Suppose $\beta > 1$, $\sigma \leq \frac{\varepsilon^\beta}{\sqrt{-4(d+5)\log \varepsilon}}$, and $\| \eta_k \|_{\mathbb{R}^D} \leq \varepsilon^\beta$, then

$$C_\varepsilon(y_k) = \varepsilon^{d+2} \left(\frac{|S^{d-1}|P(x_k)}{d(d+2)} \begin{bmatrix} I_{d \times d} & 0 \\ 0 & 0 \end{bmatrix} + \begin{bmatrix} O(\varepsilon^{\beta-1} + \varepsilon^2) & O(\varepsilon^{2\beta-2} + \varepsilon^2) \\ O(\varepsilon^{2\beta-2} + \varepsilon^2) & O(\varepsilon^{2\beta-2} + \varepsilon^2) \end{bmatrix} \right),$$

where the constant factors in all blocks depend on d , C^2 norm of P , the second fundamental form of $\iota(M)$ and its derivative and the Ricci curvature of M .

Suppose $\iota(x_k) = 0$ and there is no noise, then the expectation of the local covariance matrix at y_k can be expressed as follows:

$$\tilde{C}_\varepsilon(y_k) = \mathbb{E} \left\{ \iota(\mathbb{X}) \iota(\mathbb{X})^\top \chi \left(\frac{\| \iota(\mathbb{X}) \|_{\mathbb{R}^D}}{\varepsilon} \right) \right\}.$$

By Proposition 3.1 in [39],

$$(25) \quad \tilde{C}_\varepsilon(y_k) = \varepsilon^{d+2} \left(\frac{|S^{d-1}|P(x_k)}{d(d+2)} \begin{bmatrix} I_{d \times d} & 0 \\ 0 & 0 \end{bmatrix} + O(\varepsilon^2) \right),$$

where $O(\varepsilon^2)$ represents a D by D matrix whose entries are of order $O(\varepsilon^2)$. The constant factors in $O(\varepsilon^2)$ depend on d , C^2 norm of P , the second fundamental form of $\iota(M)$ and its derivative and the Ricci curvature of M . If the standard deviation of the Gaussian noise is small enough, so that $\sigma \leq \frac{\varepsilon^3}{\sqrt{-4(d+5)\log \varepsilon}}$ then

$$C_\varepsilon(y_k) = \varepsilon^{d+2} \left(\frac{|S^{d-1}|P(x_k)}{d(d+2)} \begin{bmatrix} I_{d \times d} & 0 \\ 0 & 0 \end{bmatrix} + O(\varepsilon^2) \right).$$

Comparing to Proposition 3.1 in [39], the impact of the noise on the local covariance matrix is negligible.

Remark D.2. Since $\tilde{C}_\varepsilon(y_k)$ is invariant under translation and its eigenvalues are invariant under rotation, the leading term $\varepsilon^{d+2} \frac{|S^{d-1}|P(x_k)}{d(d+2)} \begin{bmatrix} Id \times d & 0 \\ 0 & 0 \end{bmatrix}$ in (25) implies that $\tilde{C}_\varepsilon(y_k)$ has d large eigenvalues of order ε^{d+2} , while the rest of the eigenvalues are of order $O(\varepsilon^{d+4})$. Refer to Section I for an illustration.

D.1. Preliminary lemmas. We introduce some notation. Suppose S is a subset of M . Then $\chi_S(x)$ is the characteristic function on S . For $S_1, S_2 \subset M$, let $S_1 \Delta S_2 = (S_1 \setminus S_2) \cup (S_2 \setminus S_1)$ be the symmetric difference. Let $d_M(x, x')$ be the geodesic distance between x and x' in M . Let $B_r(x) \subset M$ be the open geodesic ball of radius r centered at $x \in M$.

We have the following lemma about the geodesic distance between x and x' on M and the Euclidean distance between $\iota(x)$ and $\iota(x')$ in \mathbb{R}^D . The proof of the lemma is available in [39].

Lemma D.1. Fix $x \in M$. Let $u \in T_x M \approx \mathbb{R}^d$ with $\|u\|_{\mathbb{R}^d}$ sufficiently small. Suppose $x' = \exp_x(u)$. Let $\iota_* u = \frac{d}{dr} \iota(\exp_x(ut))|_{t=0} \in T_{\iota(x)} \iota(M)$. Then

$$\iota(x') - \iota(x) = \iota_* u + \frac{1}{2} \mathbb{I}_x(u, u) + O(\|u\|_{\mathbb{R}^d}^3),$$

where \mathbb{I}_x is the second fundamental form of $\iota(M)$ at $\iota(x)$. Moreover,

$$\|\iota(x') - \iota(x)\|_{\mathbb{R}^D} = \|u\|_{\mathbb{R}^d} - \frac{1}{24} \left\| \mathbb{I}_x \left(\frac{u}{\|u\|_{\mathbb{R}^d}}, \frac{u}{\|u\|_{\mathbb{R}^d}} \right) \right\|_{\mathbb{R}^D}^2 \|u\|_{\mathbb{R}^d}^3 + O(\|u\|_{\mathbb{R}^d}^4).$$

This implies that

$$\|u\|_{\mathbb{R}^d} = \|\iota(x') - \iota(x)\|_{\mathbb{R}^D} + \frac{1}{24} \left\| \mathbb{I}_x \left(\frac{u}{\|u\|_{\mathbb{R}^d}}, \frac{u}{\|u\|_{\mathbb{R}^d}} \right) \right\|_{\mathbb{R}^D}^2 \|\iota(x') - \iota(x)\|_{\mathbb{R}^D}^3 + O(\|\iota(x') - \iota(x)\|_{\mathbb{R}^D}^4).$$

Next, we introduce the following lemma about the volume form on M . The proof of the lemma is available in [10].

Lemma D.2. Fix $x \in M$. For $u \in T_x M \approx \mathbb{R}^d$ with $\|u\|_{\mathbb{R}^d}$ sufficiently small, the volume form has the following expansion

$$dV = \left\{ 1 - \sum_{i,j=1}^d \frac{1}{6} \text{Ric}_x(e'_i, e'_j) u_i u_j + O(\|u\|_{\mathbb{R}^d}^3) \right\} du,$$

where $u = \sum_{i=1}^d u_i e'_i$ and Ric_x is the Ricci curvature tensor of M at x . Consequently,

$$\text{Vol}\{B_r(x)\} = \text{Vol}(B_1^{\mathbb{R}^d}) r^d \left\{ 1 - \frac{S_x}{6(d+2)} r^2 + O(r^4) \right\},$$

where S_x is the scalar curvature of M at x .

Recalling that $G_\sigma(\eta)$ is the $\mathcal{N}(0, \sigma^2 I_{D \times D})$ probability density function of η , we have the following Lemma describing bounds on $G_\sigma(\eta)$.

Lemma D.3. (1) If $\frac{1}{\sigma} \geq \sqrt{2}(D-2)$, then $\int_{\|\eta\|_{\mathbb{R}^D} \geq t} G_\sigma(\eta) d\eta \leq \frac{2}{\Gamma(\frac{D}{2})} e^{-\frac{t^2}{4\sigma^2}}$.

(2) $\int_{\mathbb{R}^D} \eta(i)^2 G_\sigma(\eta) d\eta \leq \sigma^2$, for $i = 1, \dots, D$.

Proof. (1) By the change of variables in the spherical coordinates,

$$\int_{\|\eta\|_{\mathbb{R}^D} \geq t} G_\sigma(\eta) d\eta = \frac{1}{(2\pi\sigma^2)^{\frac{D}{2}}} (2\sigma^2)^{\frac{D}{2}} |S^{D-1}| \int_{\frac{t}{\sqrt{2}\sigma}}^{\infty} r^{D-1} e^{-r^2} dr = \frac{|S^{D-1}|}{\pi^{\frac{D}{2}}} \int_{\frac{t}{\sqrt{2}\sigma}}^{\infty} r^{D-1} e^{-r^2} dr.$$

Since $\frac{r}{2} \geq \log(r)$ for all $r > 0$, when $r \geq D-2$, we have $D-2 \leq \frac{r^2}{2\log(r)}$. Hence, $r^{D-2}e^{-r^2} \leq e^{-\frac{r^2}{2}}$. If $\frac{t}{\sigma} \geq \sqrt{2}(D-2)$, then

$$\int_{\|\eta\|_{\mathbb{R}^D} \geq t} G_\sigma(\eta) d\eta \leq \frac{|S^{D-1}|}{\pi^{\frac{D}{2}}} \int_{\frac{t}{\sqrt{2}\sigma}}^{\infty} e^{-\frac{r^2}{2}} r dr = \frac{2}{\Gamma(\frac{D}{2})} e^{-\frac{t^2}{4\sigma^2}}.$$

(2) follows from the change of variables in the spherical coordinates and the symmetry of \mathbb{R}^D . \square

Recall that we have $\iota(x_k) = 0 \in \mathbb{R}^D$. We define the following terms for our proofs:

$$\begin{aligned} F_1\{\iota(x), \eta, \eta_k\} &= \{\iota(x) + \eta - \eta_k\} \{\iota(x) + \eta - \eta_k\}^\top \chi\left(\frac{\|\iota(x) + \eta - \eta_k\|_{\mathbb{R}^D}}{\varepsilon}\right), \\ E_1 &= \int_{\|\eta\|_{\mathbb{R}^D} < \varepsilon^\beta} \int_M F_1\{\iota(x), \eta, \eta_k\} P(x) G_\sigma(\eta) dV d\eta, \\ E_2 &= \int_{\|\eta\|_{\mathbb{R}^D} \geq \varepsilon^\beta} \int_M F_1\{\iota(x), \eta, \eta_k\} P(x) G_\sigma(\eta) dV d\eta, \\ E_3 &= \int_{\|\eta\|_{\mathbb{R}^D} < \varepsilon^\beta} \int_M \{\iota(x) + \eta - \eta_k\} \{\iota(x) + \eta - \eta_k\}^\top \chi_{B_\varepsilon(x_k)}(x) P(x) G_\sigma(\eta) dV d\eta. \end{aligned}$$

Lemma D.4. *Suppose ε is small enough depending on d and D . For $\beta > 1$, if $\sigma \leq \frac{\varepsilon^\beta}{\sqrt{-4(d+5)\log\varepsilon}}$, then $|e_i^\top E_2 e_j| \leq \varepsilon^{d+5}$ for all $1 \leq i, j \leq D$.*

Proof. When $\|\iota(x) + \eta - \eta_k\|_{\mathbb{R}^D} \leq \varepsilon$, $\chi\left(\frac{\|\iota(x) + \eta - \eta_k\|_{\mathbb{R}^D}}{\varepsilon}\right) \leq 1$. When $\|\iota(x) + \eta - \eta_k\|_{\mathbb{R}^D} > \varepsilon$, $\chi\left(\frac{\|\iota(x) + \eta - \eta_k\|_{\mathbb{R}^D}}{\varepsilon}\right) = 0$. Hence, for all $1 \leq i, j \leq D$ and all x , we have

$$|e_i^\top \{\iota(x) + \eta - \eta_k\} \{\iota(x) + \eta - \eta_k\}^\top e_j| \chi\left(\frac{\|\iota(x) + \eta - \eta_k\|_{\mathbb{R}^D}}{\varepsilon}\right) \leq \varepsilon^2.$$

Next, we bound $|e_i^\top E_2 e_j|$,

$$\begin{aligned} |e_i^\top E_2 e_j| &\leq \int_{\|\eta\|_{\mathbb{R}^D} \geq \varepsilon^\beta} \int_M |e_i^\top \{\iota(x) + \eta - \eta_k\} \{\iota(x) + \eta - \eta_k\}^\top e_j| \\ &\quad \times \chi\left(\frac{\|\iota(x) + \eta - \eta_k\|_{\mathbb{R}^D}}{\varepsilon}\right) P(x) G_\sigma(\eta) dV d\eta \\ &\leq \int_{\|\eta\|_{\mathbb{R}^D} \geq \varepsilon^\beta} \int_M \varepsilon^2 P(x) G_\sigma(\eta) dV d\eta = \int_{\|\eta\|_{\mathbb{R}^D} \geq \varepsilon^\beta} \varepsilon^2 G_\sigma(\eta) d\eta \int_M P(x) dV \\ &\leq \int_{\|\eta\|_{\mathbb{R}^D} \geq \varepsilon^\beta} \varepsilon^2 G_\sigma(\eta) d\eta. \end{aligned}$$

We apply Fubini's theorem in the second to last step and the fact that $P(x)$ is a probability density function on M in the last step. Based on the assumption of the lemma, when ε is small enough based on d and D , $\frac{\varepsilon^\beta}{\sigma} \geq \sqrt{-4(d+5)\log\varepsilon} \geq 2\sqrt{2}(D-2)$. Then by Lemma D.3, $|e_i^\top E_2 e_j| \leq \frac{2\varepsilon^2}{\Gamma(\frac{D}{2})} e^{-\frac{\varepsilon^{2\beta}}{4\sigma^2}}$. Since $\Gamma(\frac{D}{2}) > 1$, when $\varepsilon \leq \frac{1}{2}$, a straightforward calculation shows that $\sigma \leq \frac{\varepsilon^\beta}{\sqrt{-4(d+5)\log\varepsilon}}$ implies $|e_i^\top E_2 e_j| \leq \frac{2\varepsilon^2}{\Gamma(\frac{D}{2})} e^{-\frac{\varepsilon^{2\beta}}{4\sigma^2}} \leq \varepsilon^{d+5}$. \square

Lemma D.5. *Suppose ε is small enough depending on the second fundamental form of $\iota(M)$. For $x \in M$, define $W_{ij}(x) = |e_i^\top \{\iota(x) + \eta - \eta_k\} \{\iota(x) + \eta - \eta_k\}^\top e_j|$. Suppose $1 < \beta \leq 3$. If $\|\eta\|_{\mathbb{R}^D} \leq \varepsilon^\beta$ and*

$\|\eta_k\|_{\mathbb{R}^D} \leq \varepsilon^\beta$, then for $x \in B_{\varepsilon+3\varepsilon^\beta}(x_k)$

$$\begin{aligned} W_{ij}(x) &\leq 49\varepsilon^2, \quad (1 \leq i, j \leq d), \\ W_{ij}(x) &\leq C_3(\varepsilon^3 + \varepsilon^{1+\beta}), \quad (1 \leq i \leq d; d+1 \leq j \leq D), \\ W_{ij}(x) &\leq C_3(\varepsilon^3 + \varepsilon^{1+\beta}), \quad (d+1 \leq i \leq D; 1 \leq j \leq d), \\ W_{ij}(x) &\leq C_3(\varepsilon^4 + \varepsilon^{2\beta}), \quad (d+1 \leq i, j \leq D), \end{aligned}$$

where C_3 is a constant depending on the second fundamental form of $\iota(M)$.

Suppose $\beta > 3$. If $\|\eta\|_{\mathbb{R}^D} \leq \varepsilon^\beta$ $\|\eta_k\|_{\mathbb{R}^D} \leq \varepsilon^\beta$, then for $x \in B_{\varepsilon+3\varepsilon^\beta}(x_k)$

$$\begin{aligned} W_{ij}(x) &\leq 49\varepsilon^2, \quad (1 \leq i, j \leq d), \\ W_{ij}(x) &\leq 2C_3\varepsilon^3, \quad (1 \leq i \leq d; d+1 \leq j \leq D), \\ W_{ij}(x) &\leq 2C_3\varepsilon^3, \quad (d+1 \leq i \leq D; 1 \leq j \leq d), \\ W_{ij}(x) &\leq 2C_3\varepsilon^4, \quad (d+1 \leq i, j \leq D). \end{aligned}$$

Proof. Since $\|\eta\|_{\mathbb{R}^D} < \varepsilon^\beta$ and $\|\eta_k\|_{\mathbb{R}^D} \leq \varepsilon^\beta$, we have

$$\begin{aligned} (26) \quad &|e_i^\top \{\iota(x) + \eta - \eta_k\} \{\iota(x) + \eta - \eta_k\}^\top e_j| \\ &\leq (|e_i^\top \iota(x)| + |e_i^\top \eta| + |e_i^\top \eta_k|)(|\iota(x)^\top e_j| + |\eta^\top e_j| + |\eta_k^\top e_j|) \\ &\leq (|e_i^\top \iota(x)| + 2\varepsilon^\beta)(|\iota(x)^\top e_j| + 2\varepsilon^\beta). \end{aligned}$$

For any $x \in B_{\varepsilon+3\varepsilon^\beta}(x_k)$, suppose $x = \exp_{x_k}(u)$ for $u \in T_{x_k}M \approx \mathbb{R}^d$. Then, $\|u\|_{\mathbb{R}^d} \leq \varepsilon + 3\varepsilon^\beta$. Since $\iota(x_k) = 0$, by Lemma D.1, we have

$$\iota(x) = \iota_* u + \frac{1}{2} \mathbb{I}_{x_k}(u, u) + O(\|u\|_{\mathbb{R}^d}^3),$$

where $\iota_* u = \frac{d}{dt} \iota(\exp_{x_k}(ut))|_{t=0} \in T_{\iota(x_k)}\iota(M)$. Since $\{e_1, \dots, e_d\}$ form a basis of $T_{\iota(x_k)}\iota(M)$, they are perpendicular to $\mathbb{I}_{x_k}(u, u)$. Since $1 < \beta$, when ε is small enough depending on the second fundamental form of $\iota(M)$, we have $|e_i^\top \iota(x)| \leq 5\varepsilon$ for $i = 1, \dots, d$. Similarly, since $\{e_{d+1}, \dots, e_D\}$ form a basis of $T_{\iota(x_k)}\iota(M)^\perp$, they are perpendicular to $\iota_* u$. When ε is small enough depending on the second fundamental form of $\iota(M)$, we have $|e_i^\top \iota(x)| \leq C_2\varepsilon^2$ for $i = d+1, \dots, D$, where C_2 is a constant depending on the second fundamental form of $\iota(M)$. If we substitute the bounds of $|e_i^\top \iota(x)|$ into (26), then after the simplification, for any $\|\eta\|_{\mathbb{R}^D} < \varepsilon^\beta$, $\|\eta_k\|_{\mathbb{R}^D} \leq \varepsilon^\beta$ and $x \in B_{\varepsilon+3\varepsilon^\beta}(x_k)$, we have

$$\begin{aligned} &|e_i^\top \{\iota(x) + \eta - \eta_k\} \{\iota(x) + \eta - \eta_k\}^\top e_j| \leq 49\varepsilon^2, \quad (1 \leq i, j \leq d), \\ &|e_i^\top \{\iota(x) + \eta - \eta_k\} \{\iota(x) + \eta - \eta_k\}^\top e_j| \leq C_3(\varepsilon^3 + \varepsilon^{1+\beta}), \quad (1 \leq i \leq d; d+1 \leq j \leq D), \\ &|e_i^\top \{\iota(x) + \eta - \eta_k\} \{\iota(x) + \eta - \eta_k\}^\top e_j| \leq C_3(\varepsilon^3 + \varepsilon^{1+\beta}), \quad (d+1 \leq i \leq D; 1 \leq j \leq d) \\ &|e_i^\top \{\iota(x) + \eta - \eta_k\} \{\iota(x) + \eta - \eta_k\}^\top e_j| \leq C_3(\varepsilon^4 + \varepsilon^{2\beta}), \quad (d+1 \leq i, j \leq D), \end{aligned}$$

where C_3 is a constant depending on the second fundamental form of $\iota(M)$. The proof for the case when $\beta > 3$ is similar. \square

Lemma D.6. Suppose ε is small enough depending on the scalar curvature of M and the second fundamental form of $\iota(M)$. Suppose $1 < \beta$. If $\|\eta_k\|_{\mathbb{R}^D} \leq \varepsilon^\beta$ then

$$E_1 = E_3 + \begin{bmatrix} O(\varepsilon^{d+1+\beta} + \varepsilon^{d+4}) & O(\varepsilon^{d+2+\beta} + \varepsilon^{d+2\beta} + \varepsilon^{d+5}) \\ O(\varepsilon^{d+2+\beta} + \varepsilon^{d+2\beta} + \varepsilon^{d+5}) & O(\varepsilon^{d+3+\beta} + \varepsilon^{d-1+3\beta} + \varepsilon^{d+6}) \end{bmatrix},$$

where the top left block is a d by d matrix and the constant factors in the four blocks depend on d , P_M and the second fundamental form of $\iota(M)$.

Proof. Let $A(\eta) = \{x \in M \mid \|\iota(x) + \eta - \eta_k\|_{\mathbb{R}^D} \leq \varepsilon \text{ for a fixed } \|\eta\|_{\mathbb{R}^D} < \varepsilon^\beta\}$. Since $\|\eta\|_{\mathbb{R}^D} < \varepsilon^\beta$ and $\|\eta_k\|_{\mathbb{R}^D} \leq \varepsilon^\beta$, by the triangle inequality, if $x \in A(\eta)$, then $\varepsilon - 2\varepsilon^\beta \leq \|\iota(x)\|_{\mathbb{R}^D} \leq \varepsilon + 2\varepsilon^\beta$. If $1 < \beta \leq 3$, when ε is small enough depending on the second fundamental form of $\iota(M)$, by Lemma D.1, we have $\varepsilon - 2\varepsilon^\beta \leq d(x, x_k) < \varepsilon + 3\varepsilon^\beta$. Hence, $B_{\varepsilon-2\varepsilon^\beta}(x_k) \subset A(\eta) \subset B_{\varepsilon+3\varepsilon^\beta}(x_k)$ which implies $A(\eta)\Delta B_\varepsilon \subset B_{\varepsilon+3\varepsilon^\beta}(x_k) \setminus B_{\varepsilon-2\varepsilon^\beta}(x_k)$. Since $1 < \beta \leq 3$, when ε is small enough depending on the scalar curvature of M , by Lemma D.2, for all $\|\eta\|_{\mathbb{R}^D} < \varepsilon^\beta$ we have

$$\text{Vol}\{A(\eta)\Delta B_\varepsilon(x_k)\} \leq \text{Vol}\{B_{\varepsilon+3\varepsilon^\beta}(x_k)\} - \text{Vol}\{B_{\varepsilon-2\varepsilon^\beta}(x_k)\} \leq 6\text{Vol}(B_1^{\mathbb{R}^d})d\varepsilon^{d-1+\beta} = C_1(d)\varepsilon^{d-1+\beta},$$

where $C_1(d) = 6d\text{Vol}(B_1^{\mathbb{R}^d})$ is a constant only depending on d . Similarly, if $\beta > 3$, then for all $\|\eta\|_{\mathbb{R}^D} < \varepsilon^\beta$ we have $A(\eta)\Delta B_\varepsilon \subset B_{\varepsilon+3\varepsilon^3}(x_k) \setminus B_{\varepsilon-2\varepsilon^3}(x_k)$ and

$$\text{Vol}\{A(\eta)\Delta B_\varepsilon(x_k)\} \leq C_1(d)\varepsilon^{d+2}.$$

Observe that for a fixed $\|\eta\|_{\mathbb{R}^D} < \varepsilon^\beta$, $|\chi_{A(\eta)}(x) - \chi_{B_\varepsilon(x_k)}(x)| \leq \chi_{A(\eta)\Delta B_\varepsilon(x_k)}(x)$. Moreover, we have $\chi_{A(\eta)}(x) = \chi\left(\frac{\|\iota(x) + \eta - \eta_k\|_{\mathbb{R}^D}}{\varepsilon}\right)$. Hence,

(27)

$$\begin{aligned} & |e_i^\top (E_1 - E_3)e_j| \\ & \leq \int_{\|\eta\|_{\mathbb{R}^D} < \varepsilon^\beta} \int_M |e_i^\top \{\iota(x) + \eta - \eta_k\} \{\iota(x) + \eta - \eta_k\}^\top e_j| \chi_{A(\eta)}(x) - \chi_{B_\varepsilon(x_k)}(x) |P(x)G_\sigma(\eta)| dV d\eta \\ & \leq \int_{\|\eta\|_{\mathbb{R}^D} < \varepsilon^\beta} \int_M |e_i^\top \{\iota(x) + \eta - \eta_k\} \{\iota(x) + \eta - \eta_k\}^\top e_j| \chi_{A(\eta)\Delta B_\varepsilon(x_k)}(x) P(x)G_\sigma(\eta) dV d\eta \\ & \leq \left(\sup_{\|\eta\|_{\mathbb{R}^D} < \varepsilon^\beta, x \in A(\eta)\Delta B_\varepsilon(x_k)} |e_i^\top \{\iota(x) + \eta - \eta_k\} \{\iota(x) + \eta - \eta_k\}^\top e_j| \right) \\ & \quad \times \int_{\|\eta\|_{\mathbb{R}^D} < \varepsilon^\beta} \int_M \chi_{A(\eta)\Delta B_\varepsilon(x_k)}(x) P(x)G_\sigma(\eta) dV d\eta \\ & \leq \left(\sup_{\|\eta\|_{\mathbb{R}^D} < \varepsilon^\beta, x \in A(\eta)\Delta B_\varepsilon(x_k)} |e_i^\top \{\iota(x) + \eta - \eta_k\} \{\iota(x) + \eta - \eta_k\}^\top e_j| \right) P_M \left(\sup_{\|\eta\|_{\mathbb{R}^D} < \varepsilon^\beta} \text{Vol}\{A(\eta)\Delta B_\varepsilon(x_k)\} \right) \end{aligned}$$

Recall that if $1 < \beta \leq 3$, for any $\|\eta\|_{\mathbb{R}^D} < \varepsilon^\beta$, $A(\eta)\Delta B_\varepsilon(x_k) \subset B_{\varepsilon+3\varepsilon^\beta}(x_k) \setminus B_{\varepsilon-2\varepsilon^\beta}(x_k) \subset B_{\varepsilon+3\varepsilon^\beta}(x_k)$. Hence, if we substitute the bounds in Lemma D.5 into (27), then we conclude that when $1 < \beta \leq 3$ and ε is small enough depending on the scalar curvature of M and the second fundamental form of $\iota(M)$,

$$E_1 = E_3 + \begin{bmatrix} O(\varepsilon^{d+1+\beta}) & O(\varepsilon^{d+2+\beta} + \varepsilon^{d+2\beta}) \\ O(\varepsilon^{d+2+\beta} + \varepsilon^{d+2\beta}) & O(\varepsilon^{d+3+\beta} + \varepsilon^{d-1+3\beta}) \end{bmatrix},$$

where the top left block is a d by d matrix and the constant factors depend on d , P_M and the second fundamental form of $\iota(M)$.

When $\beta > 3$ and ε is small enough depending on the scalar curvature of M and the second fundamental form of $\iota(M)$, we have $A(\eta)\Delta B_\varepsilon \subset B_{\varepsilon+3\varepsilon^3}(x_k) \setminus B_{\varepsilon-2\varepsilon^3}(x_k)$. Hence, if we substitute the bounds in Lemma D.5 into (27), then

$$E_1 = E_3 + \begin{bmatrix} O(\varepsilon^{d+4}) & O(\varepsilon^{d+5}) \\ O(\varepsilon^{d+5}) & O(\varepsilon^{d+6}) \end{bmatrix},$$

where the top left block is a d by d matrix and the constant factors depend on d , P_M and the second fundamental form of $\iota(M)$. The statement of the lemma follows from combining the cases when $1 < \beta \leq 3$ and $\beta > 3$. \square

Lemma D.7. *Suppose ε is small enough depending on d , D , and the scalar curvature of M . Suppose $\beta > 1$, $\sigma \leq \frac{\varepsilon^\beta}{\sqrt{-4(d+5)\log\varepsilon}}$, and $\|\eta_k\|_{\mathbb{R}^D} \leq \varepsilon^\beta$. Then*

$$E_3 = \frac{|S^{d-1}|P(x_k)}{d(d+2)} \varepsilon^{d+2} \begin{bmatrix} I_{d \times d} & 0 \\ 0 & 0 \end{bmatrix} + O(\varepsilon^{d+4} + \varepsilon^{d+2\beta}),$$

where $O(\varepsilon^{d+4} + \varepsilon^{d+2\beta})$ represents a D by D matrix whose entries are of order $O(\varepsilon^{d+4} + \varepsilon^{d+2\beta})$. The constants in $O(\varepsilon^{d+4} + \varepsilon^{d+2\beta})$ depend on d , C^2 norm of P , the second fundamental form of $\iota(M)$ and its derivative and the Ricci curvature of M .

Proof.

(28)

$$\begin{aligned} E_3 &= \int_{\|\eta\|_{\mathbb{R}^D} < \varepsilon^\beta} \int_M \{\iota(x) + \eta - \eta_k\} \{\iota(x) + \eta - \eta_k\}^\top \chi_{B_\varepsilon(x_k)}(x) P(x) G_\sigma(\eta) dV d\eta \\ &= \int_{\|\eta\|_{\mathbb{R}^D} < \varepsilon^\beta} \int_M \{\iota(x)\iota(x)^\top + \eta\iota(x)^\top - \eta_k\iota(x)^\top + \iota(x)\eta^\top + \eta\eta^\top \\ &\quad - \eta_k\eta^\top - \iota(x)\eta_k^\top - \eta\eta_k^\top + \eta_k\eta_k^\top\} \chi_{B_\varepsilon(x_k)}(x) P(x) G_\sigma(\eta) dV d\eta \\ &= \int_{\|\eta\|_{\mathbb{R}^D} < \varepsilon^\beta} \int_M \{\iota(x)\iota(x)^\top - \eta_k\iota(x)^\top + \eta\eta^\top - \iota(x)\eta_k^\top + \eta_k\eta_k^\top\} \chi_{B_\varepsilon(x_k)}(x) P(x) G_\sigma(\eta) dV d\eta, \end{aligned}$$

where we use the symmetry of the region $\{\|\eta\|_{\mathbb{R}^D} < \varepsilon^\beta\}$ and the symmetry of the function $G_\sigma(\eta)$ in the last step.

When ε is small enough depending on the scalar curvature of M , by Lemma D.2, we have $\text{Vol}\{B_\varepsilon(x_k)\} \leq C_4(d)\varepsilon^d$, where $C_4(d) = 2\text{Vol}(B_1^{\mathbb{R}^d})$ is a constant only depending on d . We have

$$\begin{aligned} &\left| \int_{\|\eta\|_{\mathbb{R}^D} < \varepsilon^\beta} \int_M e_i^\top \eta \eta^\top e_j \chi_{B_\varepsilon(x_k)}(x) P(x) G_\sigma(\eta) dV d\eta \right| \\ &\leq \left| \int_{\|\eta\|_{\mathbb{R}^D} < \varepsilon^\beta} e_i^\top \eta \eta^\top e_j G_\sigma(\eta) d\eta \right| \left| \int_M \chi_{B_\varepsilon(x_k)}(x) dV P(x) \right| \\ &\leq \left| \int_{\|\eta\|_{\mathbb{R}^D} < \varepsilon^\beta} e_i^\top \eta \eta^\top e_j G_\sigma(\eta) d\eta \right| C_4(d) \varepsilon^d. \end{aligned}$$

By the symmetry of the region $\{\|\eta\|_{\mathbb{R}^D} < \varepsilon^\beta\}$ and the symmetry of the function $G_\sigma(\eta)$,

$$\int_{\|\eta\|_{\mathbb{R}^D} < \varepsilon^\beta} e_i^\top \eta \eta^\top e_j G_\sigma(\eta) d\eta = 0, \quad (i \neq j).$$

By Lemma D.3,

$$\left| \int_{\|\eta\|_{\mathbb{R}^D} < \varepsilon^\beta} e_i^\top \eta \eta^\top e_j G_\sigma(\eta) d\eta \right| \leq \sigma^2 \leq \varepsilon^{2\beta}. \quad (i = j).$$

In conclusion

$$(29) \quad \int_{\|\eta\|_{\mathbb{R}^D} < \varepsilon^\beta} \int_M \eta \eta^\top \chi_{B_\varepsilon(x_k)}(x) P(x) G_\sigma(\eta) dV d\eta = O(\varepsilon^{d+2\beta}) I_{D \times D},$$

where the constant in $O(\varepsilon^{d+2\beta})$ depends on d .

Similarly, for $1 \leq i, j \leq D$,

$$(30) \quad \int_{\|\eta\|_{\mathbb{R}^D} < \varepsilon^\beta} \int_M e_i^\top \eta_k \eta_k^\top e_j \chi_{B_\varepsilon(x_k)}(x) P(x) G_\sigma(\eta) dV d\eta = O(\varepsilon^{d+2\beta}),$$

where the constant in $O(\varepsilon^{d+2\beta})$ depends on d .

Next, we have

$$\begin{aligned} & \left| \int_{\|\eta\|_{\mathbb{R}^D} < \varepsilon^\beta} \int_M e_i^\top \iota(x) \eta_k^\top e_j \chi_{B_\varepsilon(x_k)}(x) P(x) G_\sigma(\eta) dV d\eta \right| \\ & \leq \left| \int_M e_i^\top \iota(x) \chi_{B_\varepsilon(x_k)}(x) P(x) dV \right| \left| \int_{\|\eta\|_{\mathbb{R}^D} < \varepsilon^\beta} G_\sigma(\eta) d\eta \right| \left| \eta_k^\top e_j \right| \\ & \leq \varepsilon^\beta \left| \int_M e_i^\top \iota(x) \chi_{B_\varepsilon(x_k)}(x) P(x) dV \right|. \end{aligned}$$

Based on the proof of Lemma SI.5 in [39], $|\int_M e_i^\top \iota(x) \chi_{B_\varepsilon(x_k)}(x) P(x) dV| = O(\varepsilon^{d+2})$ for $i = 1, \dots, d$, where the constant in $O(\varepsilon^{d+2})$ depends on d and the $C^{(1)}$ norm of P . $|\int_M e_i^\top \iota(x) \chi_{B_\varepsilon(x_k)}(x) P(x) dV| = O(\varepsilon^{d+2})$ for $i = d+1, \dots, D$, where the constant in $O(\varepsilon^{d+2})$ depends on d , P_M and the second fundamental form of $\iota(M)$. In conclusion, for $1 \leq i, j \leq D$,

$$(31) \quad \int_{\|\eta\|_{\mathbb{R}^D} < \varepsilon^\beta} \int_M e_i^\top \iota(x) \eta_k^\top e_j \chi_{B_\varepsilon(x_k)}(x) P(x) G_\sigma(\eta) dV d\eta = O(\varepsilon^{d+2+\beta}),$$

where the constant in $O(\varepsilon^{d+2})$ depends on d , the $C^{(1)}$ norm of P and the second fundamental form of $\iota(M)$. Next, observe that

$$(32) \quad \begin{aligned} & \int_{\|\eta\|_{\mathbb{R}^D} < \varepsilon^\beta} \int_M \eta_k \iota(x)^\top \chi_{B_\varepsilon(x_k)}(x) P(x) G_\sigma(\eta) dV d\eta \\ & = \left\{ \int_{\|\eta\|_{\mathbb{R}^D} < \varepsilon^\beta} \int_M \iota(x) \eta_k^\top \chi_{B_\varepsilon(x_k)}(x) P(x) G_\sigma(\eta) dV d\eta \right\}^\top. \end{aligned}$$

At last,

$$\begin{aligned} & \int_{\|\eta\|_{\mathbb{R}^D} < \varepsilon^\beta} \int_M \iota(x) \iota(x)^\top \chi_{B_\varepsilon(x_k)}(x) P(x) G_\sigma(\eta) dV d\eta \\ & = \int_M \iota(x) \iota(x)^\top \chi_{B_\varepsilon(x_k)}(x) P(x) dV \int_{\|\eta\|_{\mathbb{R}^D} < \varepsilon^\beta} G_\sigma(\eta) d\eta \\ & = \int_M \iota(x) \iota(x)^\top \chi_{B_\varepsilon(x_k)}(x) P(x) dV \left(1 - \int_{\|\eta\|_{\mathbb{R}^D} \geq \varepsilon^\beta} G_\sigma(\eta) d\eta \right). \end{aligned}$$

Based on the proof of Proposition 3.1 in [39],

$$\int_M \iota(x) \iota(x)^\top \chi_{B_\varepsilon(x_k)}(x) P(x) dV = \frac{|S^{d-1}| P(x_k)}{d(d+2)} \varepsilon^{d+2} \begin{bmatrix} I_{d \times d} & 0 \\ 0 & 0 \end{bmatrix} + \begin{bmatrix} O(\varepsilon^{d+4}) & O(\varepsilon^{d+4}) \\ O(\varepsilon^{d+4}) & O(\varepsilon^{d+4}) \end{bmatrix},$$

where the constant in $O(\varepsilon^{d+4})$ depends on d , C^2 norm of P , the second fundamental form of $\iota(M)$ and its derivative and the Ricci curvature of M .

Based on the assumption of the lemma, when ε is small enough based on d and D , $\frac{\varepsilon^\beta}{\sigma} \geq \sqrt{-4(d+5) \log \varepsilon} \geq 2\sqrt{2}(D-2)$. Then by Lemma D.3, $0 < \int_{\|\eta\|_{\mathbb{R}^D} \geq \varepsilon^\beta} G_\sigma(\eta) d\eta \leq \frac{2}{\Gamma(\frac{D}{2})} e^{-\frac{\varepsilon^{2\beta}}{4\sigma^2}}$. Since $\Gamma(\frac{D}{2}) > 1$, when $\varepsilon \leq \frac{1}{2}$, a straightforward calculation shows that $\sigma \leq \frac{\varepsilon^\beta}{\sqrt{-4(d+5) \log \varepsilon}}$ implies $0 < \int_{\|\eta\|_{\mathbb{R}^D} \geq \varepsilon^\beta} G_\sigma(\eta) d\eta \leq \varepsilon^2$.

In conclusion,

$$(33) \quad \begin{aligned} & \int_{\|\eta\|_{\mathbb{R}^D} < \varepsilon^\beta} \int_M \iota(x) \iota(x)^\top \chi_{B_\varepsilon(x_k)}(x) P(x) G_\sigma(\eta) dV d\eta \\ & = \frac{|S^{d-1}| P(x_k)}{d(d+2)} \varepsilon^{d+2} \begin{bmatrix} I_{d \times d} & 0 \\ 0 & 0 \end{bmatrix} + \begin{bmatrix} O(\varepsilon^{d+4}) & O(\varepsilon^{d+4}) \\ O(\varepsilon^{d+4}) & O(\varepsilon^{d+4}) \end{bmatrix}, \end{aligned}$$

where the constant in $O(\varepsilon^{d+4})$ depends on d , C^2 norm of P , the second fundamental form of $\iota(M)$ and its derivative and the Ricci curvature of M . If we substitute (29), (30), (31), (32) and (33) into (28), then we have

$$E_3 = \frac{|S^{d-1}|P(x_k)}{d(d+2)} \varepsilon^{d+2} \begin{bmatrix} I_{d \times d} & 0 \\ 0 & 0 \end{bmatrix} + O(\varepsilon^{d+4} + \varepsilon^{d+2+\beta} + \varepsilon^{d+2\beta}),$$

where $O(\varepsilon^{d+4} + \varepsilon^{d+2+\beta} + \varepsilon^{d+2\beta})$ represents a D by D matrix whose entries are of order $O(\varepsilon^{d+4} + \varepsilon^{d+2+\beta} + \varepsilon^{d+2\beta})$. The constants in $O(\varepsilon^{d+4} + \varepsilon^{d+2+\beta} + \varepsilon^{d+2\beta})$ depend on d , C^2 norm of P , the second fundamental form of $\iota(M)$ and its derivative and the Ricci curvature of M . Observe that if $\beta > 2$, then $\varepsilon^{d+4} + \varepsilon^{d+2+\beta} + \varepsilon^{d+2\beta}$ is bounded by $3\varepsilon^{d+4}$. If $\beta \leq 2$, then $\varepsilon^{d+4} + \varepsilon^{d+2+\beta} + \varepsilon^{d+2\beta}$ is bounded by $3\varepsilon^{d+2\beta}$. The statement of the lemma follows. \square

D.2. Proof of Proposition D.1. Observe that

$$\mathbb{E}[\{\iota(\mathbb{X}) + \mathbb{H} - \eta_k\} \{\iota(\mathbb{X}) + \mathbb{H} - \eta_k\}^\top \chi\left(\frac{\|\iota(\mathbb{X}) + \mathbb{H} - \eta_k\|_{\mathbb{R}^D}}{\varepsilon}\right)] = E_1 + E_2 = E_3 + (E_1 - E_3) + E_2.$$

By combining Lemmas D.4, D.6 and D.7, we have

$$C_\varepsilon(y_k) = \varepsilon^{d+2} \frac{|S^{d-1}|P(x_k)}{d(d+2)} \begin{bmatrix} I_{d \times d} & 0 \\ 0 & 0 \end{bmatrix} + \begin{bmatrix} O(\varepsilon^{d+1+\beta} + \varepsilon^{d+2\beta} + \varepsilon^{d+4}) & O(\varepsilon^{d+2+\beta} + \varepsilon^{d+2\beta} + \varepsilon^{d+4}) \\ O(\varepsilon^{d+2+\beta} + \varepsilon^{d+2\beta} + \varepsilon^{d+4}) & O(\varepsilon^{d+3+\beta} + \varepsilon^{d-1+3\beta} + \varepsilon^{d+2\beta} + \varepsilon^{d+4}) \end{bmatrix},$$

where the constant factors in all the blocks depend on d , C^2 norm of P , the second fundamental form of $\iota(M)$ and its derivative and the Ricci curvature of M . Since $1 < \beta$, we have $\varepsilon^{d+2\beta} < \varepsilon^{d+1+\beta}$, $\varepsilon^{d+3+\beta} < \varepsilon^{d+4}$ and $\varepsilon^{d-1+3\beta} < \varepsilon^{d+2\beta}$. If $\beta > 2$, then $\varepsilon^{d+4} + \varepsilon^{d+2+\beta} + \varepsilon^{d+2\beta}$ is bounded by $3\varepsilon^{d+4}$. If $\beta \leq 2$, then $\varepsilon^{d+4} + \varepsilon^{d+2+\beta} + \varepsilon^{d+2\beta}$ is bounded by $3\varepsilon^{d+2\beta}$. Hence

$$C_\varepsilon(y_k) = \varepsilon^{d+2} \frac{|S^{d-1}|P(x_k)}{d(d+2)} \begin{bmatrix} I_{d \times d} & 0 \\ 0 & 0 \end{bmatrix} + \begin{bmatrix} O(\varepsilon^{d+1+\beta} + \varepsilon^{d+4}) & O(\varepsilon^{d+2\beta} + \varepsilon^{d+4}) \\ O(\varepsilon^{d+2\beta} + \varepsilon^{d+4}) & O(\varepsilon^{d+2\beta} + \varepsilon^{d+4}) \end{bmatrix}.$$

APPENDIX E. PROOF OF THEOREM 3.1 AND THEOREM 3.2

E.1. Preliminary lemmas. Suppose $U, V \in \mathbb{R}^{m \times n}$. Recall that the Hadamard product of U and V is defined as $(U \circ V)_{ij} = U_{ij}V_{ij}$ for $1 \leq i \leq m$ and $1 \leq j \leq n$. Then $U^{(2)} = U \circ U$ is the Hadamard square of U . We start by considering the second moment of the local covariance matrix:

$$\mathbb{E}\left(\left[\{\iota(\mathbb{X}) + \mathbb{H} - \eta_k\} \{\iota(\mathbb{X}) + \mathbb{H} - \eta_k\}^\top\right]^{(2)} \chi\left\{\frac{\|\iota(\mathbb{X}) + \mathbb{H} - \eta_k\|_{\mathbb{R}^D}}{\varepsilon}\right\}\right)$$

Next, we define the following matrices E_4 and E_5 to simplify our discussion:

$$F_2\{\iota(x), \eta, \eta_k\} = \left[\{\iota(x) + \eta - \eta_k\} \{\iota(x) + \eta - \eta_k\}^\top\right]^{(2)} \chi\left\{\frac{\|\iota(x) + \eta - \eta_k\|_{\mathbb{R}^D}}{\varepsilon}\right\},$$

$$E_4 = \int_{\|\eta\|_{\mathbb{R}^D} < \varepsilon^\beta} \int_M F_2\{\iota(x), \eta, \eta_k\} P(x) G_\sigma(\eta) dV d\eta,$$

$$E_5 = \int_{\|\eta\|_{\mathbb{R}^D} \geq \varepsilon^\beta} \int_M F_2\{\iota(x), \eta, \eta_k\} P(x) G_\sigma(\eta) dV d\eta.$$

Note that for $1 \leq i, j \leq D$,

$$e_i^\top E_5 e_j = \int_{\|\eta\|_{\mathbb{R}^D} \geq \varepsilon^\beta} \int_M [e_i^\top \{\iota(x) + \eta - \eta_k\}]^2 [\{\iota(x) + \eta - \eta_k\}^\top e_j]^2 \times \chi\left\{\frac{\|\iota(x) + \eta - \eta_k\|_{\mathbb{R}^D}}{\varepsilon}\right\} P(x) G_\sigma(\eta) dV d\eta.$$

When $\|\iota(x) + \eta - \eta_k\|_{\mathbb{R}^D} \leq \varepsilon$, $\chi\left\{\frac{\|\iota(x) + \eta - \eta_k\|_{\mathbb{R}^D}}{\varepsilon}\right\} \leq 1$. When $\|\iota(x) + \eta - \eta_k\|_{\mathbb{R}^D} > \varepsilon$, $\chi\left\{\frac{\|\iota(x) + \eta - \eta_k\|_{\mathbb{R}^D}}{\varepsilon}\right\} = 0$. Hence, for all $1 \leq i, j \leq D$ and all x , we have

$$[e_i^\top \{\iota(x) + \eta - \eta_k\}]^2 [\{\iota(x) + \eta - \eta_k\}^\top e_j]^2 \chi\left\{\frac{\|\iota(x) + \eta - \eta_k\|_{\mathbb{R}^D}}{\varepsilon}\right\} \leq \varepsilon^4.$$

By applying the same argument as Lemma D.4, we have the following lemma about E_5 .

Lemma E.1. *Suppose ε is small enough depending on d and D . For $\beta > 1$, if $\sigma \leq \frac{\varepsilon^\beta}{\sqrt{-4(d+5)\log\varepsilon}}$, then $|e_i^\top E_5 e_j| \leq \varepsilon^{d+8}$ for all $1 \leq i, j \leq D$.*

Now we are ready to bound the second moment of the local covariance matrix.

Lemma E.2. *Suppose ε is small enough depending on d , D , the scalar curvature of M and the second fundamental form of $\iota(M)$. Suppose $\beta > 1$, $\sigma \leq \frac{\varepsilon^\beta}{\sqrt{-4(d+5)\log\varepsilon}}$, and $\|\eta_k\|_{\mathbb{R}^D} \leq \varepsilon^\beta$, then*

$$\begin{aligned} & \mathbb{E}\left([\{\iota(\mathbb{X}) + \mathbb{H} - \eta_k\} \{\iota(\mathbb{X}) + \mathbb{H} - \eta_k\}^\top]^{(2)} \chi\left\{\frac{\|\iota(\mathbb{X}) + \mathbb{H} - \eta_k\|_{\mathbb{R}^D}}{\varepsilon}\right\}\right) \\ &= \begin{bmatrix} O(\varepsilon^{d+4}) & O(\varepsilon^{d+6} + \varepsilon^{d+2+2\beta}) \\ O(\varepsilon^{d+6} + \varepsilon^{d+2+2\beta}) & O(\varepsilon^{d+8} + \varepsilon^{d+4\beta}) \end{bmatrix}, \end{aligned}$$

where the top left block is a d by d matrix and the constant factors in all blocks depend on d , P_M and the second fundamental form of $\iota(M)$.

Proof. Recall that $B_r(x)$ is a geodesic ball of radius r centered at $x \in M$. Let $A(\eta) = \{x \in M \mid \|\iota(x) + \eta - \eta_k\|_{\mathbb{R}^D} \leq \varepsilon \text{ for a fixed } \|\eta\|_{\mathbb{R}^D} < \varepsilon^\beta\}$. Since $\|\eta\|_{\mathbb{R}^D} < \varepsilon^\beta$ and $\|\eta_k\|_{\mathbb{R}^D} \leq \varepsilon^\beta$, by the triangle inequality, if $x \in A(\eta)$, then $\varepsilon - 2\varepsilon^\beta \leq \|\iota(x)\|_{\mathbb{R}^D} \leq \varepsilon + 2\varepsilon^\beta$. If $1 < \beta \leq 3$, when ε is small enough depending on the second fundamental form of $\iota(M)$, by Lemma D.1, we have $d(x, x_k) < \varepsilon + 3\varepsilon^\beta$. Hence, $A(\eta) \subset B_{\varepsilon+3\varepsilon^\beta}(x_k)$. Since $1 < \beta \leq 3$, when ε is small enough depending on the scalar curvature of M , by Lemma D.2, for all $\|\eta\|_{\mathbb{R}^D} < \varepsilon^\beta$, we have

$$\text{Vol}\{A(\eta)\} \leq \text{Vol}\{B_{\varepsilon+3\varepsilon^\beta}(x_k)\} \leq 4^d \text{Vol}(B_1^{\mathbb{R}^d}) \varepsilon^d = C_5(d) \varepsilon^d,$$

where $C_5(d) = 4^d \text{Vol}(B_1^{\mathbb{R}^d})$ is a constant depending on d . Similarly, if $\beta > 3$ and ε is small enough depending on the second fundamental form of $\iota(M)$ and the scalar curvature of M , then we have $A(\eta) \subset B_{\varepsilon+3\varepsilon^3}(x_k)$ and $\text{Vol}\{A(\eta)\} \leq C_5(d) \varepsilon^d$.

Observe that for a fixed η , we have $\chi_{A(\eta)}(x) = \chi\left\{\frac{\|\iota(x) + \eta - \eta_k\|_{\mathbb{R}^D}}{\varepsilon}\right\}$.

Let $Q_{ij}(x, \eta, \eta_k) = [e_i^\top \{\iota(x) + \eta - \eta_k\}]^2 [\{\iota(x) + \eta - \eta_k\}^\top e_j]^2$, then

$$\begin{aligned} (34) \quad |e_i^\top E_4 e_j| &= \left| \int_{\|\eta\|_{\mathbb{R}^D} < \varepsilon^\beta} \int_M e_i^\top F_2 \{\iota(x), \eta, \eta_k\} e_j P(x) G_\sigma(\eta) dV d\eta \right| \\ &= \int_{\|\eta\|_{\mathbb{R}^D} < \varepsilon^\beta} \int_M Q_{ij}(x, \eta, \eta_k) \chi_{A(\eta)}(x) P(x) G_\sigma(\eta) dV d\eta \\ &\leq \sup_{\|\eta\|_{\mathbb{R}^D} < \varepsilon^\beta, x \in A(\eta)} Q_{ij}(x, \eta, \eta_k) \int_{\|\eta\|_{\mathbb{R}^D} < \varepsilon^\beta} \int_M \chi_{A(\eta)}(x) P(x) G_\sigma(\eta) dV d\eta \\ &\leq \sup_{\|\eta\|_{\mathbb{R}^D} < \varepsilon^\beta, x \in A(\eta)} Q_{ij}(x, \eta, \eta_k) P_M \sup_{\|\eta\|_{\mathbb{R}^D} < \varepsilon^\beta} \text{Vol}\{A(\eta)\} \\ &\leq \sup_{\|\eta\|_{\mathbb{R}^D} < \varepsilon^\beta, x \in A(\eta)} Q_{ij}(x, \eta, \eta_k) P_M C_5(d) \varepsilon^d. \end{aligned}$$

If $1 < \beta \leq 3$ and $\|\eta\|_{\mathbb{R}^D} < \varepsilon^\beta$, then $x \in A(\eta) \subset B_{\varepsilon+3\varepsilon^\beta}(x_k)$. By Lemma D.5, when ε is small enough depending on the second fundamental form of $\iota(M)$, for any $\|\eta\|_{\mathbb{R}^D} < \varepsilon^\beta$, $\|\eta_k\|_{\mathbb{R}^D} \leq \varepsilon^\beta$ and $x \in B_{\varepsilon+3\varepsilon^\beta}(x_k)$, we have

$$\begin{aligned} Q_{ij}(x, \eta, \eta_k) &\leq (49)^2 \varepsilon^4, \quad (1 \leq i, j \leq d), \\ Q_{ij}(x, \eta, \eta_k) &\leq C_3^2 (\varepsilon^3 + \varepsilon^{1+\beta})^2 \leq 2C_3^2 (\varepsilon^6 + \varepsilon^{2+2\beta}), \quad (1 \leq i \leq d; d+1 \leq j \leq D), \\ Q_{ij}(x, \eta, \eta_k) &\leq C_3^2 (\varepsilon^3 + \varepsilon^{1+\beta})^2 \leq 2C_3^2 (\varepsilon^6 + \varepsilon^{2+2\beta}), \quad (d+1 \leq i \leq D; 1 \leq j \leq d), \\ Q_{ij}(x, \eta, \eta_k) &\leq C_3^2 (\varepsilon^4 + \varepsilon^{2\beta})^2 \leq 2C_3^2 (\varepsilon^8 + \varepsilon^{4\beta}), \quad (d+1 \leq i, j \leq D), \end{aligned}$$

where C_3 is a constant depending on the second fundamental form of $\iota(M)$. Therefore, we can substitute the above bounds into (34). We conclude that when ε is small enough depending on the scalar curvature of M and the second fundamental form of $\iota(M)$,

$$E_4 = \begin{bmatrix} O(\varepsilon^{d+4}) & O(\varepsilon^{d+6} + \varepsilon^{d+2+2\beta}) \\ O(\varepsilon^{d+6} + \varepsilon^{d+2+2\beta}) & O(\varepsilon^{d+8} + \varepsilon^{d+4\beta}) \end{bmatrix},$$

where the top left block is a d by d matrix and the constant factors depend on d , P_M and the second fundamental form of $\iota(M)$.

If $\beta > 3$ and $\|\eta\|_{\mathbb{R}^D} < \varepsilon^\beta$, then $x \in A(\eta) \subset B_{\varepsilon+3\varepsilon^3}(x_k)$. By Lemma D.5, when ε is small enough depending on the second fundamental form of $\iota(M)$, for any $\|\eta\|_{\mathbb{R}^D} < \varepsilon^\beta$, $\|\eta_k\|_{\mathbb{R}^D} \leq \varepsilon^\beta$ and $x \in B_{\varepsilon+3\varepsilon^3}(x_k)$, we have

$$\begin{aligned} Q_{ij}(x, \eta, \eta_k) &\leq (49)^2 \varepsilon^4, \quad (1 \leq i, j \leq d), \\ Q_{ij}(x, \eta, \eta_k) &\leq 4C_3^2 \varepsilon^6, \quad (1 \leq i \leq d; d+1 \leq j \leq D), \\ Q_{ij}(x, \eta, \eta_k) &\leq 4C_3^2 \varepsilon^6, \quad (d+1 \leq i \leq D; 1 \leq j \leq d), \\ Q_{ij}(x, \eta, \eta_k) &\leq 4C_3^2 \varepsilon^8, \quad (d+1 \leq i, j \leq D), \end{aligned}$$

where C_3 is a constant depending on the second fundamental form of $\iota(M)$. Therefore, we can substitute the above bounds into (34). We conclude that when ε is small enough depending on the scalar curvature of M and the second fundamental form of $\iota(M)$,

$$E_4 = \begin{bmatrix} O(\varepsilon^{d+4}) & O(\varepsilon^{d+6}) \\ O(\varepsilon^{d+6}) & O(\varepsilon^{d+8}) \end{bmatrix},$$

where the top left block is a d by d matrix and the constant factors depend on d , P_M and the second fundamental form of $\iota(M)$. Since

$$\mathbb{E} \left(\left[\{ \iota(\mathbb{X}) + \mathbb{H} - \eta_k \} \{ \iota(\mathbb{X}) + \mathbb{H} - \eta_k \}^\top \right]^{(2)} \chi \left\{ \frac{\| \iota(\mathbb{X}) + \mathbb{H} - \eta_k \|_{\mathbb{R}^D}}{\varepsilon} \right\} \right) = E_4 + E_5,$$

this lemma follows from combining the cases when $1 < \beta \leq 3$ and $\beta > 3$ with Lemma E.1. \square

E.2. Proof of Theorem 3.1. When ε is small enough based on d and D , $\frac{\varepsilon^\beta}{\sigma} \geq \sqrt{-4(d+5) \log \varepsilon} \geq 2\sqrt{2}(D-2)$. Thus, we are allowed to apply Lemma D.3 to bound $\text{pr}(\|\eta_i\|_{\mathbb{R}^D} \geq \varepsilon^\beta)$. For a fixed i , $\text{pr}(\|\eta_i\|_{\mathbb{R}^D} \geq \varepsilon^\beta) \leq \frac{2}{\Gamma(\frac{D}{2})} e^{-\frac{\varepsilon^{2\beta}}{4\sigma^2}} \leq 2e^{-\frac{\varepsilon^{2\beta}}{4\sigma^2}}$, where we use $\frac{2}{\Gamma(\frac{D}{2})} \leq 2$ in the last step.

If $\sigma \leq \frac{\varepsilon^\beta}{\sqrt{12 \log(2n)}}$, then by a straightforward calculation, we have

$$\text{pr}(\|\eta_i\|_{\mathbb{R}^D} \geq \varepsilon^\beta) \leq 2e^{-\frac{\varepsilon^{2\beta}}{4\sigma^2}} \leq \frac{1}{4n^3}.$$

Since $\{\eta_i\}_{i=1}^n$ are i.i.d. samples, by a straightforward union bound, we have

$$\Pr(\|\eta_i\|_{\mathbb{R}^D} \leq \varepsilon^\beta | i = 1, \dots, n) \geq 1 - \frac{1}{4n^2}.$$

Suppose $\|\eta_k\|_{\mathbb{R}^D} \leq \varepsilon^\beta$. Since $y_k = \iota(x_k) + \eta_k$ with $\iota(x_k) = 0$, for each $a, b = 1, \dots, D$, we denote

$$\begin{aligned} F_{a,b,i,k} &= e_a^\top (y_i - y_k)(y_i - y_k)^\top e_b \chi\left(\frac{\|y_i - y_k\|_{\mathbb{R}^D}}{\varepsilon}\right) \\ &= e_a^\top \{\iota(x_i) + \eta_i - \eta_k\} \{\iota(x_i) + \eta_i - \eta_k\}^\top e_b \chi\left\{\frac{\|\iota(x_i) + \eta_i - \eta_k\|_{\mathbb{R}^D}}{\varepsilon}\right\} \end{aligned}$$

$\{F_{a,b,i,k}\}$ for $i = 1, \dots, n$ and $i \neq k$ are independent and identically distributed realizations of

$$F_{a,b,k} = e_a^\top \{\iota(\mathbb{X}) + \mathbb{H} - \eta_k\} \{\iota(\mathbb{X}) + \mathbb{H} - \eta_k\}^\top e_b \chi\left\{\frac{\|\iota(\mathbb{X}) + \mathbb{H} - \eta_k\|_{\mathbb{R}^D}}{\varepsilon}\right\}.$$

If $\|\iota(x) + \eta - \eta_k\|_{\mathbb{R}^D} \leq \varepsilon$, then $\chi\left\{\frac{\|\iota(x) + \eta - \eta_k\|_{\mathbb{R}^D}}{\varepsilon}\right\} = 1$, $|e_a^\top \{\iota(x) + \eta - \eta_k\}| \leq \varepsilon$ and $|\{\iota(x) + \eta - \eta_k\}^\top e_b| \leq \varepsilon$. Hence, $|F_{a,b,k}|$ is uniformly bounded by $c = \varepsilon^2$, for all $1 \leq a, b \leq D$.

By Proposition D.1, when ε is small enough depending on d, D , the second fundamental form of $\iota(M)$ and the scalar curvature of M ,

$$\begin{aligned} & \mathbb{E}\left[\{\iota(\mathbb{X}) + \mathbb{H} - \eta_k\} \{\iota(\mathbb{X}) + \mathbb{H} - \eta_k\}^\top \chi\left\{\frac{\|\iota(\mathbb{X}) + \mathbb{H} - \eta_k\|_{\mathbb{R}^D}}{\varepsilon}\right\}\right] \\ &= \varepsilon^{d+2} \left(\frac{|\mathcal{S}^{d-1}| P(x_k)}{d(d+2)} \begin{bmatrix} I_{d \times d} & 0 \\ 0 & 0 \end{bmatrix} + \begin{bmatrix} O(\varepsilon^{\beta-1} + \varepsilon^2) & O(\varepsilon^{2\beta-2} + \varepsilon^2) \\ O(\varepsilon^{2\beta-2} + \varepsilon^2) & O(\varepsilon^{2\beta-2} + \varepsilon^2) \end{bmatrix} \right), \end{aligned}$$

where the constant factors in the four blocks depend on d, C^2 norm of P , the second fundamental form of $\iota(M)$ and its derivative and the Ricci curvature of M . Let

$$\begin{aligned} \Omega &= \mathbb{E}\left(\left[\{\iota(\mathbb{X}) + \mathbb{H} - \eta_k\} \{\iota(\mathbb{X}) + \mathbb{H} - \eta_k\}^\top\right]^{(2)} \chi\left\{\frac{\|\iota(\mathbb{X}) + \mathbb{H} - \eta_k\|_{\mathbb{R}^D}}{\varepsilon}\right\}\right) \\ &\quad - \left(\mathbb{E}\left[\{\iota(\mathbb{X}) + \mathbb{H} - \eta_k\} \{\iota(\mathbb{X}) + \mathbb{H} - \eta_k\}^\top \chi\left\{\frac{\|\iota(\mathbb{X}) + \mathbb{H} - \eta_k\|_{\mathbb{R}^D}}{\varepsilon}\right\}\right]\right)^{(2)}. \end{aligned}$$

The variance of the random variable $F_{a,b,k}$ is $e_a^\top \Omega e_b$. By combining Proposition D.1 and Lemma E.2,

$$e_a^\top \Omega e_b \leq C_6 \varepsilon^{d+4} \quad (1 \leq a, b \leq d).$$

If $d < a \leq D$ or $d < b \leq D$,

$$e_a^\top \Omega e_b \leq C_6 (\varepsilon^{d+6} + \varepsilon^{d+2+2\beta}).$$

C_6 is a constant depending on d, C^2 norm of P , the second fundamental form of $\iota(M)$ and its derivative and the Ricci curvature of M .

Observe that

$$e_a^\top C_{n,\varepsilon}(y_k) e_b = \frac{1}{n} \sum_{i=1}^n F_{a,b,i,k} = \frac{n-1}{n} \left(\frac{1}{n-1} \sum_{i \neq k, i=1}^n F_{a,b,i,k} \right).$$

Since $\frac{n-1}{n} \rightarrow 1$ as $n \rightarrow \infty$, the error incurred by replacing $\frac{1}{n}$ by $\frac{1}{n-1}$ is of order $\frac{1}{n}$, which is negligible asymptotically. Thus, we can simply focus on analyzing $\frac{1}{n-1} \sum_{i \neq k, i=1}^n F_{a,b,i,k}$. By Bernstein's inequality,

$$\Pr\left\{\left|\frac{1}{n-1} \sum_{i \neq k, i=1}^n F_{a,b,i,k} - \mathbb{E}(F_{a,b,k})\right| > \gamma\right\} \leq \exp\left\{-\frac{(n-1)\gamma^2}{2e_a^\top \Omega e_b + \frac{2}{3}c\gamma}\right\} \leq \exp\left(-\frac{n\gamma^2}{4e_a^\top \Omega e_b + \frac{4}{3}c\gamma}\right).$$

For fixed a, b with $1 \leq a, b \leq d$, we choose γ_1 so that $\frac{\gamma_1}{\varepsilon^{d+2}} \rightarrow 0$ as $\varepsilon \rightarrow 0$, then we have $4e_a^\top \Omega e_b + \frac{4}{3}c\gamma_1 \leq (4C_6 + 2)\varepsilon^{d+4}$. Hence,

$$\exp\left(-\frac{n\gamma_1^2}{4e_a^\top \Omega e_b + \frac{4}{3}c\gamma_1}\right) \leq \exp(-C_7 n \gamma_1^2 \varepsilon^{-d-4}),$$

where $C_7 = \frac{1}{4C_6 + 2}$.

For fixed a, b with $d+1 \leq a \leq D$ or $d+1 \leq b \leq D$, we choose γ_2 so that $\frac{\gamma_2}{\varepsilon^{d+2\beta} + \varepsilon^{d+4}} \rightarrow 0$ as $\varepsilon \rightarrow 0$, then we have $4e_a^\top \Omega e_b + \frac{4}{3}c\gamma_2 \leq (4C_6 + 2)(\varepsilon^{d+2+2\beta} + \varepsilon^{d+6}) \leq (8C_6 + 4)\varepsilon^{d+2+\min(4,2\beta)}$. Hence,

$$\exp\left(-\frac{n\gamma_2^2}{4e_a^\top \Omega e_b + \frac{4}{3}c\gamma_2}\right) \leq \exp\left(-\frac{C_7}{2}n\gamma_2^2 \varepsilon^{-d-2-\min(4,2\beta)}\right).$$

If $\gamma_1 = C_8 \sqrt{\frac{\log(n)\varepsilon^{d+4}}{n}}$ and $\gamma_2 = C_9 \sqrt{\frac{\log(n)\varepsilon^{d+2+\min(4,2\beta)}}{n}}$ for some constants C_8 and C_9 depending on C_7 and D , then $\exp(-C_7 n \gamma_1^2 \varepsilon^{-d-4}) = \frac{1}{4D^2 n^3}$ and $\exp(-\frac{C_7}{2}n\gamma_2^2 \varepsilon^{-d-2-\min(4,2\beta)}) = \frac{1}{4D^2 n^3}$. Hence, for fixed a, b , we have

$$\Pr\left\{\left|\frac{1}{n-1} \sum_{i \neq k, i=1}^n F_{a,b,i,k} - \mathbb{E}(F_{a,b,k})\right| > C_8 \sqrt{\frac{\log(n)\varepsilon^{d+4}}{n}}\right\} \leq \frac{1}{4D^2 n^3} \quad (1 \leq a, b \leq d).$$

If $d < a \leq D$ or $d < b \leq D$,

$$\Pr\left\{\left|\frac{1}{n-1} \sum_{i \neq k, i=1}^n F_{a,b,i,k} - \mathbb{E}(F_{a,b,k})\right| > C_9 \sqrt{\frac{\log(n)\varepsilon^{d+2+\min(4,2\beta)}}{n}}\right\} \leq \frac{1}{4D^2 n^3}.$$

By considering the conditional probability such that $\|\eta_k\|_{\mathbb{R}^D} \leq \varepsilon^\beta$ for $k = 1, \dots, n$ and taking a trivial union bound for all $1 \leq a, b \leq D$ and $1 \leq k \leq n$, we conclude that for all x_k with probability greater than $1 - \frac{1}{n^2}$

$$|e_a^\top C_{n,\varepsilon}(y_k) e_b - \mathbb{E}(F_{a,b,k})| < C_8 \sqrt{\frac{\log(n)\varepsilon^{d+4}}{n}} \quad (1 \leq a, b \leq d).$$

If $d < a \leq D$ or $d < b \leq D$,

$$|e_a^\top C_{n,\varepsilon}(y_k) e_b - \mathbb{E}(F_{a,b,k})| < C_9 \sqrt{\frac{\log(n)\varepsilon^{d+2+\min(4,2\beta)}}{n}}.$$

The conclusion of the proposition follows.

E.3. Proof of Theorem 3.2. For any $\beta > 1$, suppose ε is small enough depending on d, D , the second fundamental form of $\iota(M)$ and the scalar curvature of M . We apply Theorem 3.1. In the conclusion of Theorem 3.1, note that $\sqrt{\frac{\log n}{n\varepsilon^d}} \leq \varepsilon^{\min(\beta-1,1)}$ is equivalent to $\frac{\log n}{n} \leq \varepsilon^{d+2\min(\beta-1,1)}$ and $\sqrt{\frac{\log n}{n\varepsilon^{d-2\min(\beta-1,1)}}} \leq \varepsilon^{2\min(\beta-1,1)}$ is equivalent to $\frac{\log n}{n} \leq \varepsilon^{d+2\min(\beta-1,1)}$. Hence, if $\varepsilon^{-d-2\min(\beta-1,1)} \leq \frac{n}{\log n}$ and $\sigma \leq \min\left(\frac{1}{\sqrt{-4(d+5)\log \varepsilon}}, \frac{1}{\sqrt{12\log(2n)}}\right)\varepsilon^\beta$, then for all x_k , with probability greater than $1 - \frac{1}{n^2}$,

$$C_{n,\varepsilon}(y_k) = \varepsilon^{d+2} \left(\frac{|S^{d-1}|P(x_k)}{d(d+2)} \begin{bmatrix} I_{d \times d} & 0 \\ 0 & 0 \end{bmatrix} + \begin{bmatrix} O(\varepsilon^{\min(\beta-1,1)}) & O(\varepsilon^{2\min(\beta-1,1)}) \\ O(\varepsilon^{2\min(\beta-1,1)}) & O(\varepsilon^{2\min(\beta-1,1)}) \end{bmatrix} \right),$$

where the constant factors depend on d , C^2 norm of P , the second fundamental form of $\iota(M)$ and its derivative and the Ricci curvature of M . Hence,

$$C_{n,\varepsilon}(y_k) = \varepsilon^{d+2} \frac{|S^{d-1}|P(x_k)}{d(d+2)} \left(\begin{bmatrix} I_{d \times d} + E_1 & 0 \\ 0 & 0 \end{bmatrix} + \begin{bmatrix} E_2 & E_3 \\ E_4 & E_5 \end{bmatrix} \right),$$

where the entries of E_1 are bounded by $C_{10}\varepsilon^{\min(\beta-1,1)}$ and the entries of E_2, E_3, E_4 and E_5 are bounded by $C_{10}\varepsilon^{2\min(\beta-1,1)}$. C_{10} depends on d, P_m, C^2 norm of P , the second fundamental form of $\iota(M)$ and its derivative and the Ricci curvature of M .

The scalar curvature is the trace of the Ricci curvature tensor. We will simplify any dependence on the scalar curvature by the dependence on d and the Ricci curvature. Note that the operator norms of E_1 and $\begin{bmatrix} E_2 & E_3 \\ E_4 & E_5 \end{bmatrix}$ can be bounded by $dC_{10}\varepsilon^{\min(\beta-1,1)}$ and $DC_{10}\varepsilon^{2\min(\beta-1,1)}$ respectively. Therefore, if we further require that ε is small enough depending on β, d, D, P_m, C^2 norm of P , the second fundamental form of $\iota(M)$ and its derivative and the Ricci curvature of M , then the operator norms of E_1 and $\begin{bmatrix} E_2 & E_3 \\ E_4 & E_5 \end{bmatrix}$ are bounded by $\frac{1}{3}$. Since $\begin{bmatrix} I_{d \times d} + E_1 & 0 \\ 0 & 0 \end{bmatrix}$ and $\begin{bmatrix} E_2 & E_3 \\ E_4 & E_5 \end{bmatrix}$ are symmetric matrices, based on Weyl's theorem, all the eigenvalues of $I_{d \times d} + E_1$ and the first d largest eigenvalues of $\begin{bmatrix} I_{d \times d} + E_1 & 0 \\ 0 & 0 \end{bmatrix} + \begin{bmatrix} E_2 & E_3 \\ E_4 & E_5 \end{bmatrix}$ are bounded below by $\frac{2}{3}$ and the remaining $D-d$ eigenvalues of $\begin{bmatrix} I_{d \times d} + E_1 & 0 \\ 0 & 0 \end{bmatrix} + \begin{bmatrix} E_2 & E_3 \\ E_4 & E_5 \end{bmatrix}$ are bounded above by $\frac{1}{3}$. Consider the eigen decomposition of $C_{n,\varepsilon}(y_k)$ as $C_{n,\varepsilon}(y_k) = U_{n,\varepsilon}(y_k)\Lambda_{n,\varepsilon}(y_k)U_{n,\varepsilon}(y_k)^\top$ with $U_{n,\varepsilon}(y_k) \in \mathbb{O}(D)$. Then, by Davis-Kahan theorem

$$U_{n,\varepsilon}(y_k) = \begin{bmatrix} X_1 & 0 \\ 0 & X_2 \end{bmatrix} + O(\varepsilon^{2\min(\beta-1,1)}),$$

where $X_1 \in \mathbb{O}(d), X_2 \in \mathbb{O}(D-d)$. $O(\varepsilon^{2\min(\beta-1,1)})$ represent a D by D matrix whose entries are of order $O\{\varepsilon^{2\min(\beta-1,1)}\}$, where the constant factors depend on d, D, P_m, C^2 norm of P , the second fundamental form of $\iota(M)$ and its derivative and the Ricci curvature of M .

APPENDIX F. PROOF OF THEOREM 3.3

We first define a map from \mathbb{R}^D to \mathbb{R}^d generalizing the map $\mathcal{P}_{y_k}(y)$.

Definition F.1. Fix $x \in M$. Suppose $U \in \mathbb{O}(D)$. For any vector $a \in \mathbb{R}^D$, we define a projection map for $y \in \mathbb{R}^D$ associated with the first d column vectors of U :

$$\mathcal{P}_{U,\iota(x)+a}(y) = J^\top U^\top \{y - \iota(x) - a\}.$$

Based on the above definition, $\mathcal{P}_{y_k}(y) = \mathcal{P}_{U_{n,\varepsilon,\iota(x_k)} + \eta_k}(y)$. We show that, under suitable conditions on a and U , the map $\mathcal{P}_{U,\iota(x)+a}(y)$ is a local diffeomorphism when it is restricted on $\iota(M)$. Intuitively, for any $x \in M$, if we have a d dimension subspace of \mathbb{R}^D which does not deviate too far away from the tangent space $T_{\iota(x)}\iota(M)$, then for any point $\iota(x) + a \in \mathbb{R}^D$ that remains close to $\iota(x)$ and any y around $\iota(x) + a$ on $\iota(M)$, the projection of $y - \iota(x) - a$ onto the subspace is a diffeomorphism. Hence, the map $\mathcal{P}_{U,\iota(x)+a}(y)$ can be used to construct a chart. Our next proposition formalizes this argument and serves as a key component in proving Theorem 3.3.

Before we state the proposition. We make the following observation. For any $y \in \iota(M)$, the map $\mathcal{P}_{U,\iota(x)+a}(y)$ is invariant under translations of the manifold in \mathbb{R}^D : for any b , we have

$$\mathcal{P}_{U,\iota(x)+a}(y) = J^\top U^\top \{y - \iota(x) - a\} = J^\top U^\top [y + b - \{\iota(x) + b\} - a]^\top.$$

Moreover, $\mathcal{P}_{U, \iota(x)+a}(y)$ is invariant under orthogonal transformation in \mathbb{R}^D : for any $V \in \mathbb{O}(D)$,

$$\mathcal{P}_{U, \iota(x)+a}(y) = J^\top U^\top \{y - \iota(x) - a\} = J^\top U^\top V^\top V \{y - \iota(x) - a\}.$$

Hence, when we discuss the map $\mathcal{P}_{U, \iota(x)+a}(y)$, we can always translate $\iota(M)$ and apply an orthogonal transformation in \mathbb{R}^D so that $\iota(x) = 0 \in \mathbb{R}^D$ and $T_{\iota(x)}\iota(M)$ is generated by $\{e_i\}_{i=1}^d$.

Proposition F.1. *For $x \in M$, suppose we translate $\iota(M)$ and apply an orthogonal transformation in \mathbb{R}^D so that $\iota(x) = 0 \in \mathbb{R}^D$ and $\{Xe_i\}_{i=1}^d$ form a basis of $T_{\iota(x)}\iota(M)$ where $X = \begin{bmatrix} X_1 & 0 \\ 0 & X_2 \end{bmatrix} \in \mathbb{O}(D)$ with $X_1 \in \mathbb{O}(d)$ and $X_2 \in \mathbb{O}(D-d)$. Suppose $U \in \mathbb{O}(D)$ and $E = U - X$ with $|E_{ij}| < r$. For any $0 < \xi \leq \frac{3\tau_{\iota(M)}}{16}$ and $r \leq \frac{1}{30d^{\frac{3}{2}}}$, if $\|a\|_{\mathbb{R}^D} < \frac{\xi}{3}$, then we have the following facts:*

- (1) $\mathcal{P}_{U, \iota(x)+a}$ is a diffeomorphism from $B_{\frac{\xi}{3}}^{\mathbb{R}^D} \{\iota(x) + a\} \cap \iota(M)$ onto its image $O \subset \mathbb{R}^d$. O is homeomorphic to $B_1^{\mathbb{R}^d}(0)$.
- (2) There is a point u_0 in O such that $0 \in B_R^{\mathbb{R}^d}(u_0) \subset O \subset B_{\frac{R}{\xi}}^{\mathbb{R}^d}(0)$. Let $A = 1 - d^{\frac{3}{2}}r$ and $B = \frac{8\xi/3 + 2\|a\|_{\mathbb{R}^D}}{\tau_{\iota(M)}}$. Then $R \geq (\sqrt{A^2 - A^2B} - \sqrt{B - A^2B})(\xi - \|a\|_{\mathbb{R}^D})$.

F.1. Preliminary lemmas for the proof of Proposition F.1. In order to prove Proposition F.1, we need to define the angle between two subspaces of the same dimension in \mathbb{R}^D .

Definition F.2. *The angle $\phi_{V,W}$ between two subspaces of the same dimension in \mathbb{R}^D , V and W , is*

$$\phi_{V,W} = \max_{v \in V} \min_{w \in W} \arccos \left(\frac{|v^\top w|}{\|v\|_{\mathbb{R}^D} \|w\|_{\mathbb{R}^D}} \right).$$

Based on the definition, we have $0 \leq \phi_{V,W} \leq \frac{\pi}{2}$.

We summarize the basic properties of the angle between two subspaces of the same dimension in the following lemma.

Lemma F.1. *Suppose V, W, Z are three subspaces of the same dimension in \mathbb{R}^D . Then, we have the following properties:*

- (1) $\cos(\phi_{V,W}) = \min_{v \in V} \max_{w \in W} \frac{|v^\top w|}{\|v\|_{\mathbb{R}^D} \|w\|_{\mathbb{R}^D}}$.
- (2) If there is a vector $v \in V$ which is perpendicular to W , then $\phi_{V,W} = \frac{\pi}{2}$.
- (3) The angle is invariant under orthogonal transformation of \mathbb{R}^D . In other words, if $X \in \mathbb{O}(D)$, then $\phi_{XV, XW} = \phi_{V,W}$.
- (4) The angle is a metric on the set of all subspaces of the same dimension in \mathbb{R}^D . Specifically, we have
 - (a) (Non-negativeness) $\phi_{V,W} \geq 0$.
 - (b) (Identification) $\phi_{V,W} = 0$ implies $V = W$.
 - (c) (Symmetry) $\phi_{V,W} = \phi_{W,V}$.
 - (d) (Triangle inequality) $\phi_{V,Z} \leq \phi_{V,W} + \phi_{W,Z}$.

Proof. (1) follows from the definition and the fact that cosine is decreasing on $[0, \frac{\pi}{2}]$. (2) and (3) follow directly from the definition. A proof of (4) can be found in [38] \square

We refer the reader to [38] for more discussion about the angle between two subspaces of different dimensions. Next, we prove a lemma which bounds the angle for two sufficiently close subspaces.

Lemma F.2. *Suppose $X \in \mathbb{O}(D)$ such that $X = \begin{bmatrix} X_1 & 0 \\ 0 & X_2 \end{bmatrix}$ with $X_1 \in \mathbb{O}(d)$ and $X_2 \in \mathbb{O}(D-d)$. Suppose $U \in \mathbb{O}(D)$ such that $E = U - X$ with $|E_{ij}| < r$. Let $\{Xe_i\}_{i=1}^d$ be a basis of V and $\{Ue_i\}_{i=1}^d$ be a basis of*

W. Suppose $\phi_{V,W}$ is the angle between V and W , then $\cos(\phi_{V,W}) \geq 1 - d^{\frac{3}{2}}r$. In particular, if $r \leq \frac{1}{30d^{\frac{3}{2}}}$, then $\cos(\phi_{V,W}) \geq \frac{29}{30}$.

Proof. We write $E = \begin{bmatrix} E_1 & E_2 \\ E_3 & E_4 \end{bmatrix}$ with $E_1 \in \mathbb{R}^{d \times d}$. Let $u \in \mathbb{R}^d$ be an arbitrary unit vector. Then $\begin{bmatrix} X_1 \\ 0 \end{bmatrix} u$ is an arbitrary vector unit in V and $\begin{bmatrix} X_1 + E_1 \\ E_3 \end{bmatrix} u$ is a unit vector in W . By (1) in Lemma F.1, we have

$$\cos(\phi_{V,W}) \geq \left| u^\top [X_1^\top, 0] \begin{bmatrix} X_1 + E_1 \\ E_3 \end{bmatrix} u \right| = |u^\top X_1^\top (X_1 + E_1)u| = |1 + u^\top X_1^\top E_1 u|$$

By the Cauchy-Schwarz inequality, each entry of $X_1^\top E_1$ is bounded by \sqrt{dr} and each entry of $X_1^\top E_1 u$ is bounded by dr . Hence, $|u^\top X_1^\top E_1 u| \leq d^{\frac{3}{2}}r$. The conclusion follows. \square

Suppose $x, x' \in M$, then the next lemma describes the angle between the tangent spaces of two points $\iota(x)$ and $\iota(x')$ when they are close in the Euclidean distance. The proof is a combination of Proposition 6.2 and Proposition 6.3 in [27].

Lemma F.3. *Suppose $x, x' \in M$. Let $\phi_{V,W}$ be the angle between $V = T_{\iota(x)}\iota(M)$ and $W = T_{\iota(x')}\iota(M)$. If $\|\iota(x) - \iota(x')\| \leq \frac{\tau_{\iota(M)}}{2}$, then $\cos(\phi_{V,W}) \geq \sqrt{1 - \frac{2\|\iota(x) - \iota(x')\|}{\tau_{\iota(M)}}}$. In particular, if $\|\iota(x) - \iota(x')\| \leq \frac{\tau_{\iota(M)}}{4}$, then $\cos(\phi_{V,W}) \geq \frac{1}{\sqrt{2}}$.*

F.2. Proof of Proposition F.1. Proof of part 1 of Proposition F.1

Since we assume $\iota(x) = 0$, we express $\mathcal{P}_{U,\iota(x)+a}(y)$ as $\mathcal{P}_{U,a}(y)$ for notation simplicity. By proposition B.2, suppose we choose $0 < \xi_1 \leq \frac{\tau_{\iota(M)}}{4}$, then any $y \in B_{\xi_1}^{\mathbb{R}^D}(0) \cap \iota(M)$, $\mathcal{P}_{U,a}(y)$ can be represented in the chart as follows,

$$\mathcal{P}_{U,a}(y) = J^\top U^\top \begin{bmatrix} u \\ G_x(u) \end{bmatrix} - J^\top U^\top a,$$

where $u \in V_x \subset B_{\xi_1}^{\mathbb{R}^d}(0) \subset \mathbb{R}^d$. V_x contains 0 and is homeomorphic to $B_1^{\mathbb{R}^d}(0)$.

Since $\iota(M)$ is smooth, $\mathcal{P}_{U,a}(y)$ is smooth. By Proposition B.1, $B_{\xi_1}^{\mathbb{R}^D}(0) \cap \iota(M)$ is homeomorphic to $B_1^{\mathbb{R}^d}(0)$. Hence, we can show that $\mathcal{P}_{U,a}(y)$ is a diffeomorphism from $B_{\xi_1}^{\mathbb{R}^D}(0) \cap \iota(M)$ onto its image by applying the inverse function theorem. Note that

$$D\mathcal{P}_{U,a}(y) = J^\top U^\top \begin{bmatrix} I_{d \times d} \\ DG_x(u) \end{bmatrix}.$$

The column vectors of $\begin{bmatrix} I_{d \times d} \\ DG_x(u) \end{bmatrix}$ are a basis of the tangent space $V = T_y \iota(M)$, while the column vectors of UJ are a basis of a subspace W . Hence, $D\mathcal{P}_{U,a}(y)$ is not singular if and only if there is no vector in V that is perpendicular to W . By (2) in Lemma F.1, it is sufficient to show the angle $\phi_{V,W}$ between V and W is less than $\frac{\pi}{2}$. By Lemma F.2, if $r \leq \frac{1}{30d^{\frac{3}{2}}}$, then $\cos(\phi_{T_{\iota(x)}\iota(M),W}) \geq \frac{29}{30}$. Since $y \in B_{\xi_1}^{\mathbb{R}^D}(0) \cap \iota(M)$, by Lemma F.3, we have $\cos(\phi_{T_{\iota(x)}\iota(M),V}) \geq \frac{1}{\sqrt{2}}$. By (4) in Lemma F.1 and a straightforward calculation,

$$(35) \quad \phi_{V,W} \leq \phi_{T_{\iota(x)}\iota(M),W} + \phi_{T_{\iota(x)}\iota(M),V} \leq \alpha = \arccos\left(\frac{29}{30}\right) + \arccos\left(\frac{1}{\sqrt{2}}\right) < \frac{\pi}{2}.$$

By the inverse function theorem, $\mathcal{P}_{U,\iota(x)+a}(y)$ is a diffeomorphism from $B_{\xi_1}^{\mathbb{R}^D}(0) \cap \iota(M)$ onto its image. Choose $\xi = \frac{3\xi_1}{4}$. If $\|a\|_{\mathbb{R}^D} < \frac{\xi}{3} = \frac{\xi_1}{4}$, then the closure of $B_{\xi}^{\mathbb{R}^D}(a) \cap \iota(M)$ is contained in $B_{\xi_1}^{\mathbb{R}^D}(0) \cap \iota(M)$.

Hence, $\mathcal{P}_{U,a}(y)$ is a diffeomorphism from the closure of $B_{\xi}^{\mathbb{R}^D}(a) \cap \iota(M)$ onto its image. By Proposition B.1, $B_{\xi}^{\mathbb{R}^D}(a) \cap \iota(M)$ is homeomorphic to $B_1^{\mathbb{R}^d}(0)$.

Proof of part 2 of Proposition F.1

Let $O \subset \mathbb{R}^d$ be the image of $B_{\xi}^{\mathbb{R}^D}(a) \cap \iota(M)$ under $\mathcal{P}_{U,a}(y)$. Then, O is homeomorphic to $B_1^{\mathbb{R}^d}(0)$. Let \bar{O} be the closure of O in \mathbb{R}^d . Suppose $\Phi: \bar{O} \rightarrow \mathbb{R}^D$ is the inverse of $\mathcal{P}_{U,a}(y)$. Then the restriction of Φ on O is a chart of $\iota(M)$. Since $\|a\|_{\mathbb{R}^D} < \frac{\xi}{3}$, we have $0 = \iota(x) \in B_{\xi}^{\mathbb{R}^D}(a) \cap \iota(M)$. Hence, $u_0 = \mathcal{P}_{U,a}(0) = \mathcal{P}_{U,a}(\iota(x)) \in O$. Based on the definition of $\mathcal{P}_{U,a}$ in Definition F.1, Φ can be expressed as

$$\Phi(u) = a + U \begin{bmatrix} u \\ F(u), \end{bmatrix}$$

where $F(u): \bar{O} \rightarrow \mathbb{R}^{D-d}$ is a smooth function. For any $u \in O$, $\Phi(u) \in B_{\xi_1}^{\mathbb{R}^D}(0) \cap \iota(M)$. Hence, we apply the same argument as in the proof of part (a). Recall that W is the subspace generated by the column vectors of UJ . If $V(u)$ is the tangent space of $\iota(M)$ at $\Phi(u)$ for $u \in O$. By Lemma F.2, $\cos(\phi_{T_{\iota(x)}\iota(M),W}) \geq 1 - d^{\frac{3}{2}}r$. By Lemma F.3, we have $\cos(\phi_{T_{\iota(x)}\iota(M),V(u)}) \geq \sqrt{1 - \frac{2(\xi_1 + \|a\|_{\mathbb{R}^D})}{\tau_{\iota(M)}}}$. Hence, by (4) in Lemma F.1,

$$(36) \quad \phi_{V(u),W} \leq \phi_{T_{\iota(x)}\iota(M),W} + \phi_{T_{\iota(x)}\iota(M),V(u)} \leq \arccos\left(\sqrt{1 - \frac{2(\xi_1 + \|a\|_{\mathbb{R}^D})}{\tau_{\iota(M)}}}\right) + \arccos(1 - d^{\frac{3}{2}}r).$$

In particular, by (35), for $u \in O$,

$$(37) \quad \cos(\phi_{V(u),W}) \geq \cos(\alpha) > 0.5$$

Suppose $B_R^{\mathbb{R}^d}(u_0)$ is the largest open ball centered at u_0 and contained in O , i.e. there is u_1 on the boundary of O such that $\|u_0 - u_1\|_{\mathbb{R}^d} = R$. Thus, we have

$$\|\iota(x) - \Phi(u_1)\|_{\mathbb{R}^D}^2 = \|\Phi(u_0) - \Phi(u_1)\|_{\mathbb{R}^D}^2 = \|u_0 - u_1\|_{\mathbb{R}^d}^2 + \|F(u_0) - F(u_1)\|_{\mathbb{R}^{D-d}}^2.$$

Since $B_R^{\mathbb{R}^d}(u_0)$ is contained in O , any point on the segment between u_0 and u_1 is in O . By the mean value inequality, there is $u^* \in O$ on the segment between u_0 and u_1 such that

$$\|F(u_0) - F(u_1)\|_{\mathbb{R}^{D-d}} \leq \|DF(u^*)v\|_{\mathbb{R}^{D-d}} \|u_0 - u_1\|_{\mathbb{R}^d}^2,$$

where $v = \frac{u_0 - u_1}{\|u_0 - u_1\|_{\mathbb{R}^d}}$. In other words,

$$(38) \quad \|\iota(x) - \Phi(u_1)\|_{\mathbb{R}^D} \leq R \sqrt{1 + \|DF(u^*)v\|_{\mathbb{R}^{D-d}}^2}.$$

Based on the definition of Φ , $U \begin{bmatrix} v \\ DF(u^*)v \end{bmatrix}$ is a vector in $V(u^*)$, the tangent space of $\iota(M)$ at $\Phi(u^*)$.

Hence, $\frac{1}{\sqrt{1 + \|DF(u^*)v\|_{\mathbb{R}^{D-d}}^2}} \begin{bmatrix} v \\ DF(u^*)v \end{bmatrix}$ is a unit vector in $U^\top V(u^*)$. By (3) in Lemma F.1, $\phi_{U^\top V(u^*), U^\top W} = \phi_{V(u^*), W}$. Observe that any unit vector in $U^\top W$ is in the form of $\begin{bmatrix} w \\ 0 \end{bmatrix}$, where w is a unit vector in \mathbb{R}^d .

We choose the w such that $\begin{bmatrix} w \\ 0 \end{bmatrix}^\top \frac{1}{\sqrt{1 + \|DF(u^*)v\|_{\mathbb{R}^{D-d}}^2}} \begin{bmatrix} v \\ DF(u^*)v \end{bmatrix}$ attains the maximum, then we have

$$\begin{aligned} \cos(\phi_{V(u^*),W}) &= \cos(\phi_{U^\top V(u^*),U^\top W}) \leq \begin{bmatrix} w \\ 0 \end{bmatrix}^\top \frac{1}{\sqrt{1 + \|DF(u^*)v\|_{\mathbb{R}^{D-d}}^2}} \begin{bmatrix} v \\ DF(u^*)v \end{bmatrix} \\ &= \frac{w^\top v}{\sqrt{1 + \|DF(u^*)v\|_{\mathbb{R}^{D-d}}^2}} \leq \frac{1}{\sqrt{1 + \|DF(u^*)v\|_{\mathbb{R}^{D-d}}^2}}. \end{aligned}$$

By (38), we have $\|\iota(x) - \Phi(u_1)\|_{\mathbb{R}^D} \leq \frac{R}{\cos(\phi_{V(u^*),W})}$. Note that since u_1 is on the boundary of O , $\Phi(u_1)$ is on the boundary of $B_{\frac{R}{\xi}}^{\mathbb{R}^D}(a) \cap \iota(M)$. Hence,

$$\xi = \|a - \Phi(u_1)\|_{\mathbb{R}^D} = \|\iota(x) + a - \Phi(u_1)\|_{\mathbb{R}^D} \leq \|\iota(x) - \Phi(u_1)\|_{\mathbb{R}^D} + \|a\|_{\mathbb{R}^D} \leq \frac{R}{\cos(\phi_{V(u^*),W})} + \|a\|_{\mathbb{R}^D}.$$

We conclude that $R \geq (\xi - \|a\|_{\mathbb{R}^D}) \cos(\phi_{V(u^*),W})$. By (36), we have

$$\cos(\phi_{V(u^*),W}) \geq (1 - d^{\frac{3}{2}}r) \sqrt{1 - \frac{2(\xi_1 + \|a\|_{\mathbb{R}^D})}{\tau_{\iota(M)}}} - \sqrt{\frac{2(\xi_1 + \|a\|_{\mathbb{R}^D})}{\tau_{\iota(M)}}} \sqrt{1 - (1 - d^{\frac{3}{2}}r)^2}.$$

The lower bound for R follows by substituting $\xi_1 = \frac{4\xi}{3}$.

To show that $0 \in O \subset \mathbb{R}^d$, we prove that $\|u_0\|_{\mathbb{R}^d} < R$. First, by (37),

$$R \geq (\xi - \|a\|_{\mathbb{R}^D}) \cos(\phi_{V(u^*),W}) \geq \cos(\alpha)(\xi - \|a\|_{\mathbb{R}^D}) > 0.5(\xi - \|a\|_{\mathbb{R}^D}).$$

Moreover, $\|u_0\|_{\mathbb{R}^d} \leq \|a\|_{\mathbb{R}^D}$. Since $\|a\|_{\mathbb{R}^D} < \frac{\xi}{3}$, we have $\|a\|_{\mathbb{R}^D} < 0.5(\xi - \|a\|_{\mathbb{R}^D})$. The conclusion follows.

F.3. Proof of Theorem 3.3. Based on Theorem 3.2, for all x_i , $i = 1, \dots, n$, with probability greater than $1 - \frac{1}{n^2}$, we have $\|\eta_i\|_{\mathbb{R}^D} \leq \varepsilon^\beta$. When ε is small enough, we have $\varepsilon^\beta < \varepsilon < \frac{\tau_{\iota(M)}}{16}$. Hence, we have $\|\eta_i\|_{\mathbb{R}^D} \leq \varepsilon^\beta < \delta < \frac{\tau_{\iota(M)}}{16}$. If $y_i \in B_{\frac{\tau_{\iota(M)}}{\delta}}^{\mathbb{R}^D}(y_k)$, then by triangle inequality

$$\|\iota(x_i) - y_k\|_{\mathbb{R}^D} = \|y_i - \eta_i - y_k\|_{\mathbb{R}^D} \leq \|y_i - y_k\|_{\mathbb{R}^D} + \|\eta_i\|_{\mathbb{R}^D} < 3\delta.$$

Hence, $\iota(x_i) \in B_{\frac{\tau_{\iota(M)}}{3\delta}}^{\mathbb{R}^D}(y_k)$. Moreover,

$$U_{n,\varepsilon}(y_k) = \begin{bmatrix} X_1 & 0 \\ 0 & X_2 \end{bmatrix} + E.$$

By Theorem 3.2, $|E_{ij}| < C\varepsilon^{2\min(\beta-1,1)}$, where C is a constant depending on d, D, P_m, C^2 norm of P , the second fundamental form of $\iota(M)$ and its derivative and the Ricci curvature of M . Hence, when ε is small enough depending on β, d, D, P_m, C^2 norm of P , the second fundamental form of $\iota(M)$ and its derivative and the Ricci curvature of M , $C\varepsilon^{2\min(\beta-1,1)} \leq \frac{1}{30d^2}$. Note that $\mathcal{P}_{y_k}(y) = \mathcal{P}_{U_{n,\varepsilon,\iota(x_k)+\eta_k}(y)}$.

The conditions in Proposition F.1 are satisfied with $\xi = 3\delta$, $a = \eta_k$ and $r = C\varepsilon^{2\min(\beta-1,1)}$. (1) and (2) of Theorem 3.3 follows. Since $\|\eta_i\|_{\mathbb{R}^D} \leq \varepsilon^\beta$, we have $B = \frac{8/3(3\delta)+2\|\eta_k\|_{\mathbb{R}^D}}{\tau_{\iota(M)}} \leq \frac{8\delta+2\varepsilon^\beta}{\tau_{\iota(M)}}$. (3) of Theorem 3.3 follows.

APPENDIX G. PROOF OF THEOREM 3.4

Since $\mathcal{Y}_{true} \subset \iota(M)$, $\text{dist}\{y_i, \iota(M)\} \leq \text{dist}(y_i, \mathcal{Y}_{true})$ for all i . Hence, $G\{\mathcal{Y}, \iota(M)\} \leq G\{\mathcal{Y}, \mathcal{Y}_{true}\}$. Let $N_r(x)$ be the number of samples in $B_r^{\mathbb{R}^D} \{\iota(x)\} \cap \mathcal{Y}_{true}$. Based on (3) in Theorem 2.4 in [40], if $r \rightarrow 0$ as $m \rightarrow \infty$, then with probability greater than $1 - \frac{1}{m^2}$,

$$\sup_{x \in M} \left| \frac{N_r(x)}{mr^d} - q(x) \right| \leq C \sqrt{\frac{\log m}{mr^d}},$$

where C is a constant depending on d , D , C^1 norm of q , the curvature of M and the second fundamental form of $\iota(M)$. Hence, if $\frac{q_{\min}}{2} mr^d \geq 1$ and $\frac{\log m}{mr^d} \leq \frac{q_{\min}^2}{4C^2}$, then $N_r(x) \geq \frac{q_m}{2} mr^d \geq 1$. Note that $\frac{q_{\min}}{2} mr^d \geq 1$ and $\frac{\log m}{mr^d} \leq \frac{q_{\min}^2}{4C^2}$ are satisfied when $r^d \geq \max\left(\frac{2}{q_{\min} m}, \frac{4C^2 \log m}{q_{\min}^2 m}\right)$. Hence, we choose $r^d = \max\left(\frac{2}{q_{\min}}, \left(\frac{2C}{q_{\min}}\right)^2 \frac{\log m}{m}\right)$.

Since M is compact, for any y_i , let $\iota(x'_i)$ be the point that realizes $\text{dist}\{y_i, \iota(M)\}$. Then, with probability greater than $1 - \frac{1}{m^2}$, there is a point $\iota(x_j) \in \mathcal{Y}_{true}$ such that $\iota(x_j) \in B_r^{\mathbb{R}^D} \{\iota(x'_i)\}$. Hence,

$$\begin{aligned} \text{dist}(y_i, \mathcal{Y}_{true}) - r &\leq \|y_i - \iota(x_j)\|_{\mathbb{R}^D} - r \leq \|y_i - \iota(x_j)\|_{\mathbb{R}^D} - \|\iota(x'_i) - \iota(x_j)\|_{\mathbb{R}^D} \\ &\leq \|\iota(x'_i) - y_i\|_{\mathbb{R}^D} = \text{dist}\{y_i, \iota(M)\}. \end{aligned}$$

In conclusion, we have $0 \leq \text{dist}(y_i, \mathcal{Y}_{true}) - \text{dist}\{y_i, \iota(M)\} \leq r$. Consequently,

$$0 \leq \text{dist}(y_i, \mathcal{Y}_{true})^2 - \text{dist}\{y_i, \iota(M)\}^2 \leq r(\text{dist}(y_i, \mathcal{Y}_{true}) + \text{dist}\{y_i, \iota(M)\}) \leq 2r \text{dist}\{y_i, \iota(M)\} + r^2.$$

By the definition of geometric root mean square error,

$$G(\mathcal{Y}, \mathcal{Y}_{true})^2 - G\{\mathcal{Y}, \iota(M)\}^2 \leq 2r \frac{1}{n} \sum_{i=1}^n \text{dist}\{y_i, \iota(M)\} + r^2 \leq 2rG\{\mathcal{Y}, \iota(M)\} + r^2.$$

The conclusion follows.

APPENDIX H. BRIEF REVIEW OF THE DIFFUSION MAP

We provide a briefly review of the Diffusion Map. Given samples $\{y_i\}_{i=1}^n \subset \mathbb{R}^D$, the Diffusion Map constructs a normalized graph Laplacian $L \in \mathbb{R}^{n \times n}$ by using the kernel $k(y, y') = \exp(-\|y - y'\|_{\mathbb{R}^D}^2 / \varepsilon_{DM}^2)$ as shown in the following steps.

- (1) Let $W_{ij} = \frac{k(y_i, y_j)}{q(y_i)q(y_j)} \in \mathbb{R}^{n \times n}$, $1 \leq i, j, \leq n$, where $q(y_i) = \sum_{j=1}^n k(y_i, y_j)$.
- (2) Define an $n \times n$ diagonal matrix D as $D_{ii} = \sum_{j=1}^n W_{ij}$, where $i = 1, \dots, n$.
- (3) The normalized graph Laplacian L is defined as $L = (D^{-1}W - I) / \varepsilon_{DM}^2 \in \mathbb{R}^{n \times n}$.

Suppose $(\mu_j, V_j)_{j=0}^{n-1}$ are the eigenpairs of $-L$ with $\mu_0 \leq \mu_1 \leq \dots \leq \mu_{n-1}$ and V_i normalizing in ℓ^2 . Then $\mu_0 = 0$ and V_0 is a constant vector. The map (V_1, \dots, V_ℓ) provides the coordinates of the data set $\{y_i\}_{i=1}^n$ in a low-dimensional space \mathbb{R}^ℓ .

When $\{y_i = \iota(x_i)\}_{i=1}^n$ are samples from an isometrically embedded submanifold $\iota(M) \subset \mathbb{R}^D$, then [7] shows that L approximates the Laplace-Beltrami operator Δ of M pointwisely. In particular, when the boundary of M is not empty, L pointwisely approximates Δ with Neumann boundary condition. Moreover, when M is a closed manifold, the spectral convergence rate of $-L$ to $-\Delta$ is discussed in [11, 6, 5]. Suppose the eigenvectors of $-L$ are normalized properly. [11] show that the first K eigenpairs of $-L$ approximate the corresponding eigenpairs of $-\Delta$ over $\{x_i\}_{i=1}^n$ whenever ε_{DM} is small enough depending on K and n is large enough depending on ε_{DM} . Based on the results in spectral geometry, by choosing ℓ sufficiently large, the Diffusion Map (V_1, \dots, V_ℓ) approximates the discretization of an embedding of $\iota(M)$ into \mathbb{R}^ℓ .

APPENDIX I. ESTIMATE THE DIMENSION OF THE DATA SET

Suppose data $\{y_i\}_{i=1}^n \subset \mathbb{R}^D$ satisfy Assumption 2.1. In this section, we describe a method to estimate the dimension d of the underlying manifold M by using the Diffusion Map. Let $C_{n,\varepsilon}(y_k)$ be the local covariance matrix at y_k constructed by $\{y_i\}_{i=1}^n$ as defined in (1). Suppose $\lambda_{n,\varepsilon,i}(y_k)$ is the i th largest eigenvalue of $C_{n,\varepsilon}(y_k)$. Then, we define the mean of the i th eigenvalues of the local covariance matrices as

$$(39) \quad \bar{\lambda}_{\varepsilon,i} = \frac{1}{n} \sum_{k=1}^n \lambda_{n,\varepsilon,i}(y_k).$$

We demonstrate our method by using the following example. Consider the surface of the ellipsoid in \mathbb{R}^3 described by the equation

$$\frac{x^2}{4} + \frac{y^2}{2.25} + z^2 = 1$$

We sample 800 points $\{(x'_i, y'_i, z'_i)\}_{i=1}^{800}$ uniformly on the surface. Let R be an orthogonal matrix of \mathbb{R}^3 . We rotate the surface by using R , i.e. we get 800 points $\{(x''_i, y''_i, z''_i)\}_{i=1}^{800}$ where

$$\begin{bmatrix} x''_i \\ y''_i \\ z''_i \end{bmatrix} = R \begin{bmatrix} x'_i \\ y'_i \\ z'_i \end{bmatrix}.$$

Hence, $\iota(x_i) = (0, \dots, 0, x''_i, y''_i, z''_i, 0, \dots, 0) \in \mathbb{R}^{30}$ (x''_i, y''_i , and z''_i are the 14th, 15th, and 16th coordinates, respectively) is a point on a surface of the ellipsoid $\iota(M)$ in \mathbb{R}^{30} . Suppose $\{\eta_i\}_{i=1}^{800}$ are i.i.d samples from $\mathcal{N}(0, \sigma^2 I_{30 \times 30})$ where $\sigma = 0.05$. Then $y_i = \iota(x_i) + \eta_i$ is a noisy data point around the submanifold $\iota(M)$ in \mathbb{R}^{30} . We choose the bandwidths $\varepsilon = 0.3, 0.4, 0.5, 0.6$ and find $\{\bar{\lambda}_{\varepsilon,i}\}_{i=1}^{30}$ by using $\{\iota(x_i)\}_{i=1}^{800}$. We show the plot of $\{\bar{\lambda}_{\varepsilon,i}\}_{i=1}^{30}$ for different ε in Fig 11. We can see that there are two large eigenvalues. Hence, for this example, when there is no noise, the eigenvalues of the local covariance matrices constructed from $\{\iota(x_i)\}_{i=1}^{800}$ are sufficient to determine the dimension of the underlying manifold.

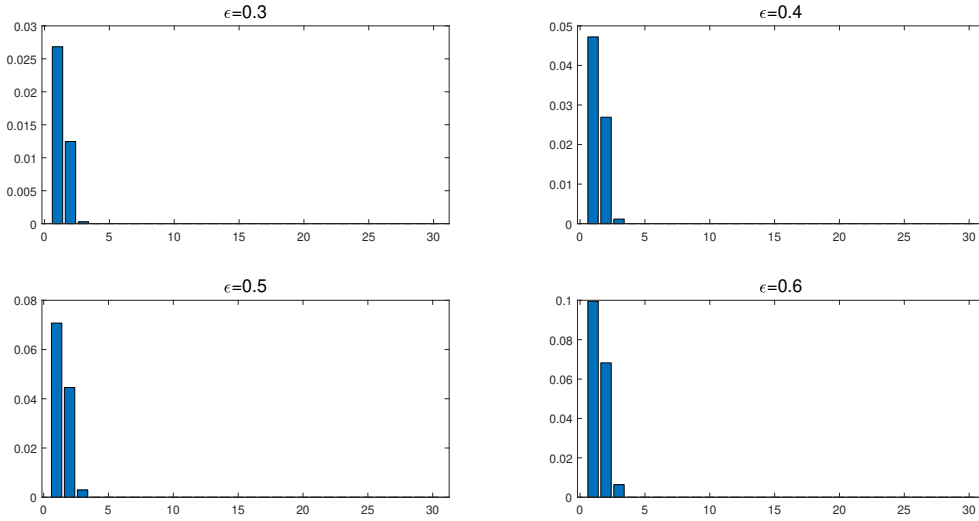


FIGURE 11. We choose the bandwidths $\varepsilon = 0.3, 0.4, 0.5, 0.6$ and find $\{\bar{\lambda}_{\varepsilon,i}\}_{i=1}^{30}$ by using $\{\iota(x_i)\}_{i=1}^{800}$. In the above plots, the horizontal axis indicates the $i = 1, \dots, 30$ and the vertical axis indicates the value of corresponding $\bar{\lambda}_{\varepsilon,i}$.

Next, we choose the bandwidths $\{\varepsilon = 0.1\ell\}_{\ell=1}^{30}$ and find $\{\bar{\lambda}_{\varepsilon,i}\}_{i=1}^{30}$ by using $\{y_i\}_{i=1}^{800}$. We show the plot of $\{\bar{\lambda}_{\varepsilon,i}\}_{i=1}^{30}$ for $\varepsilon = 0.5, 1, \dots, 3$ in Fig 12. Due to the noise, we cannot determine the dimension of $\iota(M)$ correctly by using the eigenvalues of the local covariance matrices constructed from $\{y_i\}_{i=1}^{800}$.

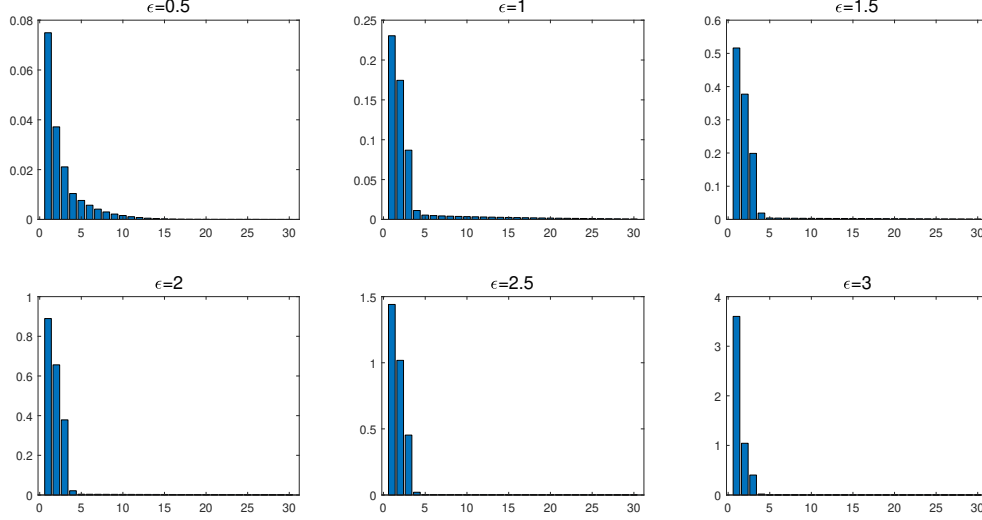


FIGURE 12. For $\{\varepsilon = 0.1\ell\}_{\ell=1}^{30}$, we find $\{\bar{\lambda}_{\varepsilon,i}\}_{i=1}^{30}$ by using $\{y_i\}_{i=1}^{800}$. We plot $\{\bar{\lambda}_{\varepsilon,i}\}_{i=1}^{30}$ for $\varepsilon = 0.5, 1, \dots, 3$. In the above plots, the horizontal axis indicates $i = 1, \dots, 30$ and the vertical axis indicates the value of the corresponding $\bar{\lambda}_{\varepsilon,i}$.

The robustness of diffusion map to noise is discussed in [13, 33, 12, 9]. Based on the description of the algorithm in Section H, we construct the normalized graph Laplacian $L \in \mathbb{R}^{n \times n}$ by using the kernel $k(y, y') = \exp(-\|y - y'\|_{\mathbb{R}^D}^2 / \varepsilon_{DM}^2)$ and the noisy data points $\{y_i\}_{i=1}^{800}$. We choose $\varepsilon_{DM} = 2$ and let $(\mu_j, V_j)_{j=0}^{n-1}$ be the eigenpairs of $-L$ with $\mu_0 \leq \mu_1 \leq \dots \leq \mu_{n-1}$ and V_i normalized in ℓ^2 . We reconstruct the noisy data points $\{y_i\}_{i=1}^{800}$ in \mathbb{R}^{2+j} by using $(V_1, \dots, V_{2+j}) \in \mathbb{R}^{800 \times (2+j)}$ and denote these data points in \mathbb{R}^{2+j} as \mathcal{X}_j for $j = 1, \dots, 4$. For each $j = 1, \dots, 4$, the diffusion map (V_1, \dots, V_{2+j}) can be regarded as an approximation of a discretization of an embedding of $\iota(M)$ into \mathbb{R}^{2+j} over the clean data point $\{\iota(x_i)\}_{i=1}^{800}$ on $\iota(M)$. Hence, \mathcal{X}_j are the samples around an embedded submanifold N_j in \mathbb{R}^{2+j} homeomorphic to M . The dimension of M is the same as the dimension of N_j . For each $j = 1, \dots, 4$, we construct the local covariance matrices by using \mathcal{X}_j with $\varepsilon = 0.3 + 0.1j$ and calculate $\{\bar{\lambda}_{\varepsilon,i}^j\}_{i=1}^{2+j}$. We plot $\{\bar{\lambda}_{\varepsilon,i}^j\}_{i=1}^{2+j}$ for each j in Figure 13. We can see that in each plot there are 2 large eigenvalues. Therefore, the dimension of the underlying manifold N_j and the dimension of M are 2.

We apply the above method to the examples in Section 4. For the Cassini Oval curve, using the local covariance matrix and (39) with the clean data $\{X(\theta_i), Y(\theta_i), Z(\theta_i)\}_{i=1}^{102}$ and $\varepsilon = 0.3$, we obtain $\bar{\lambda}_{\varepsilon,1} = 0.271$, $\bar{\lambda}_{\varepsilon,2} = 0.0078$, and $\bar{\lambda}_{\varepsilon,3} = 0.0001$. This result confirms that the clean data are sampled from a curve. In contrast, applying the local covariance matrix and (39) to the noisy data \mathcal{Y} with $\varepsilon = 0.4$ yields $\bar{\lambda}_{\varepsilon,1} = 0.2451$, $\bar{\lambda}_{\varepsilon,2} = 0.0473$, and $\bar{\lambda}_{\varepsilon,3} = 0.0122$. Here, $\bar{\lambda}_{\varepsilon,1}$ is less dominant compared to the noiseless case due to the noise. To address this, we apply the diffusion map with $\varepsilon_{DM} = 0.2$ to reduce the dimension of \mathcal{Y} , obtaining (V_1, V_2) . Applying the local covariance matrix and (39) to the lower dimensional data corresponding to (V_1, V_2) with $\varepsilon = 0.2$, we find $\bar{\lambda}_{\varepsilon,1} = 0.182$ and $\bar{\lambda}_{\varepsilon,2} = 0.0089$. Thus, our method successfully determines the dimension of the underlying manifold even in the presence of noise.

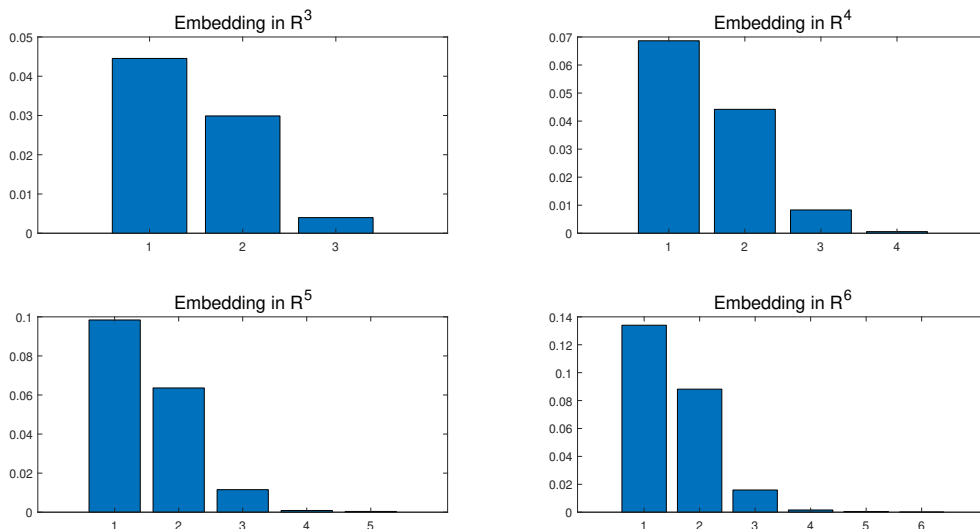


FIGURE 13. $\mathcal{X}_1, \dots, \mathcal{X}_4$ constructed by diffusion map are the samples around the embeddings of M in $\mathbb{R}^3, \dots, \mathbb{R}^6$, respectively. For each $j = 1, \dots, 4$, we construct the local covariance matrices by using \mathcal{X}_j with $\varepsilon = 0.3 + 0.1j$ and calculate $\{\bar{\lambda}_{\varepsilon,i}^j\}_{i=1}^{2+j}$. We plot $\{\bar{\lambda}_{\varepsilon,i}^j\}_{i=1}^{2+j}$ for each j . The top two plots correspond to $j = 1, 2$. The bottom two plots correspond to $j = 3, 4$. In the above plots, the horizontal axis indicates $i = 1, \dots, 2 + j$ and the vertical axis indicates the value of the corresponding $\bar{\lambda}_{\varepsilon,i}^j$.

For the torus case, using the local covariance matrix and (39) with the clean data $\{t(x_i)\}_{i=1}^{558}$ and $\varepsilon = 0.5$, we obtain $\bar{\lambda}_{\varepsilon,1} = 0.5898$, $\bar{\lambda}_{\varepsilon,2} = 0.2604$, and $\bar{\lambda}_{\varepsilon,3} = 0.0134$. In contrast, applying the local covariance matrix and (39) to the noisy data \mathcal{Y} with $\varepsilon = 0.5$ yields $\bar{\lambda}_{\varepsilon,1} = 0.5125$, $\bar{\lambda}_{\varepsilon,2} = 0.2364$, and $\bar{\lambda}_{\varepsilon,3} = 0.068$. Here, the first two average eigenvalues are less dominant compared to the noiseless case due to the noise. We apply the diffusion map with $\varepsilon_{DM} = 0.3$, obtaining (V_1, V_2, V_3, V_4) . Applying the local covariance matrix and (39) to the data corresponding to (V_1, V_2, V_3, V_4) with $\varepsilon = 0.4$, we find $\bar{\lambda}_{\varepsilon,1} = 4.179$, $\bar{\lambda}_{\varepsilon,2} = 1.41$, $\bar{\lambda}_{\varepsilon,3} = 0.024$ and $\bar{\lambda}_{\varepsilon,4} = 0.0031$.

The discussion is similar for the real projective space case in Section L in which we have a 3 dimensional manifold. Using the local covariance matrix and (39) with 1200 clean samples on the manifold and $\varepsilon = 0.25$, we obtain $\bar{\lambda}_{\varepsilon,1} = 1.2 \times 10^{-1}$, $\bar{\lambda}_{\varepsilon,2} = 5.97 \times 10^{-2}$, $\bar{\lambda}_{\varepsilon,3} = 2.32 \times 10^{-2}$, $\bar{\lambda}_{\varepsilon,4} = 2.5 \times 10^{-3}$, and $\bar{\lambda}_{\varepsilon,5} = 4 \times 10^{-4}$. In contrast, applying the local covariance matrix and (39) to the noisy data \mathcal{Y} with $\varepsilon = 0.3$ yields $\bar{\lambda}_{\varepsilon,1} = 1.8 \times 10^{-1}$, $\bar{\lambda}_{\varepsilon,2} = 1.1 \times 10^{-1}$, $\bar{\lambda}_{\varepsilon,3} = 5.78 \times 10^{-2}$, $\bar{\lambda}_{\varepsilon,4} = 2.72 \times 10^{-2}$, and $\bar{\lambda}_{\varepsilon,5} = 1.17 \times 10^{-2}$. The first three average eigenvalues are much less dominant compared to the noiseless case. We apply the diffusion map with $\varepsilon_{DM} = 0.25$ to reduce the dimension of \mathcal{Y} , resulting in (V_1, \dots, V_9) . Using the local covariance matrix and (39) to the lower dimensional data corresponding to (V_1, \dots, V_9) with $\varepsilon = 0.5$, we find $\bar{\lambda}_{\varepsilon,1} = 1.71 \times 10^{-1}$, $\bar{\lambda}_{\varepsilon,2} = 5.17 \times 10^{-2}$, $\bar{\lambda}_{\varepsilon,3} = 1.23 \times 10^{-2}$, $\bar{\lambda}_{\varepsilon,4} = 2.2 \times 10^{-3}$, and $\bar{\lambda}_{\varepsilon,5} = 4.4 \times 10^{-4}$. These average eigenvalues closely match in order with those obtained from the clean samples, demonstrating that our proposed method significantly improves upon the results of directly applying local covariance matrix to the noisy data.

APPENDIX J. AN EXAMPLE FOR SELECTION OF ε AND δ IN MrGAP

In this section, we illustrate our method for selecting the parameters ε and δ in the MrGAP algorithm. We consider $t(M)$ which is the unit circle in \mathbb{R}^2 . We uniformly sample 100 points on the circle, each

with additive Gaussian noise with $\sigma = 0.06$. Let $\mathcal{Y} = \{y_i\}_{i=1}^{100}$ be the noisy data around the circle. We also sample \mathcal{Y}_{true} consisting of 10^5 points on the circle. We use \mathcal{Y}_{true} to approximate the geometric root mean square error from samples to $\iota(M)$ with $G(\mathcal{Y}, \mathcal{Y}_{true}) = 0.0588$. Let $\varepsilon = \{0.1, 0.2, \dots, 1.8\}$ and $\delta = \{0.1, 0.2, \dots, 1.8\}$. We consider all pairs $(\varepsilon_i, \delta_j)$ with $\varepsilon \leq \delta$. Therefore, there are 171 distinct pairs. For each pair $(\varepsilon_i, \delta_j)$, we maximize $L_{ij} = \sum_{k=1}^n \log p_k(Z_k | A, \rho, \sigma)$ in Step 3 of Algorithm 1 over A, ρ, σ . We choose $(\varepsilon_i, \delta_j)$ corresponding to the largest L_{ij} . When $\varepsilon = 1.4$ and $\delta = 1.4$, $\frac{L_{ij}}{100}$ achieves maximum 338 over all pairs of $(\varepsilon_i, \delta_j)$. The corresponding Gaussian process parameters are $A^{(0)} = 0.9$, $\rho^{(0)} = 1.2$ and $\sigma^{(0)} = \sqrt{0.008}$. For $\varepsilon = 1.4$ and $\delta = 1.4$, suppose \mathcal{X}_1 is the denoised output after the first round of Algorithm 1. Then, $G(\mathcal{X}_1, \mathcal{Y}_{true}) = 0.0251$. We plot the $\frac{L_{ij}}{100}$ and the corresponding first round denoised outputs for different pairs of $(\varepsilon_i, \delta_j)$ in Figure 14.

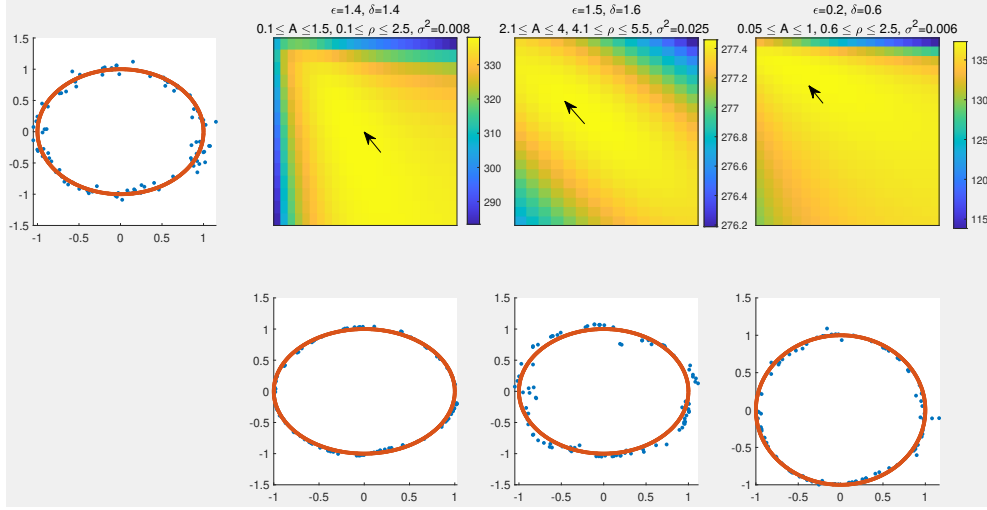


FIGURE 14. Top row: The first plot shows the noisy data \mathcal{Y} and the samples on the unit circle \mathcal{Y}_{true} . $G(\mathcal{Y}, \mathcal{Y}_{true}) = 0.0588$. For each pair $(\varepsilon_i, \delta_j)$, suppose $\frac{L_{ij}}{100}$ achieves maximum with A_{ij} , ρ_{ij} and σ_{ij} . In the second to the fourth plot, we fix σ_{ij} and we plot $\frac{L_{ij}}{100}$ over A and ρ in a neighborhood around A_{ij} and ρ_{ij} . The horizontal axis is ρ and the vertical axis is A . The arrows indicate the locations of the maximums. The maximums of $\frac{L_{ij}}{100}$ in the plots are 338, 277.46, and 137.3 respectively. Bottom row: The plots of the first round denoised outputs correspond to ε_i , δ_j , A_{ij} , ρ_{ij} and σ_{ij} in the top row. The geometric root mean square error between the first round denoised outputs and \mathcal{Y}_{true} are 0.0251, 0.0769, and 0.0366 respectively.

APPENDIX K. EXPLORATION OF THE PROPERTIES OF MRGAP ON NUMERICAL EXAMPLES

K.1. Discussion of the affine subspaces constructed in Step 1 of Algorithm 1. Suppose that $\{\iota(x_i)\}_{i=1}^n$ are samples on $\iota(M)$ and $\{y_i\}_{i=1}^n$ are the corresponding noisy data points around $\iota(M)$. Recall from the description in Section 2.5 and Step 1 of Algorithm 1 that we construct an affine subspace $\mathcal{H}_k = y_k + \mathcal{T}_k$ through y_k , where \mathcal{T}_k is the subspace spanned by the first d eigenvectors of $C_{n,\varepsilon}(y_k)$ defined in (1). In this subsection, we present an example showing that Algorithm 1 performs well even when the affine subspace \mathcal{H}_k deviates significantly from the affine space $\iota(x_k) + T_{\iota(x_k)}\iota(M)$ tangent to $\iota(M)$ at $\iota(x_k)$. This example illustrates the conclusion of Theorem 3.3, namely, that Algorithm 1 remains valid as long as $\mathcal{P}_{y_k}(y)$, defined in (3), is a local diffeomorphism, regardless of the deviation between \mathcal{H}_k and the corresponding affine space tangent to $\iota(M)$.

As described in Section 4.1, let $\iota(M)$ denote the Cassini Oval in \mathbb{R}^3 . Let $\{\iota(x_i)\}_{i=1}^{102} \subset \mathbb{R}^3$ and $\mathcal{Y} = \{y_i\}_{i=1}^{102} \subset \mathbb{R}^3$ be the points on $\iota(M)$ and the corresponding noisy data points respectively. Following Section 4.1, we choose the scale parameters $\varepsilon = 0.3$ and $\delta = 0.6$. Let $\{\hat{y}_i^{(1)}\}_{i=1}^{102}$ be the outputs after the first iteration of Algorithm 1. We focus on the point $\iota(x_{91})$. Define $\mathcal{H}_{91} = y_{91} + \mathcal{T}_{91}$ as the 1 dimensional affine subspace through y_{91} , where \mathcal{T}_{91} is the subspace generated by the first eigenvectors of $C_{102,0.3}(y_{91})$ constructed from \mathcal{Y} . Similarly, let $\hat{\mathcal{H}}_{91} = \hat{y}_{91}^{(1)} + \hat{\mathcal{T}}_{91}$ be the 1 dimensional affine subspace through $\hat{y}_{91}^{(1)}$, where $\hat{\mathcal{T}}_{91}$ is the subspace spanned by the first eigenvector of $C_{102,0.3}(\hat{y}_{91}^{(1)})$ constructed from $\{\hat{y}_i^{(1)}\}_{i=1}^{102}$. Let $\iota(x_{91}) + T_{\iota(x_{91})}\iota(M)$ be the affine subspace tangent to $\iota(M)$ at $\iota(x_{91})$. The deviation between two affine subspaces can be quantified by the angle between them, which lies in $[0, \pi/2]$. The angle between \mathcal{T}_{91} and $T_{\iota(x_{91})}\iota(M)$ is $0.613 \approx 35.6^\circ$. After the first iteration of Algorithm 1, the outputs are less noisy, and we indeed observe a smaller angle between $\hat{\mathcal{T}}_{91}$ and $T_{\iota(x_{91})}\iota(M)$, namely $0.233 \approx 13.3^\circ$. We plot \mathcal{H}_{91} and $\hat{\mathcal{H}}_{91}$, together with $\iota(x_{91}) + T_{\iota(x_{91})}\iota(M)$ in Figure 15. It is worth noting that, due to the finite sample size, the affine subspace at $\iota(x_{91})$ generated from the clean samples on $\iota(M)$, that is, the subspace spanned by the first eigenvector of $C_{102,0.3}(\iota(x_{91}))$ constructed from $\{\iota(x_i)\}_{i=1}^{102}$, still does not exactly coincide with $\iota(x_{91}) + T_{\iota(x_{91})}\iota(M)$. This result together with the results in Section 4.1 demonstrate that MrGap does not rely on the accurate estimation of the affine subspaces tangent to $\iota(M)$.

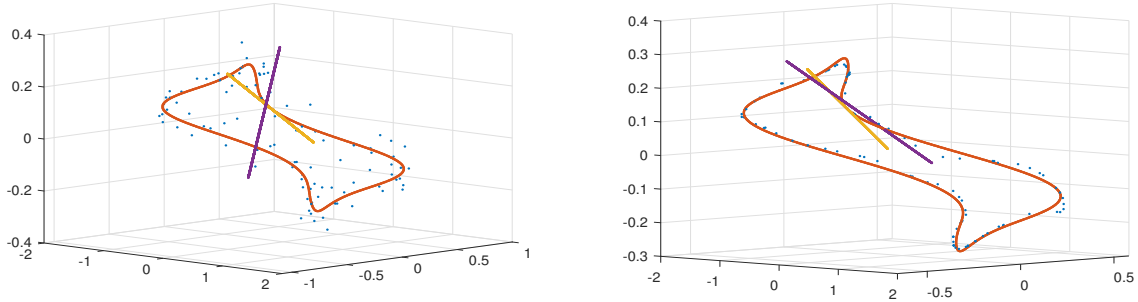


FIGURE 15. Left panel: The blue points represent $\mathcal{Y} = \{y_i\}_{i=1}^{102}$ and the red points represent $\iota(M)$. The yellow line and purple line represent \mathcal{H}_{91} and $\iota(x_{91}) + T_{\iota(x_{91})}\iota(M)$ respectively. The angle between them is $0.613 \approx 35.6^\circ$. Right panel: The blue points represent $\{\hat{y}_i^{(1)}\}_{i=1}^{102}$ and the red points represent $\iota(M)$. The yellow line and purple line represent $\hat{\mathcal{H}}_{91}$ and $\iota(x_{91}) + T_{\iota(x_{91})}\iota(M)$ respectively. The angle between them is $0.233 \approx 13.3^\circ$.

K.2. Stability of Algorithm 2 under different orders of interpolations. Suppose $\{\hat{y}_i\}_{i=1}^n$ are the final denoised output from Algorithm 1. Recall that Algorithm 2 iteratively interpolates points around each \hat{y}_i based on the index order i . In this subsection, we demonstrate through a numerical simulation that the output of Algorithm 2 remains stable regardless of the interpolation order.

Let $\mathcal{Y} = \{y_i\}_{i=1}^{102}$ be the noisy data points around the Cassini Oval in Section 4. Suppose $\{y_i^{(1)}\}_{i=1}^{102}$ are the output after applying the first round of Algorithm 1 to \mathcal{Y} . Next, we generate 100 different permutations of $\{y_i^{(1)}\}_{i=1}^{102}$. We denote these permutations as $\{\mathcal{Y}_j^{(1)}\}_{j=1}^{100}$. For each permutation $\mathcal{Y}_j^{(1)}$, we apply Algorithm 2 with $\varepsilon = 0.3$ and $\delta = 0.6$. We choose $K = 20$ and we apply the same estimated covariance parameters in the last round of Algorithm 1 i.e. $A^{(1)} = 0.048$, $\rho^{(1)} = 0.3$ and $\sigma^{(1)} = \sqrt{2} \times 10^{-5}$. Therefore, for each permutation $\mathcal{Y}_j^{(1)}$, we construct $\tilde{\mathcal{X}}_j$ consisting of 2040 interpolation points. Let \mathcal{Y}_{true} be the 10^5 points sampled on the Cassini Oval described in Section 4. We evaluate the performance of each

group of interpolations through the geometric root mean square error between $\tilde{\mathcal{X}}_j$ and the Cassini Oval through \mathcal{Y}_{true} . Let $\mathcal{E}_j = G(\tilde{\mathcal{X}}_j, \mathcal{Y}_{true})$ for $j = 1, \dots, 100$. The mean of $\{\mathcal{E}_j\}_{j=1}^{100}$ is 0.0213 with a small standard deviation 2.16×10^{-4} .

K.3. Noisy data set around a submanifold with small reach. We consider $\iota(M)$ which is a 2-d Cassini oval with a small reach. For $\theta \in [0, 2\pi)$,

$$X(\theta) = \{\cos(2\theta) + (\cos(2\theta)^2 + 0.7)^{1/2}\}^{1/2} \cos(\theta),$$

$$Y(\theta) = \{1.07 \cos(2\theta) + (\cos(2\theta)^2 + 0.2)^{1/2}\}^{1/2} \sin(\theta).$$

Let \mathcal{Y}_{true} be the collection of 10^5 points on $\iota(M)$. Suppose $y_i = \iota(x_i) + \eta_i$.

In the first example, we show that to reconstruct $\iota(M)$ accurately, it is necessary that η_i is small compared to the reach. Suppose $\mathcal{Y} = \{y_i\}_{i=1}^{102}$ in which $\eta_i \sim \mathcal{N}(0, \sigma^2 I_{3 \times 3})$, with $\sigma = 0.04$. We plot \mathcal{Y} and \mathcal{Y}_{true} in Figure 16. We choose $\varepsilon = 0.6$ and $\delta = 0.6$ by maximizing the sum of the marginal likelihood functions in the first round of Algorithm 1. We iterate Steps 1-3 of Algorithm 1 twice. The estimated covariance parameters in the last round are $A^{(1)} = 0.1$, $\rho^{(1)} = 0.5$ and $\sigma^{(1)} = \sqrt{0.012}$. We apply Algorithm 2 with the covariance parameters and output \mathcal{X}_2 consisting of 612 points. The denoised outputs \mathcal{X}_1 and the interpolations \mathcal{X}_2 are shown in Figure 16. Given the large noise and small reach, \mathcal{Y} is more likely to distribute around a figure 8 curve rather than a simple closed curve. Thus, MrGap improperly connects two regions on $\iota(M)$, resulting in the denoised points and interpolations falling along the figure 8 curve.

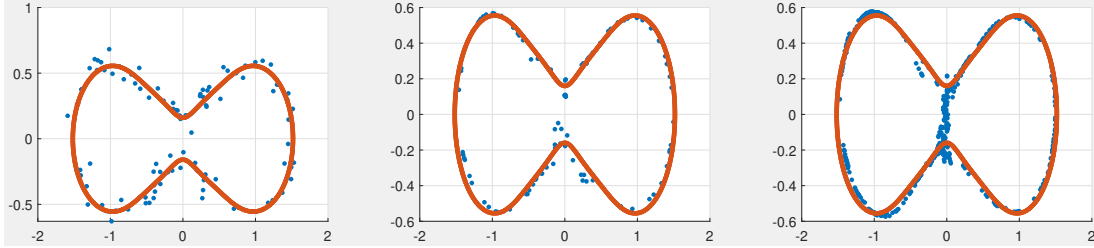


FIGURE 16. Left: The plot of \mathcal{Y} (blue) and \mathcal{Y}_{true} (red). Middle: The plot of \mathcal{X}_1 (blue) and \mathcal{Y}_{true} (red). Right: The plot of \mathcal{X}_2 (blue) and \mathcal{Y}_{true} (red)

In the second example, we apply the same $\iota(M)$. We demonstrate that regions with large curvature cannot be adequately reconstructed when the surrounding data are too sparse. Suppose $\mathcal{Y} = \{y_i\}_{i=1}^{30}$ in which $\eta_i \sim \mathcal{N}(0, \sigma^2 I_{3 \times 3})$, with $\sigma = 0.04$. We plot \mathcal{Y} and \mathcal{Y}_{true} in Figure 17. We choose $\varepsilon = 0.6$ and $\delta = 0.6$ by maximizing the sum of the marginal likelihood functions in the first round of Algorithm 1. We iterate Steps 1-3 of Algorithm 1 twice. The estimated covariance parameters in the last round are $A^{(1)} = 0.24$, $\rho^{(1)} = 1$ and $\sigma^{(1)} = \sqrt{0.0005}$. We apply Algorithm 2 with the covariance parameters and output \mathcal{X}_2 consisting of 600 points. The denoised outputs \mathcal{X}_1 and the interpolations \mathcal{X}_2 are shown in Figure 17. The highlighted regions in the figure have large curvature. Due to the lack of samples in these areas, interpolations either fail to reconstruct the region or produce a flatter representation compared to the actual curve.

K.4. MrGap on disconnected manifolds. Recall from Assumption 2.1 that we assume the manifold M is connected. However, the assumption of connectedness is made for simplicity in the statements of the main theorems and is not necessary for the functionality of MrGap. We now introduce the following assumption:

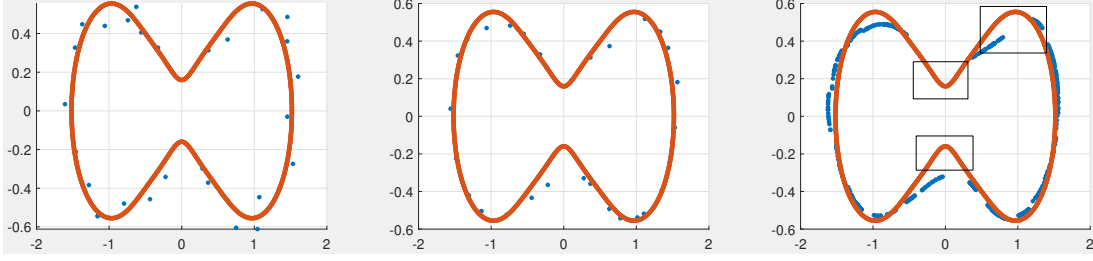


FIGURE 17. Left: The plot of \mathcal{Y} (blue) and \mathcal{Y}_{true} (red). Middle: The plot of \mathcal{X}_1 (blue) and \mathcal{Y}_{true} (red). Right: The plot of \mathcal{X}_2 (blue) and \mathcal{Y}_{true} (red)

Assumption K.1. Suppose $M = \cup_{i=1}^m M_i$ where each M_i is a d -dimensional smooth, closed, and connected Riemannian manifold and the m manifolds are mutually disjoint. M is isometrically embedded in \mathbb{R}^D though $\iota : M \rightarrow \mathbb{R}^D$. P is a probability density function on M , which is smooth, bounded from below by $P_m > 0$ and bounded from above by P_M . The observed data follow $y_i = \iota(x_i) + \eta_i$, with $x_i \sim P$ and $\eta_i \sim \mathcal{N}(0, \sigma^2 I_{D \times D})$ independently for $i = 1, \dots, n$.

Because the m manifolds are disjoint, we have

$$m_0 = \min_{i \neq j} \min_{x \in M_i, x' \in M_j} \|\iota(x) - \iota(x')\|_{\mathbb{R}^D} > 0.$$

Let $\tau_{\iota(M_i)}$ denote the reach of the embedded manifold $\iota(M_i)$. Suppose the relations between ε , σ , δ , and n in Theorem 3.3 hold. Further assume that $\varepsilon < m_0/3$ and $\delta < \min(m_0/3, \tau_{\iota(M_1)}/16, \dots, \tau_{\iota(M_m)}/16)$. Under these conditions, the conclusions of Theorem 3.3 hold. In particular, if $x_k \in M_i$, then with high probability, $B_{3\delta}^{\mathbb{R}^D}(y_k) \cap \iota(M_j) = \emptyset$ for $j \neq i$, and $B_\varepsilon^{\mathbb{R}^D}(y_k)$ and $B_\delta^{\mathbb{R}^D}(y_k)$ do not contain any $y_{k'}$ corresponding to $x_{k'} \in M_j$ for $j \neq i$. Consequently, $C_{n,\varepsilon}(y_k)$ is constructed only using $y_{k'}$ corresponding to $x_{k'}$ on M_i . The map $\mathcal{P}_{y_k}(y)$ as defined in (3) is a diffeomorphism from $B_{3\delta}^{\mathbb{R}^D}(y_k) \cap \iota(M_i)$ onto its image $O_k \subset \mathbb{R}^d$, and O_k is homeomorphic to $B_1^{\mathbb{R}^d}(0)$. In other words, applying MrGap directly over $\{y_i\}_{i=1}^n$ to reconstruct $\iota(M)$ is equivalent to applying MrGap to reconstruct each $\iota(M_i)$ separately. We illustrate the performance of MrGap on the following disconnected manifold without testing whether M is connected.

Let $\iota(M) = S_1 \cup S_2 \subset \mathbb{R}^3$ be a pair of linked circles in \mathbb{R}^3 , where S_1 is the unit circle in the XY plane centered at $(0, 0, 0)$ and S_2 is the unit circle in the YZ plane centered at $(0, 1, 0)$. Let $\{\iota(x_i)\}_{i=1}^{100}$ and $\{\iota(x_i)\}_{i=101}^{200}$ be the uniform samples distributed on S_1 and S_2 respectively. Suppose $\eta_i \sim \mathcal{N}(0, \sigma^2 I_{3 \times 3})$, with $\sigma = 0.07$. Suppose $y_i = \iota(x_i) + \eta_i$, $i = 1, \dots, 200$, and $\mathcal{Y} = \{y_i\}_{i=1}^{200}$. We uniformly sample \mathcal{Y}_{true} consisting of 5×10^5 points on $\iota(M)$. For any sample points \mathcal{S} , $G\{\mathcal{S}, \iota(M)\}$ is approximated by $G(\mathcal{S}, \mathcal{Y}_{true})$. Without denoising, we obtain $G(\mathcal{Y}, \mathcal{Y}_{true}) = 0.098$.

We choose the scale parameters $\varepsilon = 0.6$ and $\delta = 0.6$ in MrGap. We iterate Steps 1-3 of Algorithm 1 twice. The estimated covariance parameters in the first round are $A^{(0)} = 0.11$, $\rho^{(0)} = 1.2$ and $\sigma^{(0)} = \sqrt{0.007}$, while the values in the last round are $A^{(1)} = 0.22$, $\rho^{(1)} = 1$ and $\sigma^{(1)} = \sqrt{1 \times 10^{-5}}$. The denoised outputs are $\mathcal{X}_1 = \{\tilde{y}_i\}_{i=1}^{200}$, with $G(\mathcal{X}_1, \mathcal{Y}_{true}) = 0.0321$. In the interpolation phase, we construct 200 charts and interpolate $K = 10$ points in each chart. The outputs are $\mathcal{X}_2 = \{\tilde{y}_i\}_{i=1}^{2000}$ with $G(\mathcal{X}_2, \mathcal{Y}_{true}) = 0.0304$. A comparison of \mathcal{Y} , \mathcal{X}_1 , and \mathcal{X}_2 with \mathcal{Y}_{true} is provided in Figure 18.

Consider the more general case, when $M = \cup_{i=1}^m M_i$ where each M_i is a d_i -dimensional smooth, closed, and connected Riemannian manifold and the m manifolds are mutually disjoint. M is isometrically embedded in \mathbb{R}^D though $\iota : M \rightarrow \mathbb{R}^D$. Since each connected component may have a different dimension, MrGap cannot be applied directly. Given the noisy data \mathcal{Y} around M , we propose the following method:

- (1) Apply spectral clustering [26] or topological data analysis methods [27, 14, 31, 24] to separate \mathcal{Y} into groups $\{\mathcal{Y}_i\}_i^m$.

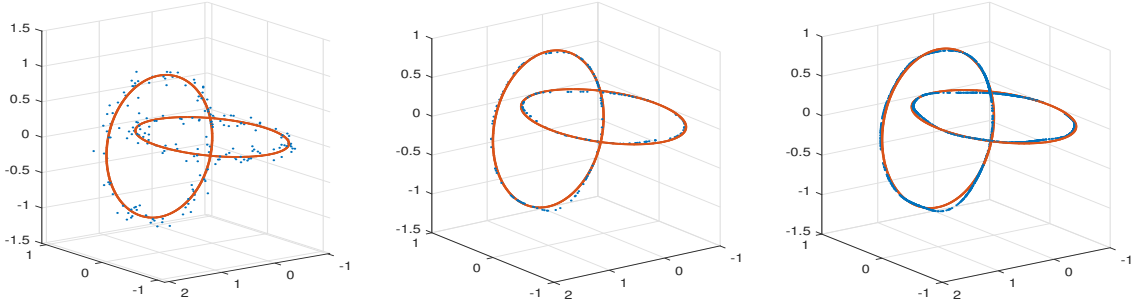


FIGURE 18. Red curves represent \mathcal{Y}_{true} consisting of 5×10^5 points on $\iota(M)$. Left panel shows data \mathcal{Y} (blue) and \mathcal{Y}_{true} ($G(\mathcal{Y}, \mathcal{Y}_{true}) = 0.098$). Middle panel shows denoised samples \mathcal{X}_1 (blue) by MrGap and \mathcal{Y}_{true} ($G(\mathcal{X}_1, \mathcal{Y}_{true}) = 0.0312$). Right panel shows interpolations \mathcal{X}_2 (blue) by MrGap and \mathcal{Y}_{true} ($G(\mathcal{X}_2, \mathcal{Y}_{true}) = 0.0304$).

- (2) For each group \mathcal{Y}_i , apply the method in Section I to detect the dimension d_i of the corresponding manifold M_i .
- (3) Apply MrGap to each \mathcal{Y}_i with the corresponding detected dimension d_i .

We illustrate the above method by the following simulation. Let $\iota(M) = \iota(M_1) \cup \iota(M_2) \subset \mathbb{R}^3$, where $\iota(M_1)$ is the circle of radius 1.6 in the XY plane centered at the origin and $\iota(M_2)$ is the sphere of radius 0.8 centered at the origin. Let $\{\iota(x_i)\}_{i=1}^{230}$ and $\{\iota(x_i)\}_{i=231}^{430}$ be the uniform samples distributed on $\iota(M_1)$ and $\iota(M_2)$ respectively. Suppose $\eta_i \sim \mathcal{N}(0, \sigma^2 I_{3 \times 3})$, with $\sigma = 0.08$. Suppose $y_i = \iota(x_i) + \eta_i$, $i = 1, \dots, 430$, and $\mathcal{Y} = \{y_i\}_{i=1}^{430}$. We uniformly sample \mathcal{Y}_{true} consisting of 4×10^6 points on $\iota(M)$ with 1.5×10^6 points on $\iota(M_1)$ and 2.5×10^6 points on $\iota(M_2)$. For any sample points \mathcal{S} , $G\{\mathcal{S}, \iota(M)\}$ is approximated by $G(\mathcal{S}, \mathcal{Y}_{true})$. Without denoising, we obtain $G(\mathcal{Y}, \mathcal{Y}_{true}) = 0.0994$.

We apply the spectral clustering method to \mathcal{Y} . We construct the random walk graph Laplacian matrix from \mathcal{Y} and find the eigenvector corresponding to the second smallest eigenvalue of the matrix. The eigenvector is plotted over \mathcal{Y} in Figure 19. The values of the eigenvector's entries partition \mathcal{Y} into two groups \mathcal{Y}_1 and \mathcal{Y}_2 . We apply the method in Section I to \mathcal{Y}_1 and \mathcal{Y}_2 respectively, and detect the dimensions $d_1 = 1$ and $d_2 = 2$.

We apply MrGap to \mathcal{Y}_1 and \mathcal{Y}_2 separately. For \mathcal{Y}_1 , we choose the scale parameters $\varepsilon = 0.8$ and $\delta = 0.8$. We iterate Steps 1-3 of Algorithm 1 twice. The estimated covariance parameters in the first round are $A^{(0)} = 0.4$, $\rho^{(0)} = 4.2$ and $\sigma^{(0)} = \sqrt{0.005}$, while the values in the last round are $A^{(1)} = 0.21$, $\rho^{(1)} = 0.8$ and $\sigma^{(1)} = \sqrt{1 \times 10^{-5}}$. The denoised outputs are $\mathcal{X}_1^1 = \{\hat{y}_i\}_{i=1}^{230}$. In the interpolation phase, we construct 230 charts and interpolate $K = 10$ points in each chart. The outputs are $\mathcal{X}_2^1 = \{\tilde{y}_i\}_{i=1}^{2300}$. For \mathcal{Y}_2 , we choose the scale parameters $\varepsilon = 0.9$ and $\delta = 0.9$. We iterate Steps 1-3 of Algorithm 1 twice. The estimated covariance parameters in the first round are $A^{(0)} = 0.74$, $\rho^{(0)} = 3.5$ and $\sigma^{(0)} = \sqrt{0.007}$, while the values in the last round are $A^{(1)} = 1.9$, $\rho^{(1)} = 5$ and $\sigma^{(1)} = \sqrt{0.002}$. The denoised outputs are $\mathcal{X}_1^2 = \{\hat{y}_i\}_{i=231}^{430}$. In the interpolation phase, we construct 200 charts and interpolate $K = 10$ points in each chart. The outputs are $\mathcal{X}_2^2 = \{\tilde{y}_i\}_{i=2301}^{4300}$. We have $G(\mathcal{X}_1^1 \cup \mathcal{X}_1^2, \mathcal{Y}_{true}) = 0.0337$ and $G(\mathcal{X}_2^1 \cup \mathcal{X}_2^2, \mathcal{Y}_{true}) = 0.0347$.

APPENDIX L. ADDITIONAL SIMULATIONS

L.1. Performance of MrGap on a real projective space. In this section, we evaluate the performance of MrGap on a simulated example in which $\iota(M)$ is an embedded 3-real projective space, $RP(3)$, in \mathbb{R}^{10} . The space $RP(3)$ is 3 dimensional closed connected manifold diffeomorphic to $SO(3)$. Letting

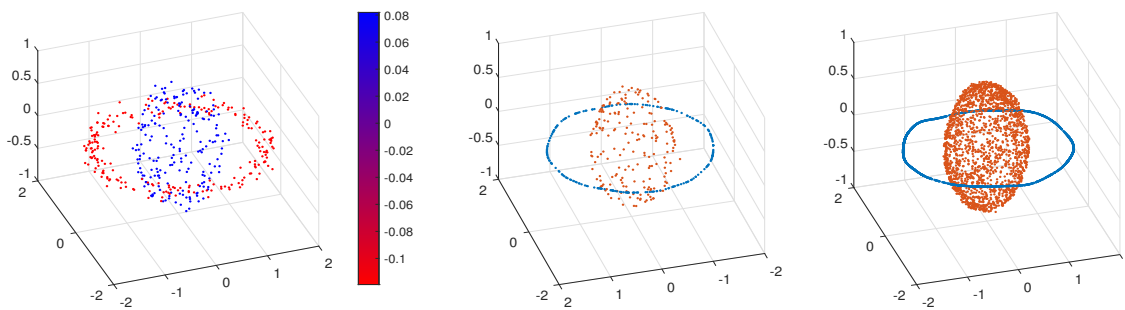


FIGURE 19. Left panel shows the plot of the eigenvector corresponding to the second smallest eigenvalue of the random walk graph Laplacian matrix over \mathcal{Y} . The values of the eigenvector's entries partition \mathcal{Y} into two groups \mathcal{Y}_1 and \mathcal{Y}_2 . Middle panel shows denoised samples \mathcal{X}_1^1 (blue) and \mathcal{X}_1^2 (red) correspondingly to \mathcal{Y}_1 and \mathcal{Y}_2 . ($G(\mathcal{X}_1^1 \cup \mathcal{X}_1^2, \mathcal{Y}_{true}) = 0.0337$). Right panel shows interpolations \mathcal{X}_2^1 (blue) and \mathcal{X}_2^2 (red). ($G(\mathcal{X}_2^1 \cup \mathcal{X}_2^2, \mathcal{Y}_{true}) = 0.0347$).

S^3 denote the 3 dimensional unit sphere: $S^3 = \{[z_1, z_2, z_3, z_4]^\top \mid z_1^2 + z_2^2 + z_3^2 + z_4^2 = 1\} \subset \mathbb{R}^4$, $\iota(M)$ is explicitly constructed through the following map:

$$(40) \quad \begin{aligned} \Phi(z) : \quad S^3 &\rightarrow \iota(M) \subset \mathbb{R}^{10} \\ z = [z_1, z_2, z_3, z_4]^\top &\rightarrow [z_1^2, z_2^2, z_3^2, z_4^2, z_1z_2, z_1z_3, z_1z_4, z_2z_3, z_2z_4, z_3z_4]^\top, \end{aligned}$$

with Φ inducing a diffeomorphism $\tilde{\Phi} : RP(3) \rightarrow \iota(M) \subset \mathbb{R}^{10}$. We uniformly sample points $\{z_i\}_{i=1}^{1200}$ on S^3 to obtain non-uniform samples $\{\Phi(z_i)\}_{i=1}^{1200}$ on $\iota(M)$. Suppose $\eta_i \sim \mathcal{N}(0, \sigma^2 I_{10 \times 10})$, with $\sigma = 0.04$, $y_i = \Phi(z_i) + \eta_i$ for $i = 1, \dots, 1200$, and $\mathcal{Y} = \{y_i\}_{i=1}^{1200}$. We uniformly sample $\{z_i\}_{i=1}^{10^6}$ on S^3 to obtain $\mathcal{Y}_{true} = \{\Phi(z_i)\}_{i=1}^{10^6}$, which is used to approximate the geometric root mean square error. Without denoising, we obtain $G(\mathcal{Y}, \mathcal{Y}_{true}) = 0.1074$.

We apply the method in Section I of the Supplementary Material and estimate the dimension $d = 3$. A detailed procedure of the estimation for this example is provided in that section. We apply MrGap with $\varepsilon = 0.5$ and $\delta = 0.5$. We iterate Steps 1-3 of Algorithm 1 twice. The estimated covariance parameters in the first round are $A^{(0)} = 0.05$, $\rho^{(0)} = 1$ and $\sigma^{(0)} = \sqrt{0.0015}$, while the values in the second round are $A^{(1)} = 0.08$, $\rho^{(1)} = 1.2$ and $\sigma^{(1)} = 0.02$. The denoised outputs are $\mathcal{X}_1 = \{\hat{y}_i\}_{i=1}^{1200}$, with $G(\mathcal{X}_1, \mathcal{Y}_{true}) = 0.0532$. We interpolate $K = 10$ points around each of the 1200 data points. The outputs are $\mathcal{X}_2 = \{\tilde{y}_i\}_{i=1}^{12000}$ with $G(\mathcal{X}_2, \mathcal{Y}_{true}) = 0.0593$.

L.2. MrGap on manifold with boundary. Let $\iota(M)$ be a half torus in \mathbb{R}^3 parametrized by $u \in [0, 2\pi)$ and $v \in (-\frac{\pi}{2}, \frac{\pi}{2})$

$$(41) \quad \begin{aligned} X(u, v) &= \{3 + 0.8 \cos(u)\} \cos(v), \\ Y(u, v) &= \{3 + 0.8 \cos(u)\} \sin(v), \\ Z(u, v) &= 0.8 \sin(u). \end{aligned}$$

We randomly sample 400 points $\{\iota(x_i)\}_{i=1}^{400}$ based on the uniform density function on $\iota(M)$. Let $\eta_i \sim \mathcal{N}(0, \sigma^2 I_{3 \times 3})$, with $\sigma = 0.12$, $y_i = \iota(x_i) + \eta_i$ for $i = 1, \dots, 400$, and $\mathcal{Y} = \{y_i\}_{i=1}^{400}$. We randomly sample 79585 points based on the uniform density function on $\iota(M)$ to form \mathcal{Y}_{true} . We calculate the geometric root mean square error from \mathcal{Y} to \mathcal{Y}_{true} which is $G(\mathcal{Y}, \mathcal{Y}_{true}) = 0.1159$. We plot \mathcal{Y} in Figure 20. We apply MrGap with $\varepsilon = 1$ and $\delta = 1$. We iterate Steps 1-3 of Algorithm 1 twice. The estimated covariance parameters in the last round are $A^{(1)} = 1.3$, $\rho^{(1)} = 5$ and $\sigma^{(1)} = \sqrt{0.002}$. The final denoised outputs are

$\mathcal{X}_1 = \{\hat{y}_i\}_{i=1}^{400}$ with $G(\mathcal{X}_1, \mathcal{Y}_{true}) = 0.0646$. We plot \mathcal{X}_1 in Figure 20. Note that η_i can be decomposed into two components: η_i^\top which is tangent to $\iota(M)$ at $\iota(x_i)$ and η_i^\perp which is perpendicular to $\iota(M)$ at $\iota(x_i)$. Due to the boundary property of the manifold, when $\iota(x_i)$ is near the boundary of $\iota(M)$, the δ neighborhood around the corresponding noisy data y_i may contain fewer data points than when $\iota(x_i)$ is away from the boundary. Since MrGap relies on a Gaussian process to reconstruct a chart associated with y_i , we may have fewer predictors and responses for the regression of the Gaussian process, which could reduce its effectiveness. Thus, the denoised data points may lie in an outward extension of $\iota(M)$ from the boundary, as we show in region 1 of Figure 20. We choose $K = 20$ in applying Algorithm 2. The outputs are $\mathcal{X}_2 = \{\tilde{y}_i\}_{i=1}^{8000}$ with $G(\mathcal{X}_2, \mathcal{Y}_{true}) = 0.0634$. We plot \mathcal{X}_2 in Figure 20.

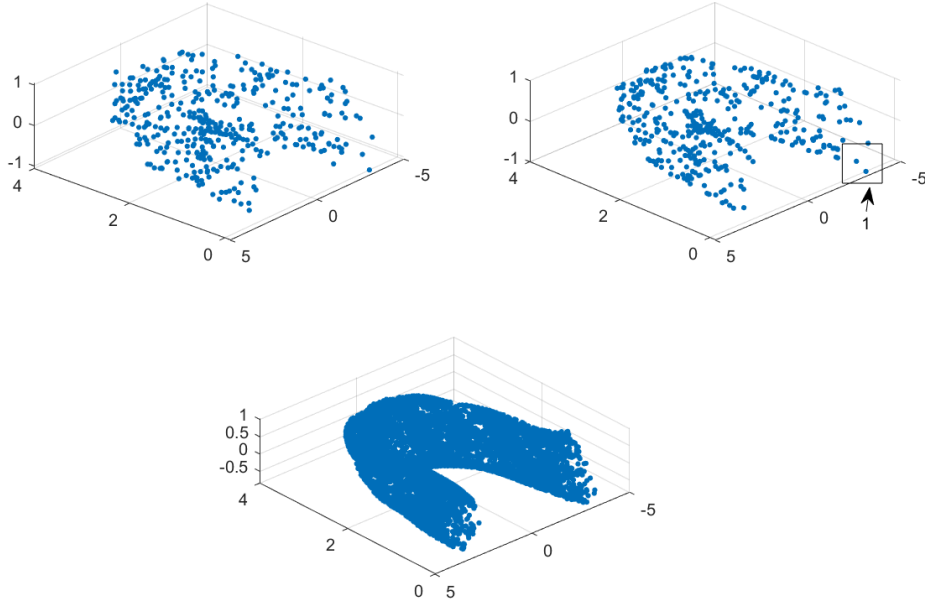


FIGURE 20. \mathcal{Y} contains 400 noisy points around the half torus $\iota(M)$ and \mathcal{Y}_{true} contains 79585 points on the torus $\iota(M)$. \mathcal{X}_1 contains 400 denoised points on $\iota(M)$ by the MrGap algorithm. \mathcal{X}_2 contains 8000 interpolated points on $\iota(M)$ by the MrGap algorithm. We use \mathcal{Y}_{true} to estimate the geometric root mean square error from samples to $\iota(M)$. Top left: Original data \mathcal{Y} with $G(\mathcal{Y}, \mathcal{Y}_{true}) = 0.1159$. Top right: Fits from MrGap \mathcal{X}_1 with $G(\mathcal{X}_1, \mathcal{Y}_{true}) = 0.0646$. Region 1 includes the denoised points on an extension $\iota(M)$ from the boundary. Bottom: Interpolated fits from MrGap \mathcal{X}_2 with $G(\mathcal{X}_2, \mathcal{Y}_{true}) = 0.0634$.

L.3. MrGap on data with bounded noise. The idea of the proof of the main result, Theorem 3.3, can be summarized as follows. Consider two conditions: (1) y_i should not deviate significantly from $\iota(x_i)$ compared to the reach of $\iota(M)$, $\tau_{\iota(M)}$, and (2) there exists a d dimensional affine subspace through y_i with an orthonormal basis deviating from an orthonormal basis of the tangent space at $\iota(x_i)$ by an order 1 term depending on d . When these conditions are met, this affine subspace can be used to construct a chart for $\iota(M)$. When η_i is a bounded error rather than Gaussian, condition (1) can be satisfied by proposing an error bound depending on the reach, while the behavior of orthonormal eigenvectors of $C_{n,\varepsilon}(y_i)$ can be explored by a similar method as in Theorem 3.2. Hence, we expect the result of Theorem

3.3 to hold with suitable relations between the error bound on η_i , ε , δ , n , and $\tau_{\iota(M)}$. We illustrate the performance of MrGap when the noise is bounded in the following example.

Let $\iota(M)$ be a half torus in \mathbb{R}^3 described by (41). Suppose \mathcal{Y}_{true} consists of 79585 points on $\iota(M)$. $\iota(M)$ is contained in a larger box $[-4.3, 4.3] \times [-4.3, 4.3] \times [-1.2, 1.2]$ in \mathbb{R}^3 . We sample 3000 points \mathcal{Y}_b non-uniformly from this box. \mathcal{Y} consists of 319 points $\{y_i\}_{i=1}^{319}$ such that if $y_i \in \mathcal{Y}_b$ and $G(y_i, \mathcal{Y}_{true}) < 0.25$, then $y_i \in \mathcal{Y}$. Hence, \mathcal{Y} are the points around $\iota(M)$ with bounded non-isotropic noise. We calculate the geometric root mean square error from \mathcal{Y} to \mathcal{Y}_{true} which is $G(\mathcal{Y}, \mathcal{Y}_{true}) = 0.1201$. We apply MrGap with $\varepsilon = 1$ and $\delta = 1$. We iterate Steps 1-3 of Algorithm 1 twice. The estimated covariance parameters in the last round are $A^{(1)} = 0.6$, $\rho^{(1)} = 3$ and $\sigma^{(1)} = \sqrt{0.002}$. The final denoised outputs are $\mathcal{X}_1 = \{\hat{y}_i\}_{i=1}^{319}$ with $G(\mathcal{X}_1, \mathcal{Y}_{true}) = 0.0698$. At last, we choose $K = 20$ in applying Algorithm 2. The outputs are $\mathcal{X}_2 = \{\tilde{y}_i\}_{i=1}^{6380}$ with $G(\mathcal{X}_2, \mathcal{Y}_{true}) = 0.0524$.

REFERENCES

- [1] Eddie Aamari and Clément Levrard. Nonasymptotic rates for manifold, tangent space and curvature estimation. *The Annals of Statistics*, 47(1):177–204, 2019.
- [2] Yariv Aizenbud and Barak Sober. Estimation of local geometric structure on manifolds from noisy data. *Journal of Machine Learning Research*, 26(64):1–89, 2025.
- [3] Mikhail Belkin and Partha Niyogi. Laplacian eigenmaps for dimensionality reduction and data representation. *Neural Computation*, 15(6):1373–1396, 2003.
- [4] Jean-Daniel Boissonnat, Andre Lieutier, and Mathijs Wintraecken. The reach, metric distortion, geodesic convexity and the variation of tangent spaces. *Journal of Applied and Computational Topology*, 3(1):29–58, 2019.
- [5] Jeff Calder, Nicolas Garcia Trillos, and Marta Lewicka. Lipschitz regularity of graph Laplacians on random data clouds. *SIAM Journal on Mathematical Analysis*, 54(1):1169–1222, 2022.
- [6] Xiuyuan Cheng and Nan Wu. Eigen-convergence of Gaussian kernelized graph Laplacian by manifold heat interpolation. *Applied and Computational Harmonic Analysis*, 61:132–190, 2022.
- [7] Ronald R Coifman and Stéphane Lafon. Diffusion maps. *Applied and Computational Harmonic Analysis*, 21(1):5–30, 2006.
- [8] Chandler Davis and William Morton Kahan. The rotation of eigenvectors by a perturbation. iii. *SIAM Journal on Numerical Analysis*, 7(1):1–46, 1970.
- [9] Xiucui Ding and Hau-Tieng Wu. Impact of signal-to-noise ratio and bandwidth on graph Laplacian spectrum from high-dimensional noisy point cloud. *IEEE Transactions on Information Theory*, 69(3):1899–1931, 2022.
- [10] Manfredo P Do Carmo. *Riemannian geometry*. Springer Science & Business Media, 2013.
- [11] David B. Dunson, Hau-Tieng Wu, and Nan Wu. Spectral convergence of graph Laplacian and heat kernel reconstruction in L^∞ from random samples. *Applied and Computational Harmonic Analysis*, 55:282–336, 2021.
- [12] David B. Dunson, Hau-Tieng Wu, and Nan Wu. Graph based Gaussian processes on restricted domains. *Journal of the Royal Statistical Society: Series B (Statistical Methodology)*, 84(2):414–439, 2022.
- [13] Nouredine El Karoui and Hau-Tieng Wu. Graph connection Laplacian methods can be made robust to noise. *The Annals of Statistics*, 44(1):346–372, 2016.
- [14] Brittany Terese Fasy, Fabrizio Lecci, Alessandro Rinaldo, Larry Wasserman, Sivaraman Balakrishnan, and Aarti Singh. Confidence sets for persistence diagrams. *The Annals of Statistics*, 42(6):2301 – 2339, 2014.
- [15] Herbert Federer. Curvature measures. *Transactions of the American Mathematical Society*, 93(3):418–491, 1959.

- [16] Charles Fefferman, Sergei Ivanov, Yaroslav Kurylev, Matti Lassas, and Hariharan Narayanan. Fitting a putative manifold to noisy data. *Proceedings of the 31st Conference On Learning Theory*, 75:688–720, 2018.
- [17] Charles Fefferman, Sergei Ivanov, Matti Lassas, and Hariharan Narayanan. Fitting a manifold of large reach to noisy data. *Journal of Topology and Analysis*, 17(02):315–396, 2025.
- [18] Trevor Hastie and Werner Stuetzle. Principal curves. *Journal of the American Statistical Association*, 84(406):502–516, 1989.
- [19] Daniel N Kaslovsky and François G Meyer. Non-asymptotic analysis of tangent space perturbation. *Information and Inference: a Journal of the IMA*, 3(2):134–187, 2014.
- [20] Slav Kirov and Dejan Slepcev. Multiple penalized principal curves: analysis and computation. *Journal of Mathematical Imaging and Vision*, 59(2):234–256, 2017.
- [21] John M Lee. *Introduction to Smooth Manifolds*. Springer, 2012.
- [22] Qi Mao, Li Wang, Ivor W Tsang, and Yijun Sun. Principal graph and structure learning based on reversed graph embedding. *IEEE Transactions on Pattern Analysis and Machine Intelligence*, 39(11):2227–2241, 2016.
- [23] Kun Meng and Ani Eloyan. Principal manifold estimation via model complexity selection. *Journal of the Royal Statistical Society: Series B (Statistical Methodology)*, 83(2):369–394, 2021.
- [24] Kun Meng, Jinyu Wang, Lorin Crawford, and Ani Eloyan. Randomness and statistical inference of shapes via the smooth Euler characteristic transform. *Journal of the American Statistical Association*, 120(549):498–510, 2025.
- [25] James R Munkres. *Analysis on manifolds*. CRC Press, 2018.
- [26] Andrew Ng, Michael Jordan, and Yair Weiss. On spectral clustering: Analysis and an algorithm. *Advances in neural information processing systems*, 14, 2001.
- [27] Partha Niyogi, Stephen Smale, and Shmuel Weinberger. Finding the homology of submanifolds with high confidence from random samples. *Discrete & Computational Geometry*, 39(1-3):419–441, 2008.
- [28] Otso Ovaskainen, et al, and David Dunson. A digital twin for real-time biodiversity forecasting with citizen science. *To appear in Nature Ecology and Evolution*, 2025.
- [29] Otso Ovaskainen, Ulisses Moliterno de Camargo, and Panu Somervuo. Animal sound identifier (ASI): software for automated identification of vocal animals. *Ecology Letters*, 21(8):1244–1254, 2018.
- [30] Nikita Puchkin and Vladimir Spokoiny. Structure-adaptive manifold estimation. *Journal of Machine Learning Research*, 23(40):1–62, 2022.
- [31] Andrew Robinson and Katharine Turner. Hypothesis testing for topological data analysis. *Journal of Applied and Computational Topology*, 1:241–261, 2017.
- [32] Sam T Roweis and Lawrence K Saul. Nonlinear dimensionality reduction by locally linear embedding. *Science*, 290(5500):2323–2326, 2000.
- [33] Chao Shen and Hau-Tieng Wu. Scalability and robustness of spectral embedding: landmark diffusion is all you need. *Information and Inference: A Journal of the IMA*, 11(4):1527–1595, 2022.
- [34] Amit Singer and Hau-Tieng Wu. Vector diffusion maps and the connection Laplacian. *Communications on Pure and Applied Mathematics*, 65(8):1067–1144, 2012.
- [35] Alexander Smola, Sebastian Mika, Bernhard Schölkopf, Robert Williamson, et al. Regularized principal manifolds. *Journal of Machine Learning Research*, 1:179–209, 2001.
- [36] Joshua B Tenenbaum, Vin De Silva, and John C Langford. A global geometric framework for nonlinear dimensionality reduction. *Science*, 290(5500):2319–2323, 2000.
- [37] H. Tyagi, E. Vural, and P. Frossard. Tangent space estimation for smooth embeddings of Riemannian manifolds. *Information and Inference*, 2(1):69–114, 2013.
- [38] Per Åke Wedin. On angles between subspaces of a finite dimensional inner product space. In *Matrix Pencils*, pages 263–285. Springer, 1983.

- [39] Hau-Tieng Wu and Nan Wu. Think globally, fit locally under the manifold setup: Asymptotic analysis of locally linear embedding. *The Annals of Statistics*, 46(6B):3805–3837, 2018.
- [40] Hau-Tieng Wu and Nan Wu. Strong uniform consistency with rates for kernel density estimators with general kernels on manifolds. *Information and Inference: A Journal of the IMA*, 11(2):781–799, 2021.
- [41] Hau-Tieng Wu and Nan Wu. When locally linear embedding hits boundary. *Journal of Machine Learning Research*, 24(69):1–80, 2023.
- [42] Zhigang Yao, Jiaji Su, Bingjie Li, and Shing-Tung Yau. Manifold fitting. *arXiv preprint arXiv:2304.07680*, 2023.
- [43] Yi Yu, Tengyao Wang, and Richard J Samworth. A useful variant of the Davis–Kahan theorem for statisticians. *Biometrika*, 102(2):315–323, 2015.

DAVID B DUNSON, DEPARTMENT OF STATISTICAL SCIENCE, DUKE UNIVERSITY, DURHAM, NC
Email address: `dunson@duke.edu`

NAN WU, DEPARTMENT OF MATHEMATICAL SCIENCES, THE UNIVERSITY OF TEXAS AT DALLAS, RICHARDSON, TX
Email address: `nan.wu@utdallas.edu`